JOINT EUROPEAN TORUS JET

JET–P(93)88

Many Authors

JET Contributions to the 15th Symposium on Fusion Engineering (SOFE),

(Hyannis, Mass, USA, 11-15 October 1993)

JET Contributions to the 15th Symposium on Fusion Engineering (SOFE), (Hyannis, Mass, USA, 11-15 October 1993)

Many Authors

JET-Joint Undertaking, Culham Science Centre, OX14 3DB, Abingdon, UK

Preprint of a paper to be submitted for publication in
the proceedings of the 15th Symposium on Fusion Engineering (SOFE),
(Hyannis, Mass, USA, 11-15 October 1993)
October 1993

Papers presented to the 15th Symposium on Fusion Engineering (SOFE) (Hyannis, Mass, USA, 11-15 October 1993)

JET Development towards Pumped Divertor Operations

E Bertolini and the JET Team.

JET Joint Undertaking, Abingdon, Oxon, OX14 3EA.

JET Development Towards Pumped Divertor Operations

E Bertolini and the JET Team
JET Joint Undertaking, Abingdon, Oxon, United Kingdom

ABSTRACT

The 1991-92 experimental campaign was completed in February 1992. The highlight of this campaign was the preliminary deuterium-tritium experiment (PTE) leading to the first ever production of controlled thermonuclear power in the megawatt range. JET then entered a major shutdown which should be completed by January 1994.
The main objective of the shutdown is the installation of a divertor inside the vacuum vessel. It consists of four poloidal coils, of target plates with graphite tiles and of cryo-pumping panels. The divertor magnetic configuration has required the addition of new radio-frequency antennae, new power supplies and new divertor relevant plasma diagnostics.
The aim of the divertor programme is to show active control of the impurities in thermonuclear grade plasma regimes for about ten seconds, a key issue for the construction of the International Tokamak Experimental Reactor (ITER).

INTRODUCTION

The Joint European Torus (JET) is the largest single project of the fusion research programme of the European Community. The essential objective of JET is to obtain and study a plasma in conditions and dimensions approaching those needed in a thermonuclear reactor. These studies are aimed at defining the parameters, the size and the working conditions of a Tokamak reactor.

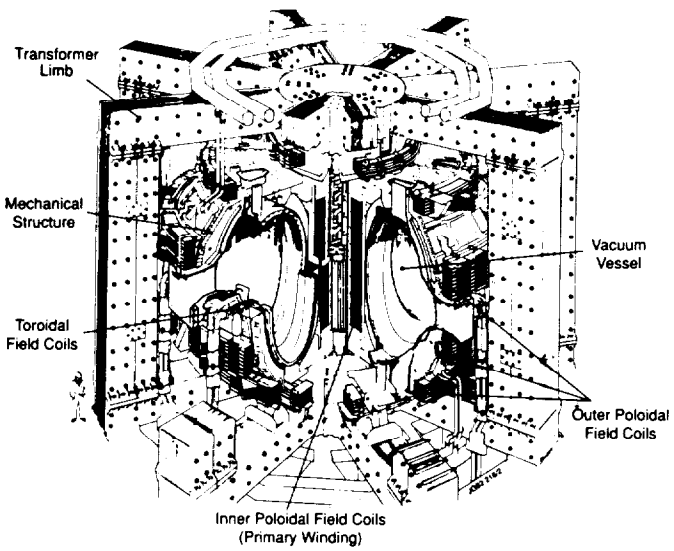

Fig.1: Schematic view of JET showing main components and key features

The realization of these objectives involves four main areas of work:

i) the scaling of plasma behaviour as parameters approach the reactor range;
ii) the plasma-wall interaction in these conditions;
iii) the study of plasma heating;
iv) the study of alpha-particle production, confinement and consequent plasma heating.

To meet these objectives, JET was designed as a large tokamak with key basic features, that were considered controversial when the design was first conceived (Fig 1). The choice of D-shaped toroidal coils and vacuum vessel, leading to elongated plasma cross-sections, of a large plasma volume with moderate toroidal magnetic field and of long flat-top currents, has proven to be a great asset for JET. It has allowed use of a large portion of the magnet volume with large plasma currents; to operate in the magnetic limiter (X-point) configuration, leading to enhanced plasma confinement; to study plasma performance in quasi steady-state conditions; and to install a pumped divertor at the bottom of the vacuum vessel, to achieve active control of the impurity influx [1].

The principal parameters, in the present configuration prior to the installation of the pumped divertor, are given in Table I.

Table I

PRINCIPAL PARAMETERS OF JET

Parameter	Value
Plasma minor radius (horizontal), a	1.25m
Plasma minor radius (vertical), b	2.10m
Plasma major radius, R_o	2.96m
Plasma aspect ratio, R_o/a	2.37
Plasma elongation ratio, $\varepsilon = b/a$	1.68
Flat top pulse length	60s
Toroidal magnetic field (plasma centre)	3.45T
Plasma current, D-shaped plasma	7.0MA
Volts-seconds available	42Vs
Total supply power	1000MW
Energy per pulse	10GJ

The additional heating systems consists of sixteen NBI (Neutral Beam Injectors) operating at 80 or at 140-160kV and of eight ICRF (Ion Cyclotron Radio Frequency) units operating at 23-57MHz. The two systems can deliver above 20MW each to the plasma [2,3].

A 10MW LCHD system (Lower Hybrid Current Drive), operating at 3.7GHz, allows studies of non inductive current drive and control of the current density profiles [4].

Vessel wall conditioning is performed by glow discharge cleaning, by carbonization or by beryllium evaporation.

Plasma fuelling is achieved in three ways: by injecting gas before and during the pulse; by neutral beam injection; and by solid ice pellets at speeds eventually up to 4km/s [5].

About fifty diagnostics systems allow measurements of plasma parameters with high time and space resolution [6].

Supply power and energy requirements (1000MW peak and up to 10,000MJ) are equally shared between the 400kV grid and two local flywheel generators [7].

Table II

PROGRESS IN JET PERFORMANCE

Experimental programme	Peak ion* densities $n_i(10^{20}m^{-3})$	Peak ion* temperature $T_i(keV)$	Energy* confinement time $\tau_E(s)$	Z_{eff}	Fusion product $n_i\tau_E T_i$ $(10^{20}m^{-3}s\ keV)$	Equivalent Q_{DT}
Ohmic heating (1983-1984)	0.4	3.0	1.0	3-10	1.2	0.01
Additional heating (1984-1986)	0.5	12.0	0.9	2-5	2.0	0.3
Machine upgrading (1986-1991)	1.2	20.0	1.2	2-3	2.5	0.3
Passive control of impurities (1988-1991)	4.0	30.0	1.8	1-2	9	1.07

* Not achieved simultaneously

JET operation is managed by CODAS (Control and Data Acquisition System), made up of on-line computers to control the machine and collect, organise and store machine and plasma diagnostics data [8].

The nuclear systems, required for D-T operation include a variety of remote handling tools and equipment and the AGHS (Active Gas Handling System), a fuel processing plant [9,10].

EXPERIMENTAL RESULTS AND ENGINEERING DEVELOPMENT

A great variety of plasma and fusion physics issues have been addressed during the ten years of JET operations. The results have been reported in a large number of papers presented to major international conferences and published in scientific journals. In the following only the progress in main plasma parameters toward reactor relevant conditions will be briefly reviewed (Table II).

This progress has been made possible by a carefully planned experimental programme and by the inherent flexibility 'built in' in the original JET design. Physics results can suggest engineering modifications and machine upgrading, leading to further progress in plasma performance.

Initially, plasma temperatures were only determined by *ohmic heating*. Ion temperatures exceeding 3keV and energy confinement time of 1s were measured, clearly showing that large plasma volumes and currents favour plasma performance. However plasma purity was quite poor [11].

In the following phase, *additional heating* was made available (eight ICRF antennae and eight NBI). Key areas of the vessel wall were covered by graphite tiles, eight graphite limiters were installed, leading to a total 20% of protected surface, and the system for off-pulse carbonization of the vessel walls became operational. These measures allowed the ion temperature to be increased to 12keV and the impurity content was reduced. Moreover, and more importantly, X-point magnetic configurations up to 3MA plasma currents (not foreseen in the original design) were established, by means of a special use of the poloidal electromagnetic system. This allowed compensation to the decay of the energy confinement time with heating. The beneficial effect of the plasma current on confinement was clearly established up to 5MA in limiter configuration [12,13].

These results gave new directions to the JET development and to the tokamak programme at large. A major *JET upgrade* was undertaken aimed at increasing the electro-mechanical capability of the machine up to plasma currents of 7MA in limiter configuration and up to 5MA in the magnetic limiter (X-point) configuration (Fig. 2). In addition, up to 50% of the vessel walls were covered with graphite tiles including two belt limiters, the additional heating systems were brought to full power and a multi-pellet injector capable of launching pellets up to 6mm diameter at a speed of 1.5km/s was installed. With these measures, plasma density, temperature and energy confinement time entered the reactor regime. A further reduction of impurities (seen by a fall in Z_{eff}) was also

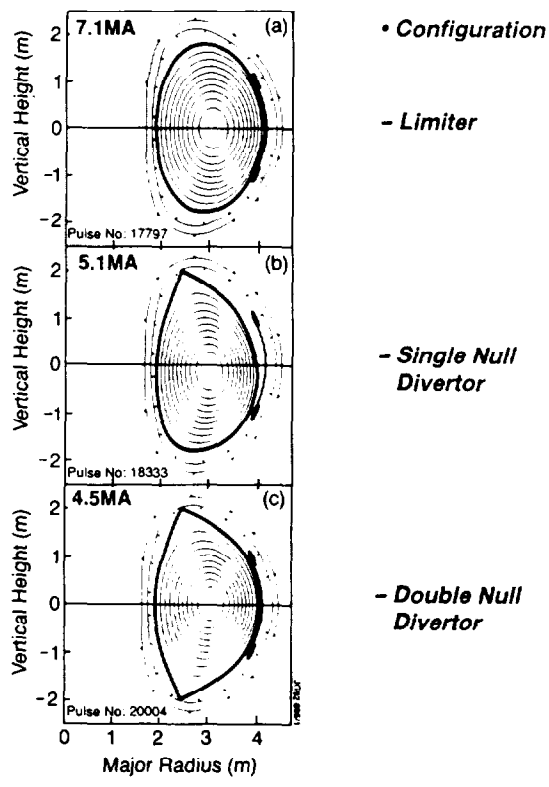

Fig 2: The three main magnetic configurations of JET, prior to the installation of the pumped divertor

achieved, although still exceeding the value required by a reactor plasma. High values of Z_{eff} lead to large radiation losses and to low values of the dilution factor n_D/n_e [14,15,16].

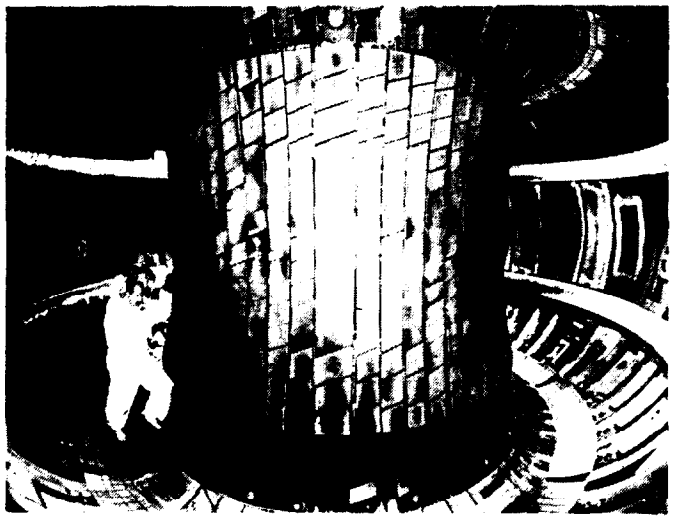

Fig 3: The vacuum vessel walls for the 1991-92 experimental campaign

In the following experimental campaign, *passive control of the impurities* was demonstrated, using beryllium as first wall material, due to its low Z and to its excellent capability of reducing oxygen (beryllium tiles were fitted at the bottom of the vessel and on the top belt limiter, and beryllium evaporators were used). A view of the vacuum vessel during the 1991-92 experimental campaign is shown in Fig.3 .

The sharp reduction of the impurity levels (Z_{eff}<2), led to a dilution factor n_D/n_e above 0.8. This allowed a further increase of the key plasma parameters. The triple fusion product ($n_D \tau_E T_D$) reached 0.9×10^{20} [m^{-3} s keV], only a factor of 6 below reactor requirements, and an equivalent Q_{DT} >1 (breakeven) was also calculated [17,18].

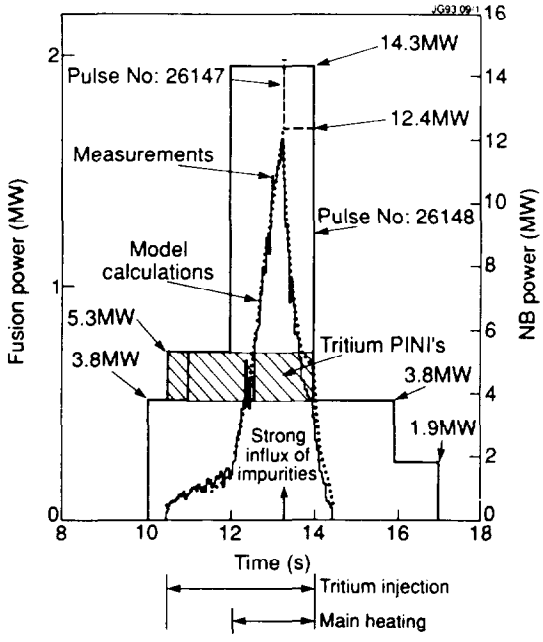

Fig 4: Neutral beam heating power and fusion power for the Preliminary Tritium Experiment at JET

This good plasma performance made it possible to conceive a preliminary D-T experiment (PTE), not originally planned, aimed at providing a firm basis for the full D-T phase; at gaining early experience in handling tritium and in tritium recovery from the vessel and from the NBI system; and at producing a fusion power in excess of 1MW for one second (Fig 4). All goals of the experiment, performed in November 1991, were achieved [19,20].

OBJECTIVES FULFILLED AND SUGGESTIONS FOR FURTHER DEVELOPMENT

After ten years of experimental and development work at JET, two objectives (semi-empirical scaling laws and plasma heating) had been fulfilled, producing experimental knowledge that contributed significantly to the conception of the International Tokamak Experimental Reactor (*ITER*) and to the choice of its main parameters. Concerning the fourth objective (alpha-particle production), work has started with the achievements of the PTE.

The key and most important issue now is to tackle the second objective more aggressively and to control the impurities. Although JET experimental results are outstanding, they show a particular limitation, in that high performance can only be achieved transiently. This is due to a combination of MHD instabilities and to the production and accumulation of impurities in the X-point region. To sustain high performance for several seconds, active control of the impurities is essential, since impurities represent the biggest threat to the progress towards a fusion reactor. JET is therefore now facing a new engineering and physics challenge, the Divertor Programme [21].

THE PUMPED DIVERTOR SHUTDOWN

It is the principal aim of the 1992-93 shutdown to install a axisymmetric pumped divertor (Mark 1) inside the vacuum vessel (Fig.5), together will all necessary auxiliary equipment [22].

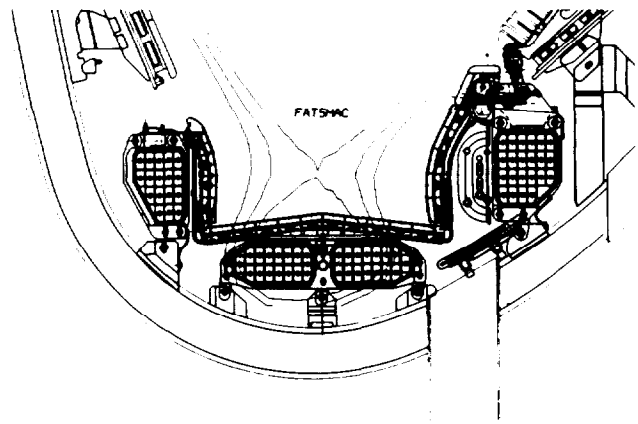

Fig 5: Schematic of JET Mark I pumped divertor showing main components: poloidal coils, target plates and cryo-pump

A. Key components of the divertor

The *four poloidal coils* can create a variety of magnetic configurations, with the X-point far away from the target

plates, including the capability of X-point sweeping to spread the thermal load. The coils are contained in a 1.2mm thick inconel casing, on which the remainder of the divertor components are installed. This calls for an extremely accurate construction of the coil-casing assembly.

The *target plates*, arranged in a U-shaped contour, will collect the power released from the plasma. They consist of an inertially water cooled structure, which support carbon fibre composite (CFC) tiles, accurately shaped to maximize the power wetted surface. The CFC tiles will be later replaced with beryllium tiles, for comparison of plasma performance.

The toroidal *cryo-pump* should allow control of the plasma density in the divertor region. It is anchored to the outer coil casing and its main components are a water cooled baffle, a liquid nitrogen cooled copper back panel, a set of helium cooled pipes and a chevron structure.

B. Other in-vessel components

The new plasma shapes, typical of the divertor configuration has required a complete re-design of the vacuum vessel first wall (Fig.6) to accommodate 'fat' plasmas, which maximize plasma cross section and more elongated 'slim' plasmas, which allow studying configurations with enhanced connection length. Limiters are still required for plasma start-up and as protection for the ICRF antennae. The existing belt limiters were replaced with a new set of 12 discrete *poloidal limiters* on the outer wall and 16 *guard limiters* on the inner wall, all covered with graphite tiles. The *ICRF antennae* require adequate proximity to the plasma to achieve effective power coupling. The plasma will have a different shape and increased wall distance in the new arrangement. A new set of eight ('A2') ICRF antennae of the appropriate shape is required and will be assembled in pairs. The LHCD *launcher* has similar requirements, therefore the grill mouth had to be re-shaped.

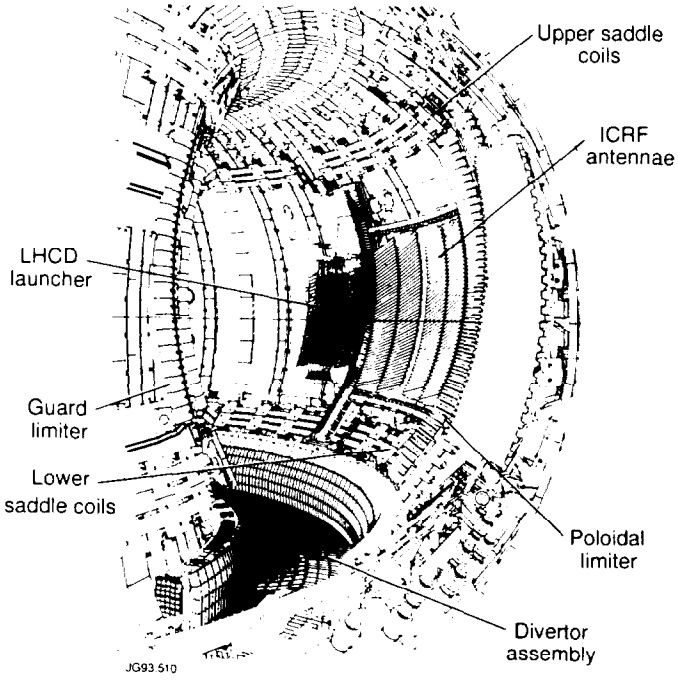

Fig 6: New configuration of the vacuum vessel.

Among the non-divertor related components to be installed inside the vessel, are eight *saddle coils* , four at the top and four at the bottom of the vessel. Their main function is to achieve control of plasma MHD instabilities (m=2, n=1 modes), through a power feedback system.

Finally to accommodate the divertor, original *diagnostics* had to be modified/relocated and a new set of diagnostics had to be designed and procured to study the divertor plasmas.

C. Progress in the shutdown

It is understandable that implementation of all these activities would require a long and carefully planned shutdown. This started in March 1992 and was arranged in three main Stages. Work has been organized in shifts, 16 to 24 hours per day for 6 to 7 days per week.

Stage 1 comprised three main activities: removal of all internal and of the required external components from the torus; replacement of toroidal coil No:4.2 (octant No:4, position 2); and preparation for the fabrication of the divertor coils.

All in vessel work was initially carried out by personnel in full air-line suits, due to the levels of tritium-in-air and beryllium-in-air concentration (10Bq/m^3 and 30μg/m^3 respectively). Towards the end of Stage 1, following the removal and storage of the in-vessel components and of the vacuum vessel wash, contamination levels dropped to those not requiring any special protection (radioactivity dose rate down from 86μSv/h to 5μSv/h, tritium and beryllium-in-air concentration down to non-detectable levels). This permitted the start of Stage 2 . At the end of Stage 1, the vacuum vessel walls were completely stripped and cleaned.

These activities were completed by the end of October 1992, six weeks later than planned, because when TF coil No:4.2 was replaced, a similar fault in coil No:4.3 became apparent. This fault had been masked by the much more serious fault on the adjacent coil No:4.2 since the interturn fault on coil No:4.2 was <3mΩ, while in coil No:4.3 it was ~ 1Ω [23].

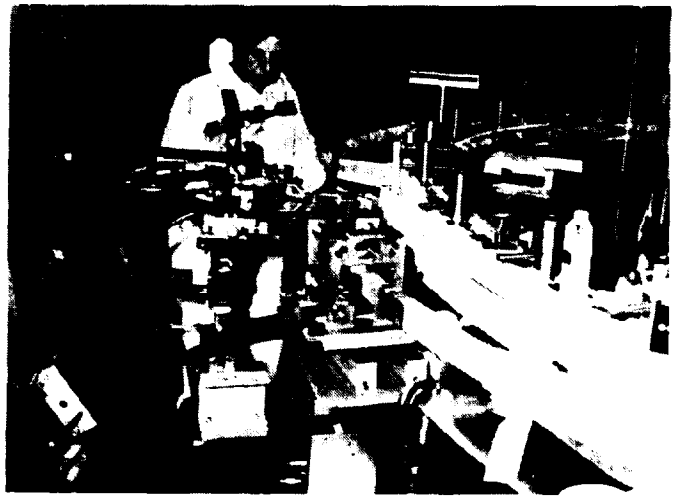

Fig 7 Divertor coil joint brazing inside the vacuum vessel

Stage 2 included fabrication of the divertor coils in the vessel [24]. This was a major task since new tools, new methods of fabrication and new procedures had to be conceived, tested and implemented. The work in factory was limited to the production of pre-formed, capton-fibreglass tape insulated copper hollow bars several metres long; to the manufacture of the required tools; and to the qualification of the brazing process. The remainder of the work was performed on site, inside the vacuum vessel. Main differences as compared with a conventional process in factory, beside the restricted space and the controlled environment, were: brazing of curved bar joints with jigs of minimal dimensions and weight, to be assembled on each joint with the required geometrical accuracy (Fig 7); tight pressure and X-ray tests of each joint; epoxy impregnation and curing inside the final casing, which would prevent observation of the result of the process; the impregnation over-pressure limited to 300mbars (instead of the usual 4-5bars) due to the thin inconel casing; and curing process not performed in an autoclave but by heating the coil conductors electrically. Not surprisingly, some problems were encountered. During the fabrication of coils No:D1 and D4, the rate of failure of the brazed joints was considerably higher than expected (20%). The reason was the inconsistent pressure values on the joints, due to the unsatisfactory and degrading performance of the brazing jigs. Subsequently these were modified and re-calibrated leading to a rate of failure for coils D2, D3 of less than 5%. A second problem became apparent after completion. When removing the resin pipes, it was discovered that, in some areas, the resin between the coil and the casing was not fully cured. Since the coil-casing system had to be an accurate reference for the installation of the other divertor components, a re-curing cycle was studied and tested on two beam models. The beams were subject to the same cycle as the coils, followed by the designed re-curing cycle. Measurements of transition temperatures on resin samples showed correct values and slices out of the model beams, subjected to shear stresses, gave values exceeding 20MPa. The re-curing process was completed successfully as part of Stage 3.

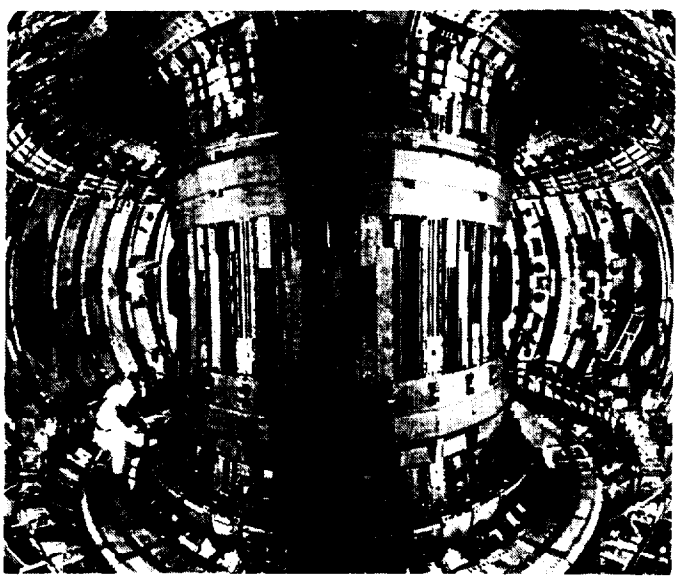

Fig 8: Status of construction work inside the vacuum vessel in September 1993

Stage 3 included the assembly of the divertor structure and of the other components associated with the vessel first wall. It started in mid-May 1993, with a thorough cleaning of the vessel by blasting frozen CO_2 pellets, to remove surface contamination (possibly caused by the coil fabrication process). The coils were located in their final position with the required accuracy (average ~ 2mm radially) and fixed to the bottom of the vessel with special clamps. The installation of upper in-vessel components, such as dump plates and saddle coils has been completed. The status of the vessel at the end of September is shown in Fig.8 [25]. It is expected to complete the shutdown in January 1994, only three weeks later than originally planned.

D. Other divertor related work

To make use of the pumped divertor, a number of major JET subsystems had to be modified and/or substantial upgraded.

Power supplies.

Four new AC/DC thyristor rectifiers, *PDFA* (Poloidal Divertor Field Amplifiers), rated 500V at 40kA, supply the divertor coils individually, allowing flexibility in establishing the divertor configuration and X-point sweeping.

The divertor plasmas will be more unstable vertically than previously. Therefore a power supply with faster response time is required. The new *FRFA* (Fast Radial Field Amplifiers) has been designed as a 'chopper', using GTO (Gate Turn Off) thyristors in four 'H-bridge', supplied at 2500V by AC/DC conventional thyristor rectifiers. The rated output is 5kV, 5kA or 10kV, 2.5kA, time of response 0.2ms in the full voltage range [26].

The *DFAS* (Disruption Feedback Amplifier System), due to supply the saddle coils for MHD stabilization experiments are of similar design as the FRFA, where IGBT's (Isolated Gate Bipolar Transistors) instead of GTO's have been used, for even faster response time (up to 10kHz), 1.5kV, up to 3kA output [27].

The addition of the new power supplies and the plan to use the full capability of the JET machine, would lead to overcome the limit of 2.5% of voltage drop on the U.K.'s 400kV grid. A 200MVAr system of *RPC* (Reactive Power Compensation), made up of capacitor banks connected via vacuum switches to the 33kV busbar system and harmonic filters had to be provided [28].

All new power supplies have been installed and commissioned.

Plasma control and machine protection

The enhanced asymmetry of the plasma configuration and the strong coupling with the divertor coils required reconsideration of essential plasma and machine control and protection, using digital techniques. A completely new *PPCC* (Plasma Position and Current Control) for plasma shape, vertical stability and current, has been designed and it is being implemented. It is based on a decoupling controller following the multi-variable approach. This system should allow a plasma-wall gap control with ~1cm precision [29]. A similar system is being implemented to *stabilize the m=2 , n=1* precursor to major disruptions, using the saddle coils and the

DFAS [30]. The new *CPS* (Coil Protection System) is based on circuit equation integration in real time. It allows on-line comparison between computed and measured coil currents, radial and vertical forces on the coils, etc [31].

Cooling systems

Freon was selected to *cool the divertor coils* (total $20m^3/hr$ and pressures up to 14 bars) with an independent circuit for each coil, allowing for recirculation of warm fluid to limit the differential coolant temperature to $\leq 20^{o}C$. This will contain the shear stresses on the electrical insulation. The toroidal magnet cooling system has therefore been extended [32].

A major upgrading of the *cryo-plant* has been necessary to care for the divertor pump, LHCD and the tritium plant, leading to the total capacity of the system of 1.3kW at $4.4^{o}K$ (450 l/hr of liquefaction capacity).

Diagnostics

Examples of new diagnostics installed to study plasma in divertor configuration are: a new instrument, located on top of the machine, consisting of three spectrometers, to measure poloidal emission profiles from different impurity ionisation stages in the divertor region; and a new microwave diagnostic, for measuring plasma electron densities and temperatures, made up of six antennae, giving two lines of transmission through the outboard divertor channel plasma and one on the inboard side (Fig.9).

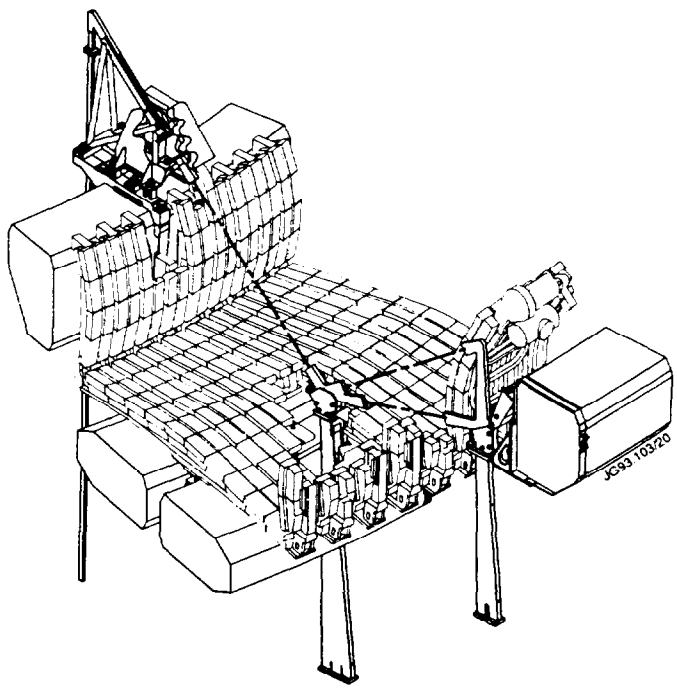

Fig 9 The new interferometer for measurements of plasma electron densities and temperatures in the divertor region

E. *Non-divertor related systems*

Use has been made of the long shutdown period for modifications and upgrading of the existing systems, for other new installation and for extended maintenance. One *NBI system*, has been modified to 80kV, 60A per beam and the other to 160kV, 30A per beam.

A high speed (up to 4km/s) *pellet injector* should be available in late 1994. A new centrifuge is under installation, capable of delivering long strings of 2 and 3mm pellets at a repetition frequency up to 40 s^{-1} and velocities up to 600m/s.

CODAS underwent a major modification and upgrading with the replacement of the 10 years old Norskdata with Sun computers, and the use of UNIX as an operating system and ETHERNET for communication.

All plant subsystems of the *AGHS*, due to handle a daily throughput of up to 5 moles of T_2 , 15 moles of D_2 and 150 moles of H_2 and required to be in full use for the JET D-T phase, have been completed and commissioned [33].

Extensive use of *remote handling tools* has been made during the shutdown for the removal and installation of in-vessel components, while further important developments took place. The articulated boom (the in-vessel transporter) has been fitted with a new controller to enhance flexibility, the TARM (Telescopic Articulated Remote Mast), for ex-vessel activities is under commissioning and the IVIS (In-Vessel Inspection System) has been fitted with new viewing tubes and neutron radiation tests are underway on most critical components.

THE FUTURE OF JET

The work summarized above represents such a major upgrading that JET should now be considered a essentially as new machine (Fig.10). Consequently a new learning process must be followed to operate the machine and provide further relevant contribution to the world fusion programme and

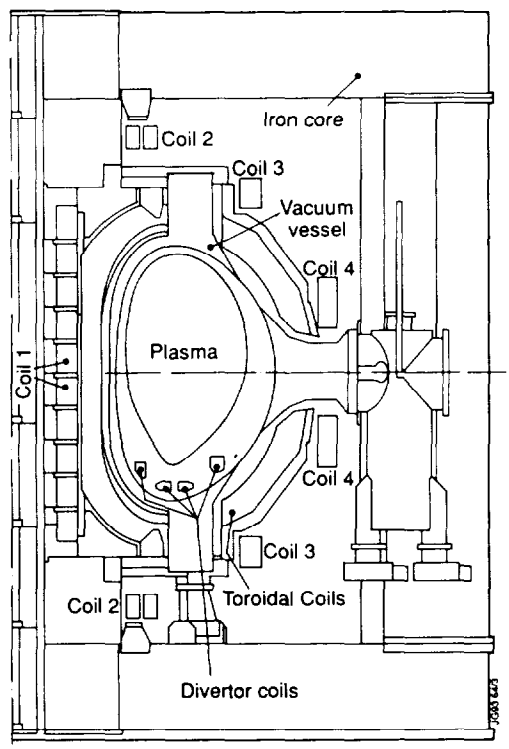

Fig 10: The new JET cross-sectional view including divertor coils

specifically to ITER. Local commissioning of major subsystems is underway and this will help in approaching the integrated commissioning with plasma in the most efficient way, thus allowing the experimental programme to start in March 1994.

A. The Mark2 divertor

The *Mark 1* divertor has always been considered an interim solution, due to its limited power handling capability and open structure. Therefore a *Mark 2* divertor has been designed and its major components are under procurement. Mark 2 will have a *closed divertor structure* (Fig 11), leading to increased impurities and neutral retention, increased radiation and reduced conducted power to the target plates. Moreover a 'continuous target design', still inertially cooled, will further increase the power handling capability, and could not require X-point sweeping. Approval for the installation of Mark 2 divertor in 1995 will be considered by the JET Council in early 1994.

Mark 2 would also permit easy changes of graphite (or beryllium) tiles to follow ITER divertor design development. However it would require an extension of JET beyond December 1996 to carry out this work and this is now been considered.

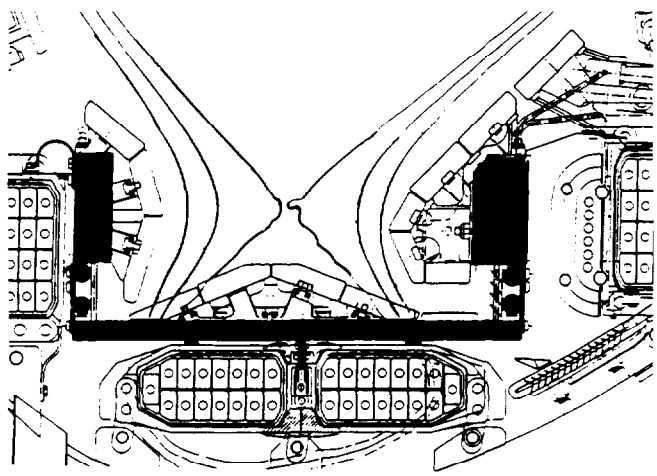

Fig 11 The structure of JET Mark 2 divertor

B. JET performance development

JET will now allow establishment of divertor configurations up to 6MA for about 10s, and up to 60s at reduced current.

The expected higher plasma purity will reduce radiation losses and bring the dilution factor close to unity.

Improved magnetic configuration, control of plasma profiles by enhanced ICRF and LHCD capability for non inductive current drive, control of disruption with saddle coils and error field compensation will further extend JET operating space.

The combination of the above measures should lead to greatly enhance global plasma performance with additional heating, leading to high neutron yield in D-T plasmas, with a thermonuclear neutron fraction up to and above 80%.

C. JET forward programme

The three main lines of the JET programme are: (a) divertor development, (b) advanced tokamak physics, and (c) D-T experiments. Parallel programme lines are: (a) physics of reactor grade plasma, (b) reactor relevant working conditions, (c) reactor technology.

The experimental plan set out for 1994 will already start tackling the various aspects of this ambitious programme, with particular emphasis on the demonstration of divertor operation and in achieving high plasma performance with divertor.

CONCLUSIONS

Ten years of JET operation has given essential contributions to the world fusion programme and in particular to the ITER design and parameters choice. Further essential contributions should be the outcome of the divertor experiments with Mark 1 and with Mark 2 pumped divertor configurations.

These configurations are expected to show divertor effectiveness in controlling impurities at $Q_{DT} \geq 1$ for several seconds and steady-state divertor operation up to 30s at plasma temperatures above 10keV.

By using the new divertor and by exploiting all JET facilities, in D-T operation, it is expected to achieve high neutron yield with a content of thermonuclear neutrons up to and above 80%.

An extension of JET beyond 1996, would allow further key contributions to the ITER programme by testing advanced divertor concepts, optimising plasma performance and demonstrating the coherence of advanced tokamak scenarios.

ACKNOWLEDGMENTS

The material for this paper is the result of extended discussions with many members of the JET Team. This collaboration is gratefully acknowledged and appreciated.

References

[1] E. Bertolini, "The JET Project: Progress Towards a Tokamak Thermonuclear Reactor", Power, 105, June 1993, vol. 7, no. 3.

[2] G. Duesing, et al., "Neutral Beam Injection System", Fusion Technology, 13, 163, January 1987.

[3] A. Kaye, et al., "Radio-Frequency Heating System", Fusion Technology, 13, 203, January 1987.

[4] C. Gormezzano, et al., "RF Heating and Current Drive: Status and Prospects for the Next Step", Proceedings of the 16th Symposium on Fusion Technology, London (UK), 3-7 September, 1990, 1; 99.

[5] K. Sonnenburg, et al., "Prototype of a High Speed Pellet Launcher for JET", Proceedings of 15th Symposium on Fusion Engineering, Utrecht (The Netherlands), 19-23 September 1988, 1, 715.

[6] M. Kelihacker, et al., "Review of Diagnostic System 1986", JET Report JET-IR(86)16.

[7] E. Bertolini, et al., "The JET Magnet Power Supplies and Plasma Control Systems", Fusion Technology, 13, 71, January 1987.

[8] H. Van der Beken, et al., "CODAS: The JET Control and Data Acquisition System", Fusion Technology, 13, 120, January 1987.

[9] J.R. Dean, T. Raimondi, "JET Remote Maintenance During Active Operation", Fusion Technology, 13, 253, January 1987.

[10] R. Haange, et al., "General Overview of the Active Gas Handling System at JET", Proceedings of the 3rd Topical Meeting on Tritium Technology in Fusion, Fission and Isotopic Applications, Toronto (Canada), 1-4 May 1988, Fusion Technology, 14, 461.

[11] PH. Rebut and the JET Team, "First Experiments in JET", Proceedings of the 10th Conference on Plasma Physics and Controlled Nuclear Fusion Research, London (UK), 12-19 September 1984. "Nuclear Fusion", IAEA Supplement, 1985, 1, 11.

[12] P.H. Rebut and the JET Team, "JET Latest Results and Future Prospects", Proceedings of the 11th Conference on Plasma Physics and Controlled Nuclear Fusion Research, Kyoto (Japan), 13-20 November 1986. "Nuclear Fusion", IAEA Supplement, 1987, 1, 31.

[13] A. Tanga, et al., "Experimental Studies in JET with Magnet Separatrix Configuration", Proceedings of the 11th Conference on Plasma Physics and Controlled Nuclear Fusion Research, Kyoto (Japan), 13-20 November 1986. "Nuclear Fusion", IAEA Supplement, 1987, 1, 65.

[14] M. Huguet, "Technical Aspects of the New JET Development Plan", Proceedings of the 14th Symposium on Fusion Engineering, Avignon (France), 8-12 September 1986, 1, 253.

[15] R.J. Bickerton and the JET Team, "Recent Progress in JET Experiments", Proceedings of the 12th Conference on Plasma Physics and Nuclear Fusion Research, Nice (France), 12-19 October 1988. "Nuclear Fusion", IAEA Supplement, 1989, 1, 41.

[16] M. Keilhacker and the JET Team, "The JET H-mode at High Currents and Power Levels", Proceedings of the 12th Conference on Plasma Physics and Nuclear Fusion Research, Nice (France) 12-19 October 1988. "Nuclear Fusion", IAEA Supplement, 1989, 1, 159.

[17] M. Huguet, E Bertolini and the JET Team, "Technical Status of JET and Future Prospects", Proceedings of the 13th Symposium on Fusion Engineering, Knoxsville (USA), 2-6 October 1989, IEEE 1990, 1, 491.

[18] P.H. Rebut and the JET Team, "Impurities in JET and their Control:, Proceedings of the 13th Symposium on Fusion Engineering, Knoxsville (USA), 2-6 October 1989, IEEE 1990, 2, 227.

[19] The JET Team, "Fusion Energy Production from a Deuterium-Tritium Plasma in the JET Tokamak", Nuclear Fusion, 32, 187 1992.

[20] E. Thompson, et al., "Experience at JET Relating to the First Production of Tritium Neutral Beams for D-T Tokamak Experiments". This Conference, 2-OB-4.

[21] P.H. Rebut, "Future Prospects for JET and Next Step Tokamaks", Proceedings of the 16th Symposium on Fusion Technology, London (UK), 3-7 September 1990, 1, 171.

[22] M. Huguet and the JET Team, "Technical Aspects of Impurity Control at JET: Status and Future Plans", Proceedings of the 9th Topical Meeting on the Technology of Fusion Energy, Oak Bay (USA), 7-10 October 1990, Fusion Technology 1991.

[23] J. Last, et al., "Toroidal Coil Faults - Detection, Diagnosis and Prevention", International Conference, Victoria, Canada, 20 - 24 September 1993. To be published.

[24] A. Tesini, "Construction and Testing of the JET Divertor Coils inside the Vacuum Vessel", This Conference, 4-OB-4.

[25] M. Pick, "The new First Wall Configuration of JET", This Conference 1-OB-5.

[26] T. Bonicelli, et al., "Analysis and Specifications of the Performance of the JET Amplifier for Vertical Stabilisation". This Conference, 5-PA-23.

[27] P.L. Mondino, et al., "The High Power Wide Bandwidth Disruption Feedback Amplifiers for JET", Fusion Technology 1990, London, 1624, North Holland.

[28] E. Bertolini et al., "Supplying JET from the UK 400kV Supergrid: A Major Engineering Achievement Relevant for the Next Step", Fusion Technology 1990, London, 233, North Holland

[29] M. Garribba, et al., "The New Control Scheme for the JET Plasma Position and Current Control System", This Conference, 2-PA-14.

[30] A. Santagiustina, et al., "Design of the M=2, N=1 Tearing Mode Control System for JET". This Conference, 3-PC-13.

[31] V. Marchese, et al., "A New Coil Protection System for the Divertor Configuration at JET". This Conference, 3-PC-13.

[32] M. Cooke, et al., "Organic Cooling Fluids for the JET Toroidal and Divertor Field Coils". This Conference, 2-PB-14.

[33] J.L. Hemmerich, et al., "Installation and Final Commissioning of the JET Active Gas Handling System (AGHS)". This Conference, 4-OB-6.

Experience at JET Relating to the First Production of Tritium Neutral Beams for D-T Tokamak Experiments

E Thompson and the JET Team.

JET Joint Undertaking, Abingdon, Oxon, OX14 3EA.

EXPERIENCE AT JET RELATING TO THE FIRST PRODUCTION OF TRITIUM NEUTRAL BEAMS FOR D-T TOKAMAK EXPERIMENTS

E Thompson and the JET Team

JET Joint Undertaking, Abingdon, Oxon, OX14 3EA, England

I. INTRODUCTION

The highest fusion yield plasmas in JET are obtained using neutral beam injection (NBI) to inject energetic beams of deuterium into low density target plasmas which are generated in single or double-null X-point magnetic configurations. Extrapolation of the measured performance of these hot-ion H-mode plasmas in deuterium to that to be expected using a D-T fuel mixture showed that significant power (~MW) would be released from controlled thermo-nuclear fusion reactions even if the tritium concentration was less than the optimum value of 50%.

It was decided to carry out an experiment in November 1991 using a small quantity of tritium in order to fulfil the following objectives:

(i) To establish a firm basis for the prediction of the performance of future D-T pulses in JET including the question of fuel mixing.

(ii) Establish safe procedures for handling tritium in compliance with the regulatory requirements and to demonstrate the technology related to tritium usage, recovery and accounting.

(iii) To demonstrate the production of 1MW of fusion power for approximately one second.

It was also decided that this First Tritium Experiment (FTE) would be executed within the following boundary conditions which were self-imposed by the Project.

- Only ~1 bar litre of tritium i.e. $\sim 7 \times 10^{13}$ Bq (2000 Ci), would be available for the total experiment.
- The integrated neutron production would be limited to $< 1.5 \times 10^{19}$ neutrons to avoid excessive activation of the JET apparatus. This was to enable the shutdown and major modifications of JET to proceed as plánned in early 1992.

Clearly these limitations restricted the number of high performance tritium discharges and also placed a high premium on having a high degree of reliability of the complete experimental scenario.

Although NBI was not the only means by which tritium could be introduced into the plasma, it was selected as the fuelling mechanism for the First Tritium Experiment (FTE) because it offered the following decisive advantages over the only other available option of gas puffing.

- The deposition profile of tritium could be predicted with a high degree of certainty. For the high fusion performance plasmas obtained in deuterium, the tritium deposition would be peaked in the high temperature core of the plasma, resulting in maximum fusion reactivity.
- The total quantity of tritium introduced into the torus is minimised.
- The necessary development, testing and commissioning could be carried out on the Neutral Beam Test Bed with minimal impact on tokamak operation.
- The NBI system had a demonstrated high degree of operational reliability and availability.

The physics aspects of high fusion performance plasmas produced in JET by NBI heating and the experimental results obtained in the FTE are described elsewhere [1,2]. In the following, we describe the major technological developments which were carried out to enable the first multi-ampère beams of tritium, essential for the successful outcome of the FTE, to be produced and injected into the JET tokamak.

II. ADVANTAGES OF NEUTRAL BEAM INJECTION FOR THE INTRODUCTION OF TRITIUM

Although simple arguments based upon energetics preclude NBI as a fuelling mechanism for an ignited fusion reactor, the advantages listed above made NBI the most advantageous fuelling mechanism for this experiment. In particular the deposition of tritium in the hot central core of the plasma completely eliminates the quantitative uncertainties regarding edge recycling and the magnitude of inward transport of tritium introduced by gas puffing. Because the primary aim was to **fuel** as opposed to heating the plasma, the 80kV configuration of the JET Positive Ion Neutral Injectors (PINI) was chosen in preference to the 160kV configuration which will be used for the final D-T phase of JET operation. In addition to computer predictions based upon the known geometry of the ion extraction and acceleration structure, the measured performance of the PINIs using H_2, D_2, ^3He and ^4He as the working gas enabled the extracted ion current of tritium and the resulting equivalent current of neutral tritium atoms injected into the tokamak to be predicted with a high degree of confidence. The tritium deposition within the plasma could then be computed using the experimentally measured radial dependencies of plasma density and temperature for the discharges typical of those to be used for the FTE. From a series of such calculations it was determined that a total fuelling ratio of up to ~14% could be obtained using a combination of two 80kV T^0 beams plus two 80kV and twelve 140kV D^0 beams. Fig. 1 shows the computed fuelling of the central region of the plasma for various injected species and energies as a function of the volume average density of the target plasma.

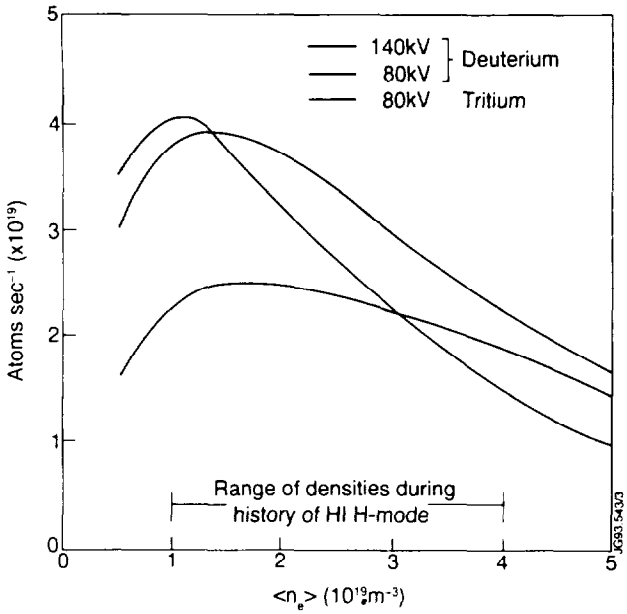

Fig.1: Computed fuelling of the Central Region of JET (r/a<0.3) per MW injected.

In addition to the above "physics" advantages, tritium NBI offered the additional major technical advantages of minimising the total quantity of tritium introduced into the torus and also enabled the usage of tritium to be quantified with sufficient precision to enable the full experimental programme for the tritium experiments to be planned in detail.

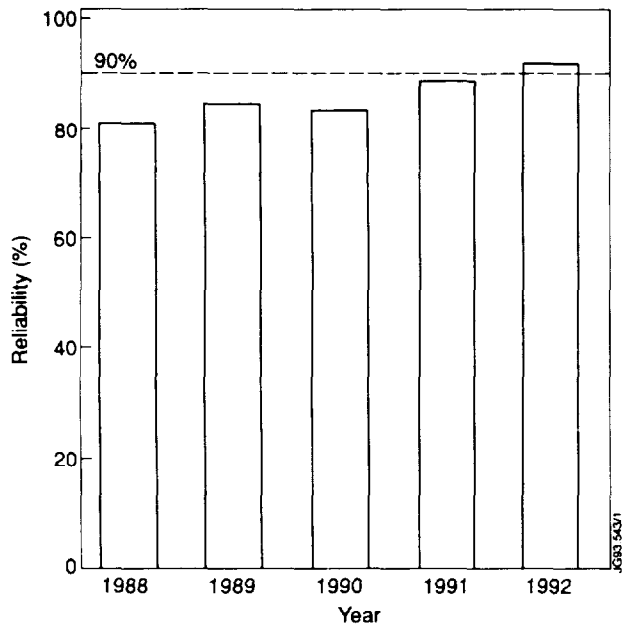

Fig.2: Measured reliability of JET NBI system (defined as ratio of energy delivered to plasma normalised to energy requested).

Clearly, the limited amount of tritium that was to be available for the FTE placed a very high premium on having a high degree of reliability for the NBI. In Fig. 2 we show how the series of steady improvements to the NBI system has resulted in a progressive increase in the system reliability to the order of 90%. It should be noted that these data include operation in H, D, ^{3}He and ^{4}He.

III. DEVELOPMENTS REQUIRED FOR TRITIUM BEAMS

Because tritium NBI is planned for the final D-T phase of JET operation, the basic injector configuration and construction is compatible with the use of tritium [3]. Nevertheless, this FTE required some of the developments already foreseen to be brought forward. The major hardware modifications which were necessary were the manufacture of a Tritium Gas Introduction System (TGIS) [4] and modifications to the Positive Ion Neutral Injectors (PINIs) [5] which were to be used for the injection of tritium. In addition, operational scenarios had to be developed in relation to isotopic exchange between D and T [6] and also in relation to the recovery of tritium condensed onto the liquid helium cooled cryopanels [7]which form the pumping surfaces inside the injectors.

A. Tritium Gas Introduction System (TGIS)

The Tritium Gas Introduction System was based upon the use of the U-bed container in which the tritium was to be transported to the JET site. A pre-requisite to designing the system was an extensive series of measurements which were designed to characterise fully this type of U-bed (using deuterium) to determine the pressure versus flow characteristics and also to examine in detail the characteristic of such a U-bed when it was close to depletion. Measurements confirmed that the U-bed operated as a constant volume source whose initial pressure is determined by the temperature of the U-bed. Therefore the TGIS was based upon the use of a constant pressure regulator in combination with a needle valve in order to give a constant gas flow. Both of these components had previously been developed by the JET Tritium Group for use in the final D-T phase of JET. The total system is shown schematically in Fig. 3. An essential feature of the TGIS is the provision of a deuterium U-bed in addition to that for tritium. This enabled the total system, including the final control and instrumentation to be tested fully and to be used in routine operation with deuterium as the working gas under the identical conditions to those foreseen to be used with tritium. Additional features built into the design included provision for the change from deuterium to tritium operation and from one to two PINI operation to be reversible and repeatable and, in particular, not to require a change of any pre-set calibrations. All internal pressures were arranged to be sub-atmospheric and the complete TGIS was housed inside a ventilated glove box with

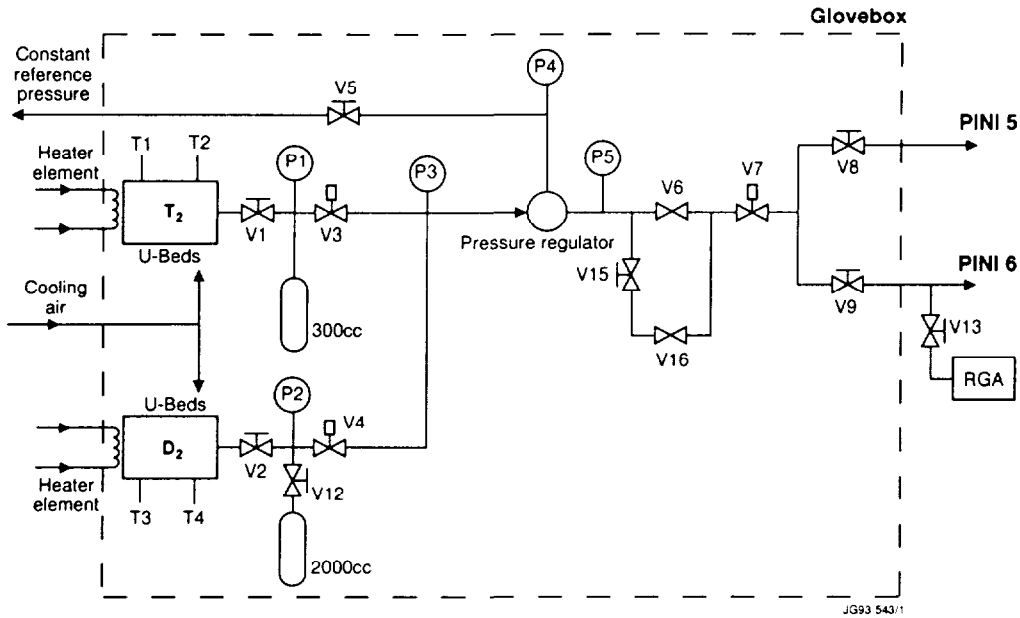

Fig.3: Schematic of Tritium Gas Introduction System.

a monitored exhaust to provide secondary containment. The unit was installed adjacent to the injectors in order to minimise pipe-runs and the associated "dead" volumes in order to maximise the utilisation of tritium.

The provision of a single, transferable U-bed heater supply and control system for **either** the D_2 **or** the T_2 U-bed in conjunction with V4 or V3 (Fig. 3) respectively, ensured no cross-contamination of D by T or *vice-versa*. It also allowed a simple fail-safe interlock to be implemented between the injector hardware and its operating software in order to recognise the use of D or T. Additional safety measures included fail-safe features on both over-pressure and over-temperature with redundant temperature and pressure monitors. The output of all sensors (including redundant transducers) was permanently displayed on a dedicated mimic diagram and all operations relating to the TGIS, including installation, commissioning, operation of hand-valves etc were governed by an extensive set of strictly enforced written procedures. The only disadvantage of this relatively simple gas introduction system was the need to enter the torus hall in order to change from D to T and *vice-versa*.

B. Modifications to Positive Ion Neutral Injectors (PINIs) for Tritium Operation

In their original configuration, the JET PINIs are supplied with gas via two independent introduction systems, one at ground potential for the neutraliser gas, plus one at high voltage in order to supply the plasma generator. For tritium operation it was decided to eliminate the gas feed at high potential since this removes the need for an insulating break in the gas line and enables an all-metallic system to be constructed with all control and instrumentation at ground potential. Therefore, it was necessary to develop and test an alternative route for gas introduction into the PINI which maximises the gas target for neutralisation and also maximises the conductance into the plasma generator in order to replace the gas which is removed in the form of beam particles. An additional constraint is that the solution must have a wide operating range against Paschen breakdown of the accelerator structure. The solution which was adopted in shown schematically in Fig. 4. By means of relatively simple modifications to the hardware it is possible to introduce gas immediately down-stream of the final grid of the ion accelerator. This results in maximum target thickness in the neutraliser and also gives maximum conductance into the plasma source via the accelerator grids. Detailed pressure measurements as a function of flow were made to fully characterise the complete system and operational tests confirmed that this solution is not at all sensitive to Paschen breakdown over a wide range of pressures. Beam neutralisation measurements made using

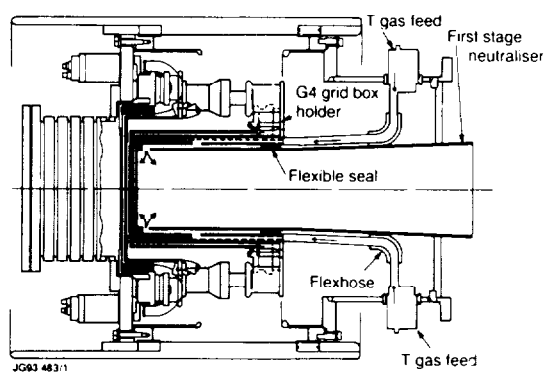

Fig.4: Modified Gas Introduction into PINI.

deuterium in a modified PINI showed that ~17 mbℓ s^{-1} T_2 would be required per PINI to convert the ion beam to neutral atoms. Two PINIs were modified in this manner and fully conditioned and characterised on the neutral beam test bed prior to installation on the tokamak.

C. *Change from D_2 to T_2 Operation*

In view of the limited amount of tritium available for the FTE, it was important to minimise the amount of tritium required to change from deuterium to tritium operation of the injector. Studies of isotopic exchange were carried out in the neutral beam test bed using hydrogen and deuterium. Data were obtained by monitoring the neutron yield from the beam-line which results from reactions between the beam and isotopes previously implanted into the beam target. In Fig. 5 we show the neutron production (normalised to the equilibrium yield of a pure deuterium beam) from the residual deuterium in the plasma generator when the working gas is changed from deuterium to hydrogen. The neutron count and hence deuterium content of the hydrogen beam decreases as a function of the integrated arc operation time. These data were taken after ten 10-second filament de-gassing pulses. This outgassing procedure resulted in approximately a factor 2 reduction in the neutron count from the first pulse following the change in working gas. From such data it was concluded that only two "isotope exchange" pulses were required prior to the injection of tritium beams into the torus.

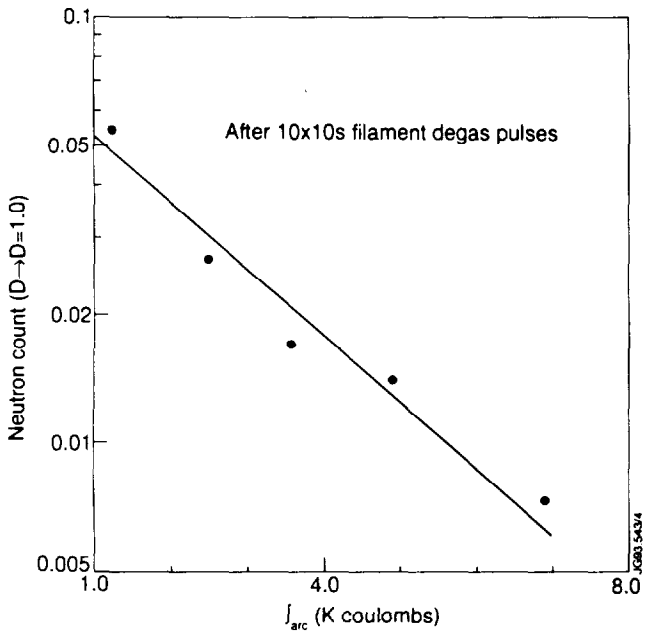

Fig.5: Neutron production during isotopic change from D_2 to H_2 operation.

IV. OPERATION OF TRITIUM BEAMS

The following pulse sequence was established for the injection of tritium beams into JET:

(i) Final optimisation of the complete scenario using full power deuterium injection into the tokamak using all 16 PINIs.
(ii) Change from D to T U-bed.
(iii) Execute 2 filament de-gassing shots on the tritium PINIs.
(iv) One 0.1s beam pulse to confirm the setting of the beam-line deflection magnet.
(v) Two beam pulses from the tritium PINIs of 0.8s duration to confirm the beam perveance and to measure the beam power.
(vi) Injection into the tokamak using the 2 tritium PINIs plus 14 deuterium PINIs.

The above pulse sequence was executed as planned and the first tritium beams were produced at 78kV. The measured beam perveance was 20% less than that predicted due to the difficulty in predicting exactly the arc current required in changing from D to T operation. However, because the first beams had been free of any electrical breakdown, it was decided not to increase the voltage or current on the tritium PINIs. Details of the tritium PINI performance are given in Table I and Fig. 6 shows the wave forms of injected power and key plasma parameters for JET pulse 26148 which was one of the two tritium shots into the tokamak both of which were successful.

Table I
Tritium PINI Performance Obtained in the FTE

Acceleration voltage	78kV
Species mix (power fractions)	Full: 79% Half: 12% Third: 9%
Injected T^0 current I^0_{inj}	13A
Injected power P_{inj}	0.8MW
T_2 gas utilisation for 3s beam pulse, including 0.8s arc stabilisation	64mbl = 163Ci = 0.016g

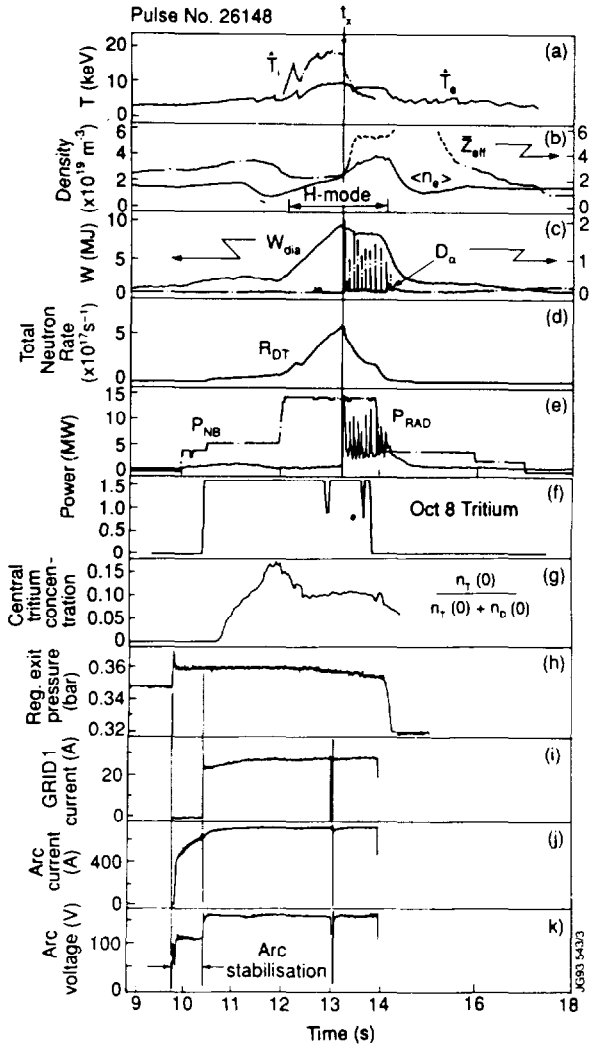

Fig.6: Time development of JET FTE Pulse No: 26148. (a)–(e) Plasma parameters: central temperatures; volume averaged electron density; line averaged effective ionic charge (Z_{eff}); plasma diamagnetic energy; D_α emission; total neutron rate and total input NBI power and radiated power. The time t_x indicates the sudden collapse of plasma performance accompanied by a strong influx of carbon impurity (X-event). (f) tritium power input from NBI (g) central tritium concentration, calculated on the basis of equal radial transport coefficients for tritium and deuterium [1]. (h) output pressure of tritium pressure regulator. (i)–(k) injector waveforms of one of the tritium PINIs: extracted beam current; arc current; arc voltage.

V. TRITIUM INPUT AND SUBSEQUENT RECOVERY FROM THE INJECTOR [8,9]

The total quantity of tritium removed from the U-bed was determined from a detailed analysis of the pressure transducers on the Tritium Gas Introduction System coupled with an analysis of the composition of the gas remaining on the U-bed after the experiment. The distribution of this total quantity of tritium was then calculated from the injector performance and confirmed where possible by water flow calorimeter on injector components. The calculated tritium distribution was as follows:

- 87% condensed onto injector cryopanels,
- 7.7% implanted into injector components,
- 4.9% injected into torus,
- 0.5% implanted into the torus duct.

Values of implantation assumed 100% implantation of the incident tritium beam fluence.

The tritium condensed on the injector cryopanels was removed immediately after the experiment, using a previously developed and tested "fast regeneration" scenario. Helium gas at room temperature was introduced into the liquid helium circuit of the cryopanels in order to ensure that all of the condensed tritium was released and not distilled onto possible cold areas of the panels and/or associated manifolds and piping. A high capacity cool-down mode of cryopump operation was also developed and tested which would have enabled all of the gas released during a regeneration to be re-condensed onto the cryopanels should this be required.

Tritium implanted into beamline components was removed by producing beams of deuterium from the PINIs which had been operated in tritium. The depletion of implanted tritium was monitored using the neutron yield from beam-target reactions and quantified by measurements of the activity of the gas subsequently recovered from the cryopanels.

The majority of implanted tritium was recovered by operating the injectors independently of the tokamak. However, due to the effect of the stray magnetic field on the ion trajectories inside the injector, some implanted tritium was only accessible by operation of the injector in synchronism with the tokamak using the same magnetic

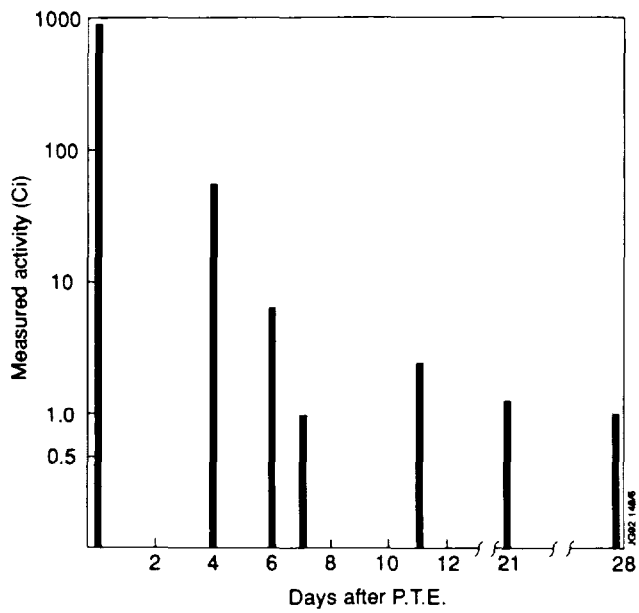

Fig.7: Measured activity of gas recovered from injector post-FTE.

configuration that had been used in the tritium tokamak experiment.

In Fig. 7 we show the measured activity of the gas recovered from the beamline at various times during the month after the FTE.

It is important to note that the amount of tritium recovered subsequent to the first regeneration of the cryopumps corresponds to the total tritium fluence that was incident onto various components inside the injector. That is, for the first tritium shots, the implantation was 100% effective.

VI. CONCLUSIONS

The first experiment using tritium NBI into the JET tokamak was an unqualified success and was executed as planned.

An essential feature of the successful production of tritium beams was the availability of the JET Neutral Beam Test Bed. This enabled not only the development of equipment to be carried out independently of tokamak operation, but, and perhaps more importantly, allowed **all** new NBI features/modifications to be extensively tested to their full operation values prior to their installation on the tokamak.

The provision of the deuterium U-bed having identical controls to that used for tritium proved invaluable in terms of giving experience and familiarity with the system prior to its use with tritium.

Finally, the experience gained during the detritiation of the injector plus the subsequent modelling of the processes involved has an important impact on future high power tritium injection.

ACKNOWLEDGMENTS

The success of the FTE is the result of the efforts of the entire JET Team. The main author wishes to acknowledge the particular contributions of A. Browne, J.F. Davies, H-D. Falter, D. Hurford, T.T.C. Jones, D. Martin, P. Massmann, W. Obert, D. Stork and L. Svensson to the work described in this paper.

REFERENCES

[1] The JET Team, "Fusion Energy Production from a Deuterium-Tritium Plasma in the JET Tokamak," *Nucl. Fusion*, vol. 32, p. 187, 1992.

[2] E. Thompson, D. Stork, H.P.L. de Esch and the JET Team, "The Use of Neutral Beam Heating to Produce High Performance Fusion Plasmas, Including the Injection of Tritium Beams into the Joint European Torus (JET)," *Phys. Fluids B*, vol. 5 (7), p. 2468, 1993.

[3] G. Duesing, H. Altmann, H. Falter, A. Goede, R. Haange, R.S. Hemsworth, P. Kupschus, D. Stork and E. Thompson, "Neutral Beam injection System, "*Fusion Technology*, vol. 11, p. 163, 1987.

[4] L. Svensson, D. Martin, A. Brown, D. Cooper, J.F. Davies, H.D. Falter, T.T.C. Jones and E. Thompson, "The Gas Introduction System used for Tritium Neutral Beam Injection into JET," *Proc. 17th Symposium in Fusion Technology, Rome, Italy*, vol. 2, pp. 1230-1234, 1992.

[5] P. Massmann, H.D. Falter, A.J. Bickley, G.H. Deschamps, D. Hurford and E. Thompson, "Modifications and Characteristics of the JET Positive Ion Neutral Injectors for the First Tritium Experiment," *ibid.*, vol. 1, pp. 574-578.

[6] H. Falter, D. Ćirić, G.H. Deschamps, H.P.L. de Esch, P. Massmann and L. Svensson, "Hydrogen Isotope Exchange in the JET Neutral Beam Injection System," *ibid.*, vol. 1, pp. 481-485.

[7] W. Obert, A. Bell, J. Davies, C. Mayaux, G. Perinić, G Saibene, R. Sartori and E. Thompson, "Regeneration and Tritium Recovery from the Large JET Neutral Injection Cryopump System after the FTE," *ibid.*, vol. 2, pp. 1191-1195.

[8] G. Saibene, R. Sartori, P. Andrew, Q. King and A.T. Peacock, "Tritium Accounting during the First Tritium Experiment at JET," *Fusion Engineering & Design*, vol. 19, pp. 133-147, 1992.

[9] D. Ćirić, A.J. Bickley, H.P.L. de Esch and H.D. Falter, "Measurements and Calculations of Isotopic Exchange between Deuterium and Tritium and their Implications to Neutral Beam Injection," these proceedings - to be published.

An Analysis of Induction Brazed Beryllium on Copper Alloy Substrates

H Altmann, E B Deksnis, C Ibbott, C Sborchia, R Tivey, R Viola.

JET Joint Undertaking, Abingdon, Oxon, OX14 3EA.

An Analysis of Induction Brazed Beryllium on Copper Alloy Substrates

H. Altmann, E.B. Deksnis, C.Ibbott, C. Sborchia, R. Tivey, R. Viola
JET Joint Undertaking, Abingdon, Oxon, England, OX14 3EA

ABSTRACT

A long pulse JET Divertor requires the production of beryllium clad copper alloy hypervapotron target plates. Vacuum brazing of beryllium poses a number of problems relating to the stable beryllium oxide and ready formation of brittle intermetallics. Induction brazing offers some advantages and a rig has been developed for producing vapotron test target plates for power load testing in the Neutral Beam Test Bed. The brazed components have survived over 1000 shots at 13 MW/m^2 with an ultimate power loading capability up to 17 MW/m^2.

These results have been interpreted with respect to both localised stresses and thermal fatigue at the interface. This study analyses the power handling capability with respect to instantaneous heat flux failure, localised hot spots from target plate deflections and high cycle fatigue with a view to establishing an optimum unit size.

INTRODUCTION

Beryllium is favoured as a First Wall material, both for its low-z characteristics and its pronounced ability for gettering oxygen. Unfortunately this affinity for oxygen, together with its readiness to form intermetallic compounds, creates special difficulties in bonding it to substrates for heat removal.

The design of the JET Divertor for long pulse operation called for a study of brazing beryllium tiles on to a copper-chromium-zirconium substrate. JET has many years experience in working with this material for the manufacture of hyper-vapotron target plates [1], especially for the ease with which it can be machined, electron-beam welded and precipitation hardened.

Standard methods of beryllium brazing are based an aluminium or copper/silver brazes [2]. Aluminium brazes have the advantage of not forming brittle intermetallic compounds with beryllium but are not compatible with copper substrates and have lower strengths than copper/silver brazes. The most commonly used braze for structural purposes is Cusiltin, also known as BAg-18, with solidus and liquidus of 602°C and 718°C respectively. Vacuum oven brazing above the liquidus leads to unacceptable thick CuBe intermetallic layers so that a standard brazing cycle consists of the brazed joint being held under medium pressure at 650°C - 680°C for 30 minutes. Initial trials with this method led to widely scattered strength results (50 - 170MPa) and power loading failures of 2mm thick tiles at 7 to 12MW/m^2.

Induction brazing offers the advantages of high heating rates and short, accurately controlled dwell times. This allows the brazed joint temperature to be raised above the liquidus while the short dwell time minimises the formation of intermetallics. An active braze Incusil ABA (containing 1.25% titanium) with solidus and liquidus of 605°C and 715°C was investigated during the vacuum oven brazing program to check for any beneficial effects from the active titanium content. It appeared to be ineffective at the sub-liquidus temperatures, but was identified as a suitable candidate for induction brazing where the titanium could getter the outgassing products from the brazed joint.

EXPERIMENTAL PROGRAM

Initial trials with a 50kHz RF generator and a solenoid coil showed both that heating rates above 6°C/second were possible and that joint strengths better than those for oven brazing were possible. Consequently a development program was established to investigate the following parameters:

- dwell time above liquidus between 10 and 300 seconds,
- different brazing materials such as

a) Cusiltin - Ag (60%) Cu (30%) Sn (10%), sol. 602°C, liq. 718°C.
b) Incusil - Ag (61.5%) Cu (24%) In (14.5%), sol. 630°C, liq. 705°C.
c) Incusil ABA - Ag (59%) Cu (27.25%) In (12.5%) Ti (1.25%), sol. 605°C, liq. 715°C.

All other parameters were to be fixed as follows:

- pressure on brazed joint at 0.3MPa,
- vacuum pressure at 5 x 10^{-5}mbar,
- temperature rise rate at 8°C/second,
- temperature cooldown rate at 4°C/second,
- braze thickness at 0.1mm and 0_2 content < 50ppm.

The program would be carried out in two stages. The optimum parameters would be established through a series of brazes between 30 x 100mm tiles of 3mm thick beryllium and 6mm thick CuCrZr. The second stage would use the optimum cycle to bond Be tiles of different thicknesses on to vapotron test targets for power load testing in the JET Neutral Injection Test Bed.

APPARATUS

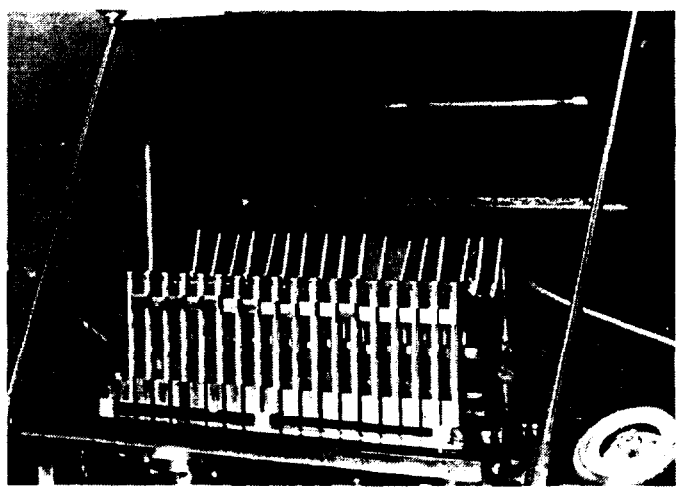

Fig.1A: Induction brazing rig.

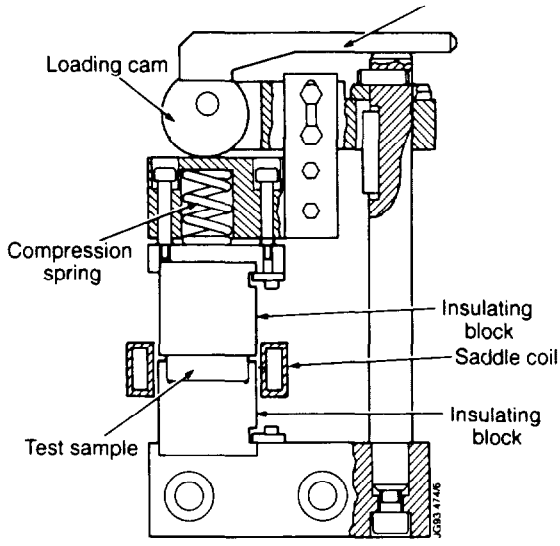

Fig.1B: Cross-section of sample loading rig.

A saddle coil design was chosen for the induction coil, both for its compatibility with the long rectangular vapotron shape and a joint clamping jig. The jig used insulating ceramic blocks to support the samples and compress the joint to 0.3MPa via lever-operated cams on to coil springs (Figure 1). A 600kW high frequency (4kHz) generator via an 18:2 matching transformer was required to achieve the heating rates. Three features were installed to achieve a rapid cooling rate, i.e. a water-cooled copper plate inside the vacuum chamber, helium backfilling to 100mbar pressure and an internal circulating fan.

Diagnostics consisted of six thermocouples, three in the beryllium tile and three in the substrate, arc-percussion welded at different depths into the sides of the tiles to monitor temperatures. The vacuum conditions were measured by a Penning gauge and RGA.

EXPERIMENTAL PROCEDURE FOR BRAZING QUALIFICATION

Each braze alloy was tested with five samples at dwell times of 10, 30, 60, 150 and 300 seconds. The standard cycle was:

a) Slow heating to 450°C.
b) Holding at 450°C for two minutes to stabilise temperatures,
c) Rapid heating (8°C/second) to 5 - 10°C above liquidus,
d) Dwell time,
e) Rapid cooling (4°C/second) down to 450°C.

A typical cycle is shown in Figure 2 where the temperature, chamber pressure and RGA were monitored throughout the cycle. The RGA scans repetitively between masses 3 and 18.

Each sample was scanned ultrasonically at 15MHz for joint defects. Thereafter they were cut-up to produce three micrographs, one from each end and centre of the specimen, plus twelve shear test specimens. Shear testing was carried out at 20°C, 250°C, 350°C and 400°C.

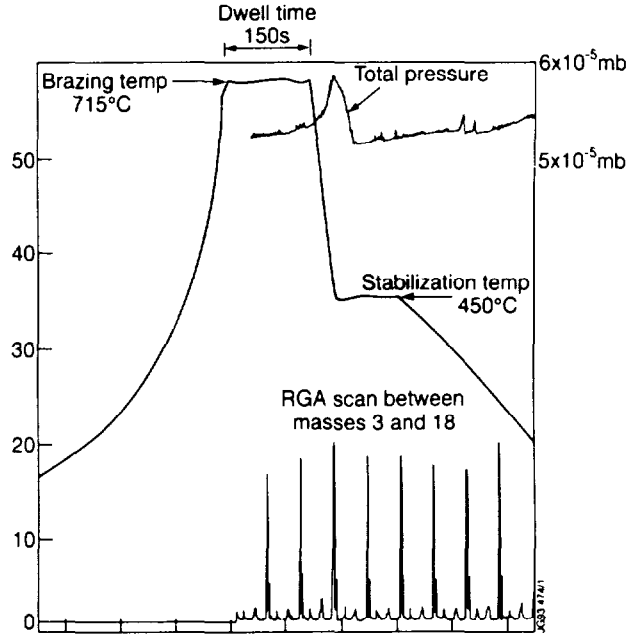

Fig.2: Measured parameters during brazing cycle

RESULTS OF BRAZING QUALIFICATION

A. *Incusil*

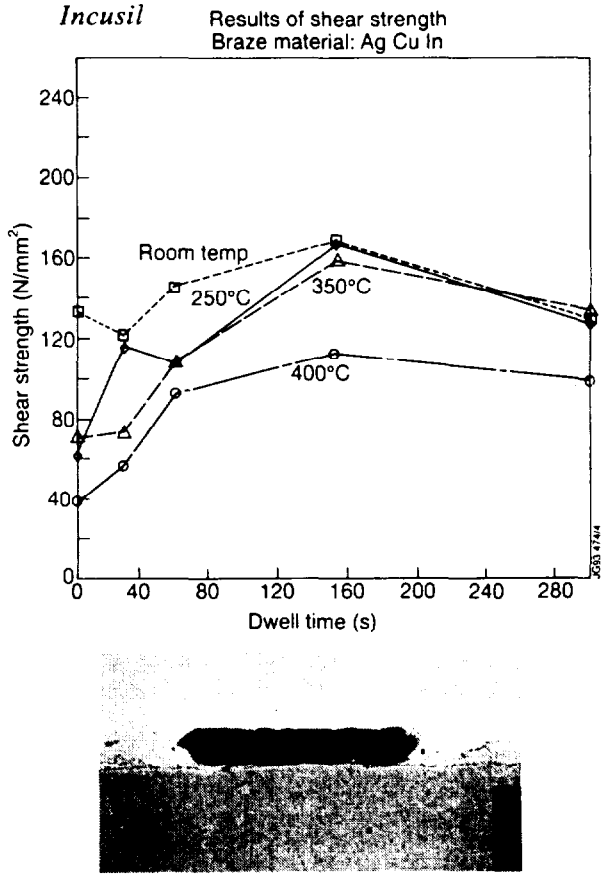

Fig.3: Micrograph and shear strength for Incusil braze.

Figure 3 shows the average shear strength versus dwell time and typical micrograph. From the shear strengths it is clear that maximum band strength is reached only after 150 seconds dwell time. All the micrographs show voids in the braze arising from the outgassing at the joint during the rapid heating phase. The average ambient shear strength is typically 150MPa but with a wide scatter, possibly arising from the voids.

B. Cusiltin

These results are similar to those for Cusiltin with average ambient shear strength of 150MPa. Both sets of samples had globules of braze along the edges of the joint, consistent with sputtering from gas bubbles in the liquid braze.

C. Incusil ABA

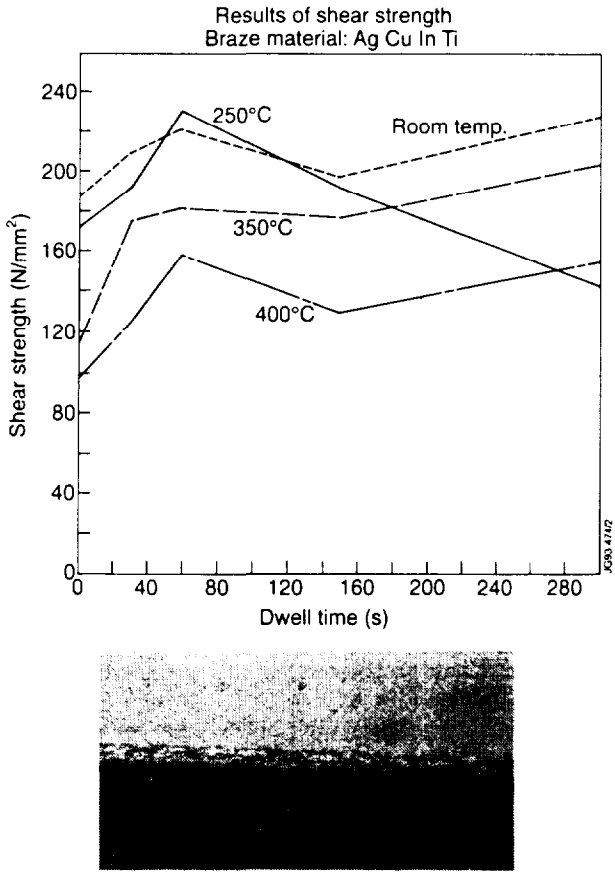

Fig.4: Micrograph and shear strength for Incusil ABA.

The results in Figure 4 show the superior performance of this braze with the average strength of 220MPa at ambient occurring after 60 seconds dwell time. The micrographs show no sign of voids and less wide scatter in shear strength. The active titanium was considered to be gettering the desorbed gas. A further five specimens were brazed at 60 seconds dwell to check for repeatibility. The shear strengths remained within a band of ± 10% as shown in figure 5.

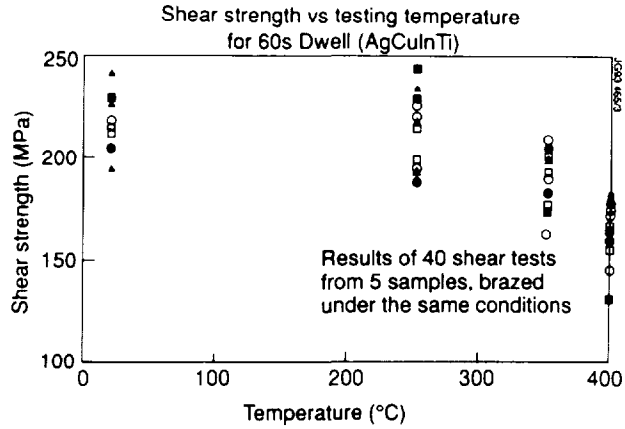

Fig.5: Repeatibility of shear strength for Incusil ABA.

POWER DENSITY TRIALS

The Incusil ABA at a dwell time of 60 seconds was identified as the optimum cycle. The brazing rig was modified to accept 500mm long vapotron test targets. Four sets of Beryllium tiles of thickness 1.5mm, 2mm (two off) and 3mm were prepared with castellated surfaces to relieve the thermal stresses under high power loading. The castellations were machined with 0.5mm wide slits down to a remaining thickness of 0.5mm in a 6mm square matrix (Fig. 6). A production proof sample was included in each brazing run.

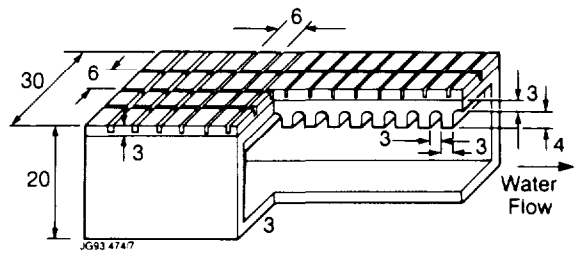

Fig.6: Sectioned Vapotron with beryllium tiles brazed to top surface.

The test program covered two phases. The first phase was chosen to determine the maximum power density to failure of each Be thickness, i.e. 1.5mm, 2mm, 3mm. The second phase was intended to check for durability by subjecting the 2mm thick Be tiles to 75% of the maximum power density for 1000 pulses. Reference [3] gives details of the Neutral Injection Test Bed facility. A dedicated beryllium test rig is used with a modified Positive Ion Neutral Injector to provide a power loading up to 50MW/m^2. Diagnostics consist of an inertial calorimeter to calibrate the beam power, an infrared camera to monitor the beryllium surface temperature and thermocouples to measure the substrate temperature.

MAXIMUM POWER DENSITY TEST

The procedure for this test was to increase the power level in small steps up to the maximum expected level, delivering 250 pulses of one second duration followed by one second off time

at each level. The tests were stopped when melting of individual castellations as shown by the IR camera started to follow in rapid succession .

The different tile thickness performed as follows:

a) 1.5mm
The first failure occurred at a power density of 14.5MW/m^2 with the next two failures within a few cycles of each other at 18 - 20MW/m^2.

b) 2.0mm
The first failure took place soon after the start of the test at 12.5MW/m^2 with the second and third failures at 17MW/m^2.

c) 3.0mm
A number of failures occurred in rapid succession at 14 - 15MW/m^2.

The initial failures in the 1.5 and 2.0mm tiles were formed on central castellations but the later defects occurred at the tile edges where the stresses are the highest. This suggests that individual castellations can melt prematurely from a local low quality brazed area but that eventual failure at the tile edge represents the overall bond strength.

FATIGUE TEST

This was carried out on the second test target with 2mm tiles at a power density of 13.5MW/m^2 compared to the maximum of 17MW/m^2 from the previous tests. The load was applied for 1000 cycles at pulse lengths from one to five seconds. No beryllium melting occurred although the IR camera did indicate high surface temperatures in a relatively low power density region.

FURTHER STUDIES

The program to carry this study further will investigate:

- the effect of a thin, ductile OFHC layer between the beryllium and copper alloy substrate,
- the optimum % of titanium in the brazing fail,
- the relevance and desirability of tile castellations,
- ion plating of the beryllium surface with different materials before brazing.

ELASTO-PLASTIC ANALYSIS OF SANDWICH STRUCTURES

The thermo-mechanical analysis of bi-metallic structures can be done analytically only for materials with temperature independent properties. The properties of both beryllium and copper show strong temperature dependence, in particular the beryllium - part of the sandwich structure would be brittle at room temperature but ductile at elected temperatures. Finite-element analysis is mandatory to assess the response of a clad structure to both thermal shock, e.g. disruptions and differential thermal expansion under steady-state loading.

A model of a vapotron with both 2 and 3mm beryllium tiles has been analysed with ABAQUS [4, 5]. It has been found that, under JET relevant conditions, there is no plastic deformation in the beryllium layers for disruptive - type loading (duration <1ms) that may vaporize part of the plasma-facing layer. No substantial loads are exerted on the beryllium-copper interface as a result.

Steady-state heat fluxes of 5 - 15MW/m^2 have been analyzed with the finite element results predicting beryllium surface temperature of 300-750°C in a 2mm thick layer. Plastic strain in the beryllium appears for fluxes approaching 7MW/m^2 with a maximum value of 0.17% at 15MW/m^2. Plasticity is found in approximately 1/3 of the beryllium thickness over almost 90% of a typical vapotron width (30 - 50mm). If the beryllium is machined right through to the substrate in a 6 x 6mm matrix, no plasticity is to be found in the beryllium for fluxes up to 15MW/m^2.

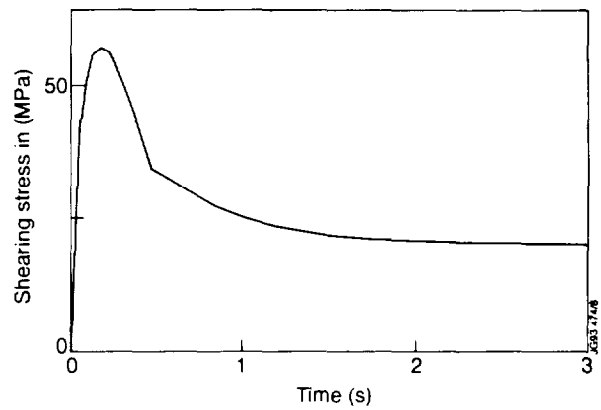

Fig.7: Computed shearing force on Cu-Be interface.

Fig.7 indicates that the stress reaches a maximum near the beginning of the pulse and later falls to a steady value. Melting of the beryllium castellations at the start of the pulse supports this analysis.

The singular stress condition at the free edge of a bi-metallic strip implies that residual micro-cracks are present in any brazed component. A non-linear code such as ABAQUS is however not capable of resolving this singularity since the range of the initial crack is only 10^{-5} - 10^{-6}mm for a copper-beryllium joint [6]. The results of the FEA for delamination loading from thermal cycling indicate that the joint shearing force on a beryllium-clad vapotron is greater for a full width uncastellated tile than for 6 x 6mm castellated tile. This has not, however, been supported by the experimental results.

REFERENCES

[1] R. Tivey, et al., "Testing of beam stopping elements using hypervapotron cooling". Proc. SOFE, Monteray (1987).

[2] D.R. Floyd and J.N. Lowe, "Beryllium Science and Technology" volume 2, 1979, Plenum Press, New York, pp 252-273.

[3] H.D. Falter, et al., "Thermal test results of the JET Divertor Plates", SPIE Vol. 1739, High Heat Flux Engineering (1992), pp 162-172.

[4] ABAQUS Users manual, Hibbit, Karlson and Svenson Inc.

[5] E. Deksnis et al., "Design of High Heat Flux Components for the JET Pumped Divertors", 16th SOFT, London 1990, pp478

[6] R. Viola, "Singular Stress Fields in Beryllium Copper Components, JET paper to be published.

Analysis and Specification of the Performances of the new JET Amplifier for the Vertical Stabilisation

T Bonicelli, M Garribba, P L Mondino[1], P Noll.

JET Joint Undertaking, Abingdon, Oxon, OX14 3EA.
[1] Present address: ITER–EDA, Naka Joint Work site, Mukouyama, Naka-machi, Naka-gun, Ibaraki-ken, Japan.

Analysis and Specification of the Performances of the new JET Amplifier for the Vertical Stabilisation

T Bonicelli, M Garribba, PL Mondino#, P Noll
JET Joint Undertaking
Abingdon, Oxfordshire, OX14 3EA, United Kingdom

#Present address: ITER EDA, Naka Joint Work Site
801-1, Mukouyama, Naka-machi, Naka-gun, Ibaraki-ken, 311-01 Japan

ABSTRACT

A new 25 MW power amplifier based on GTO inverters has been procured to cope with configurations of the JET plasma characterised by high growth rates of the vertical instability. The analysis of the future JET configurations, including a new set of four divertor field coils, resulted in the specification of the required performances of the amplifier and led to the choice of the technical solution. The new amplifier has now been fully commissioned on dummy load at the JET site.

INTRODUCTION

The vertical position of the JET plasma is unstable due to the destabilising effect of the iron magnetic circuit and of the quadrupolar component of the equilibrium magnetic field which is needed to obtain an elongated cross-section.

Active stabilisation by means of feedback techniques is therefore necessary.

An analysis of the stabilisation system based on simplified assumptions for the load and on a linear model for the amplifier shows that the response time of the amplifier must be smaller than the inverse of the "open loop" growth rate of the vertical instability [1].

Until the end of the last experimental period (February 1992), the vertical position was stabilised by controlling the current in the radial field coils with a 12-pulse line-frequency phase controlled thyristor converter (PRFA) rated for 12 MW [2].

The speed of response of the PRFA to a large amplitude variation of the reference signal is basically dependant upon the frequency of the supply voltage. The transition between maximum and minimum value of the output voltage is therefore accomplished (with a 50 Hz system and taking into account some limitations on the possible excursion of the firing angle) in ca 8 ms.

The response time to a small amplitude variation of the reference signal (up to approximately 20% of the full value) is also dependant upon the number of pulses of the converter and, for the PRFA, it is about 2 ms.

The original design of the stabilisation system was based on a limiter D-shaped plasma with an elongation ratio of 1.65.

The PRFA allowed actually even more demanding single and double-null configurations and quiescent plasmas with elongation ratios of up to ca 1.9 with growth rates of up to ca 300 s^{-1} to be controlled.

NEED FOR IMPROVED STABILISATION

The stabilisation system showed some shortcomings when it was attempted to move the X-point at a distance of about 10 cm from the wall. The control of the vertical position following plasma disruptions was also impaired in some conditions by the too long response time and the insufficient peak power of the amplifier.

Vertical instabilities can produce large forces on the JET vacuum vessel (up to 8 MN can be expected) and therefore the occurrence of such events must be limited to the maximum possible extent. This has become a more severe problem with Beryllium limiters since the plasma current I_p is sustained in cleaner plasmas during the vertical displacements z_p and the resulting forces (approximately proportional to $I_p^{2} * z_p$) become larger.

Of 317 disruptions at currents above 2.7 MA during Beryllium operation (until Oct.'90), 59 resulted in a vertical force exceeding 500 kN on the vessel supports[3].

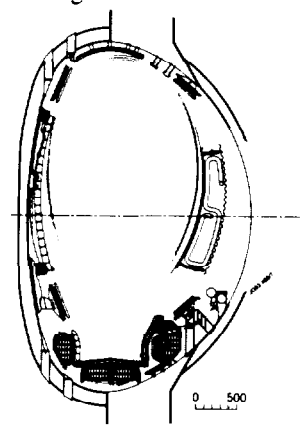

Fig. 1 Flux plot for "slim" plasma.

The need for an improved vertical position stabilisation system became even more indisputable when the analysis of the future JET divertor configurations

resulted in expected growth rates of up to 800 s^{-1} (Fig. 1) [4], far beyond the capability of the PRFA.

The analysis of the possible improvements [5] resulted in the decision to procure a new Fast Radial Field Amplifier (FRFA) and to completely re-design the plasma position and current control system to cope with the more complex magnetic configurations [6].

DEFINITION OF THE PERFORMANCES

Two fundamental aspects of the control of the plasma vertical position were considered:

- the stabilisation of quiescent plasmas
- the response to large perturbations.

A. Stabilisation of quiescent plasmas

The performance of the amplifier in stabilising quiescent plasmas (or, in other words, its small signal behaviour) is intrinsically determined by its speed. Under this point of view, the power of the amplifier is unimportant.

A linear simplified analysis of the stabilisation system demonstrated that, in order to stabilise plasma with growth rates of the vertical instability of 800 s^{-1}, an amplifier with response time of less than .5 ms was required (allowing for some safety margin). In fact, Class A linear amplifiers in the range of tens of megawatts are not a practicable solution on the ground of cost and poor efficiency.

High power amplifiers faster than the naturally line-commutated thyristor converters can be obtained by making use of switch-mode inverters supplied from a DC voltage power supply. The output voltage for this sort of amplifier can assume only discrete levels and the input/output characteristic of the amplifier is therefore inherently non-linear.

A switch-mode amplifier can be regarded, in its most basic form, as a bistable voltage source. The corresponding input/output characteristic can be of the type shown in Fig. 2a where an hysteretic control has been chosen: every time the control voltage "e " becomes larger than +H or smaller than -H an output voltage transition occurs, ideally, instantaneously.

More complex control characteristics can of course be adopted like the one shown in Fig. 2b which includes the zero output voltage level.

The study of the stability of the system was carried out by adopting a simplified linear model of the load which is described by a set of equations representing the coupling between the radial field coils, the vessel and the plasma current vertical displacement [7]. The amplifier was instead modelled as an ideal voltage source with the input/output characteristic shown in Fig. 2a. The block diagram of the system is shown in Fig. 3 where G(s) is the transfer function of the load.

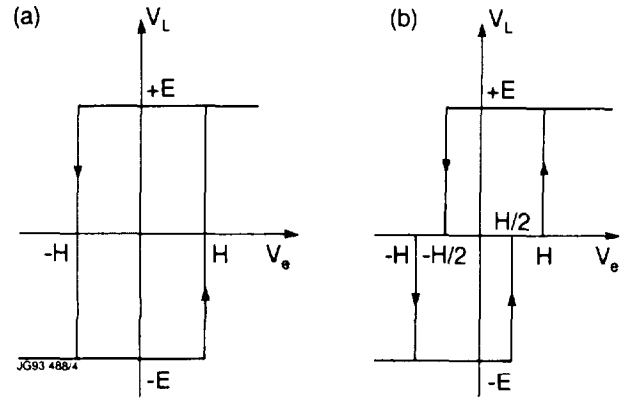

Fig. 2 Ideal Control characteristic
a) two-level hysterisis b) three-level hysteresis

A simple unity feedback speed control was adopted even though, in order to define the plasma position, a "weak" position control is added in practice.

Although the model presents some limitations and inaccuracies (for instance it does not take into account the JET mechanical shell and the double layer structure of the vessel walls), its application allows a good qualitative analysis to be carried out and some general guidelines for the specification of the amplifier to be drawn.

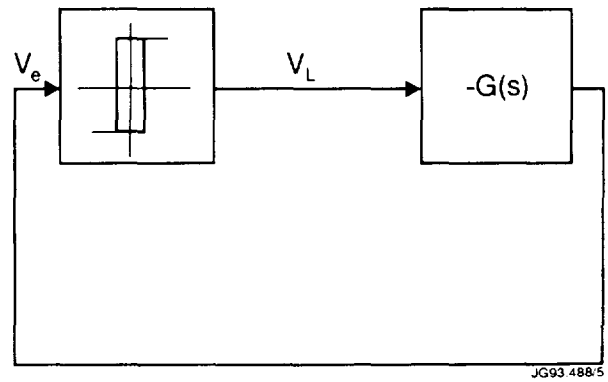

Fig. 3 Block diagram of the system

The system can be solved analytically; the plasma vertical speed settles on a stable limit cycle and oscillates between +H and -H at a frequency (disregarding the resistance of the radial field coils):

$$f = \frac{\gamma}{2}\left(\ln \frac{\frac{aE}{\gamma} + H}{\frac{aE}{\gamma} - H} \right)^{-1} \quad \text{(Hz)}$$

where : γ = growth rate of the vertical instability (s^{-1})
E = voltage per turn on the coils (V)
H = half-width of the hysterisis band (m/s)
a = parameter from the load model (m/Vs^2) including plasma current magnitude

Smaller H give higher frequencies of the limit cycle and "closer" control around zero of the vertical speed.

As H approaches the value of aE/γ (ie for "looser" control of the speed), the frequency of the limit cycle

decreases; if H exceeds that value, no stable limit cycle can be found. In principle, a stable limit cycle could therefore be reached even at a very low frequency. In practice, the region where H gets close to the limit aE/γ is not accessible since any small variation of the parameters of the system (or any inaccuracy of the model) would lead to the loss of control of the vertical position.

A more realistic limit for the minimum frequency is obtained from the "describing function" method: a stable limit cycle can be established, for the same system described in Fig. 3, only at frequencies above:

$$f_{min} = \frac{\gamma}{2\pi} \quad (Hz)$$

It is sensible that, in a practical stabilisation system, the normal working point is chosen with a good safety factor (eg 5 or 6) far from the limit also to make up for the non-idealities of the power amplifier (eg delays) and for the small disturbances always present in the plasma.

An amplifier capable of operating at frequencies in excess of at least 1 kHz was therefore deemed to be required for the new stabilisation system.

B. Response to large perturbations

Large perturbations in the plasma (for instance sudden changes in the input power) or disruptions may generate vertical instabilities [8].

If the perturbation of the vertical position is represented as a vertical force $F_z = F_{z0}\, e^{-\beta t}$, it can be shown that the capability of the stabilisation system to recover from large perturbations strongly depends upon the peak power and the amplifier delay time.

The estimated approximate scaling is [9]:

$$F_{z_{max}} \propto I_p \sqrt{P_{amp}}\, e^{-\gamma t_d}\, \frac{1+\frac{\beta}{\gamma}}{\sqrt{\gamma T_v}\,(1+\gamma T_v)}$$

where : P_{amp} = power of the amplifier
t_d = amplifier (dead) delay time
T_v = vessel time constant
I_p = plasma current

In practice, the power of the amplifier is limited by cost constraints while the delay time strongly depends upon the switching device on which the inverter is based.

At the time when the contract for the FRFA system was placed, Gate Turn Off Thyristors (GTO's) with repetitive off-state voltage (V_{DRM}) of 4500 V and peak turn-off current (I_{TGQM}) of 3000 A were available giving a power handling capability 30-40 times higher than the one of the largest Insulated Gate Bipolar Transistor (IGBT). On the other hand, the typical delay time for large GTOs is of the order of 100 μs and, though longer than the one for IGBT's (typical delays: 5-10 μs), is acceptable for the JET application.

A rated peak power for the system of 25 MVA satisfied the budgetary limits.

The maximum force F_z, normalised to the plasma current, which can be successfully counteracted is given in Fig. 4 in function of the growth rate γ for $\beta=0$ (step force) and for $\beta=100\ s^{-1}$ both for the old PRFA and the new FRFA.

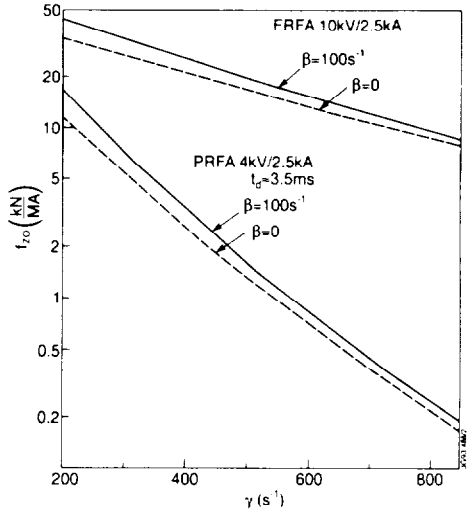

Fig. 4 Maximum vertical force permitting recovery

For growth rates of ca 300 s^{-1} (i.e. at the limit of the PRFA range of stabilisation) , the new amplifier would be capable to counteract forces up to 150 kN (for a 5 MA plasma), five times larger than the old one would do.

For a given peak power of the amplifier, an "optimal" voltage/current rating can be found in dependence of the growth rate γ and of the number of turns N of the radial field coils. For $\gamma=800\ s^{-1}$ and N=72 (number of turns of the JET coils) , the optimal rating for a 25 MVA amplifier is V=10 kV, I = 2.5 kA.

In fact, the analysis of vertical instabilities in JET shows that the apparent force perturbing the plasma vertical position could be in excess of the one which can be stabilised by the new FRFA especially in case of disruptions characterised by sudden changes of β_p or abrupt readjustements of the current profile . The vessel structure and the in-vessel components must therefore be able to withstand occasional severe vertical instabilities though it is expected that the new FRFA will help in reducing the number of such events .

Table I
Basic Performances of the FRFA system

	Config A	Config. B
Nominal Duty Cycle	30 s / 600 s	
Nominal output voltage	± 5000 V	± 10000 V
Base output current (29 s)	± 1000 A	± 500 A
Short-time output current (1 s)	± 5000 A	± 2500 A
Output switching frequency at the base current	2.5 kHz (2500 V step)	2.5 kHz (5000 V step)
Output switching frequency at the short-time current	1 kHz	
Maximum response delay time	200 μs	

SPECIFICATION OF THE PERFORMANCES

The basic performances of the system are summarised in Table I.

The system is composed of four identical subunits (each capable of delivering 2500 A/2500 V) which can be connected in two configurations [10]. For example, Configuration B, which should provide the best performances in recovering from large perturbations, is achieved by series connecting the four subunits. Five output voltage levels are available in Config. A and nine levels in Config. B.

It is expected that the FRFA is required to deliver its full power only for short time during a pulse (i.e. when large perturbations are present) while the power requirements during the quiescent periods are much reduced (20 % of the peak power was considered an adequate design value). This approach leads to a more economical design.

The nominal pulse was defined as shown in Fig. 5.

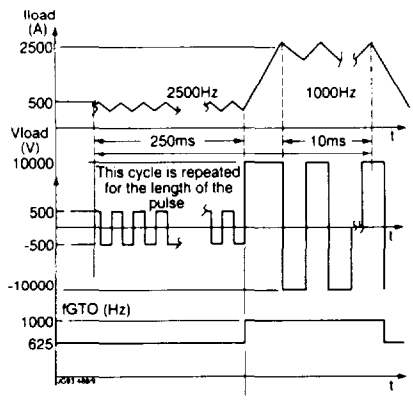

Fig. 5 Nominal pulse

The switching frequency of each GTO is limited by the thermal dissipation. Large GTO's have relatively high turn-on and turn-off losses which result in switching frequency of 200 - 300 Hz in industrial applications.

The specified output voltage switching frequency (see Table I) of the FRFA system is achieved by switching each GTO at 625 Hz during the base current periods and by switching the series connected subunits on a rota basis.

The operation of GTO's requires the respect of some interlock times to allow for the non-ideal characteristics of the devices. The response time to a voltage request will not exceed 200 μs in the worst situation.

Vertical instabilities can induce high currents in the radial field coils. The FRFA system was designed to cope with induced overcurrent of up to 20 kA which are diverted from the GTO inverters by triggering thyristor crowbars installed at the output of each subunit.

CONCLUSIONS

The FRFA system has now been installed at the JET site and commissioned with execution of power tests up to the rated performances on a 25 mH dummy load.

The final series of tests on the radial field coils and the integration with the new plasma position control system will take place at the end of the present shut-down of the JET machine at the beginning of 1994.

The new power amplifier will improve the ability to control vertical instabilities. It is expected that the highly unstable plasmas of the new JET divertor configuration can be stabilised and that recovery from minor disruptions and other perturbations is possible. Though occasional losses of the vertical position control as observed previously during major disruptions cannot be ruled out, it is believed that the number of such events will be reduced and fatigue effects on the vessel components will be lessened.

REFERENCES

[1] P Noll, M Browne, M Huart, I Piacentini, A Santagiustina, JR Watkins "The JET Plasma Position and Current Control System", Proc. 13th SOFT, pp. 503-509, 1984

[2] D Chiron, T Bonicelli, M Huart, M Garribba, PL Mondino, P Noll "Power Supplies for the stabilisation of plasma vertical position: recent upgrades and future development", Proc. 14th SOFE, pp. 513-516, 1991

[3] G Sannazzaro "Vacuum Vessel Displacement and Vertical Force before and after Dampers installation", Internal Report, Oct '90.

[4] J Last, P Barabaschi, E Bertolini, M Garribba, M Huguet, P Noll, PH Rebut, C Sborchia "The JET divertor magnetic configuration and coil design", Proc. 16th SOFT, pp. 1614-1618, 1990

[5] P Noll, internal report, EUR. FU90/JET-SC41/7

[6] M Garribba, R Litunovski, P Noll, S Puppin "The new control scheme for the JET plasma position and current control system" to be presented at 15th SOFE, 1993

[7] E Bertolini, PL Mondino, P Noll "The JET magnet power supplies and plasma control system", Fusion Technology, Vol. 11, No 1, pp. 71-119, 1987

[8] P Noll, T Bonicelli, M Garribba "Vertical instabilities in JET", Proc. 17th EPS, pp. 419-422 , 1990

[9] P Noll, Private communication

[10] PL Mondino, T Bonicelli, D Hrabal, R Klein, V Marchese, R Öström, HP Timmert "The new Fast Radial Field Amplifier for the control of the plasma vertical position in JET", Proc. 17th SOFT, pp. 907-911 , 1992

High Power RF Testing of the JET 'A2' FWCD Antennae

T Brown, V Bhatnagar, C Gormezano, J Jacquinot,
A Kaye, T Wade.

JET Joint Undertaking, Abingdon, Oxon, OX14 3EA.

HIGH POWER RF TESTING OF THE JET 'A2' FWCD ANTENNAE.

T. Brown, V Bhatnagar, C Gormezano, J Jacquinot, A Kaye, T Wade
JET Joint Undertaking, Abingdon, Oxfordshire, OX14 3EA

ABSTRACT

This paper describes the antenna assemblies, test bed and techniques used during the RF testing of the JET A2 antenna. The culmination of the programme was the successful testing of a prototype antenna to full performance.

INTRODUCTION

When JET operations resume in 1994 in the new pumped divertor configuration, eight new A2 antennae will have been installed. The antennae are grouped into four arrays to optimise FWCD as illustrated in Fig. 1. They are anticipated to couple a total of up to 24MW to the plasma for 20 seconds over the range of frequencies 23 - 57MHz.

Extensive RF testing has taken place throughout the antenna design and development to ensure routine operation above 30KV. This involved the commissioning of an enlarged RF test bed at JET to allow a full size prototype antenna to be tested.

THE A2 ANTENNA

The constraints imposed on the mechanical design by the new divertor configuration led to several design features which have had to be rigorously proven [1][2]:

- A nickel plated low heat capacity structure.
- Passive radiative cooling.
- Ceramic resistors in the faraday screen.
- Ceramic support within the antenna.
- Vacuum Transmission Line (VTL) pumped solely from the torus.
- One conductor fed via a 'crossover strip' as illustrated in Fig. 2.

THE RF TEST ASSEMBLIES

Various test assemblies have been utilised during the RF test programme:

'Flat Bed' low power model

This model was manufactured towards the start of the design process from aluminium with a greatly simplified geometry, no screen resistors and bolted construction to allow rapid adjustment of current strap size and shape. It enabled the current strap geometries to be optimised giving an equal split of current between the upper and lower current strap loops at resonance, together with characterisation of the 'crossover strip'. A four strap version of this model is presently at ORNL for design studies [3].

'Short Assembly' high power model

This model was manufactured at the end of the design process with identical design details to a full antenna. However, due to size constraints of the original test bed it comprised a single conductor loop only, representing the upper VTL-side quadrant of a full antenna. It could be configured either with a short circuit terminated current strap, or an open circuit strap. It allowed early high power RF testing of the A2 construction details, especially the ceramic support and resistors.

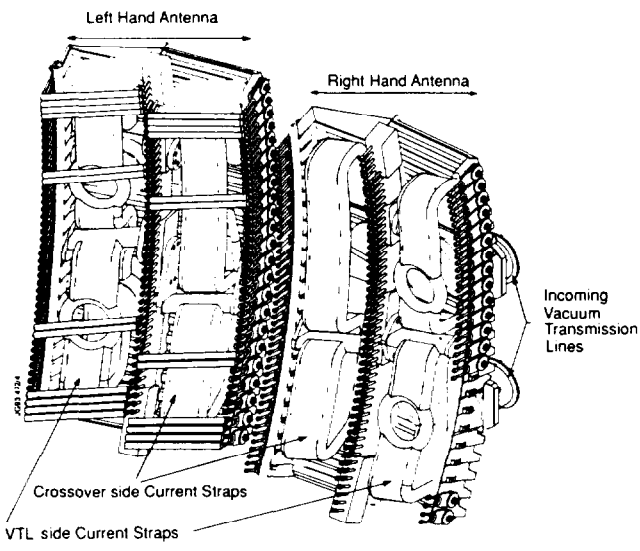

Fig. 1: A2 antenna array

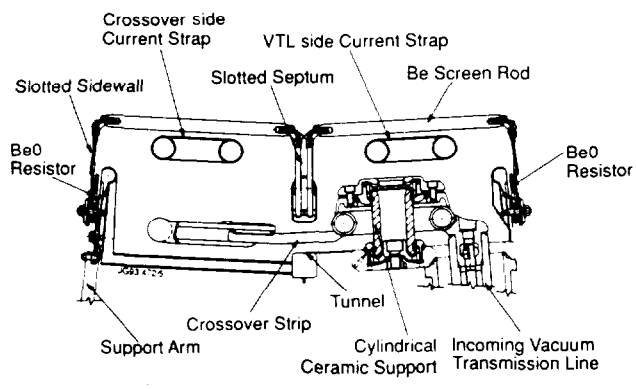

Fig. 2: Section through antenna

'Prototype antenna'

This was the first A2 antenna manufactured and was tested in a new enlarged RF test bed at JET. It was equipped with the full torus-style mechanical support structures, but with nickel plated aluminium screen rods and alumina resistors instead of the Beryllium and Beryllia torus components for ease of inspection and mechanical modifications during testing. It offered the first opportunity for high power RF testing of a complete antenna including the crossover strip geometry.

THE JET RF TEST BED

The operating parameters of the upgraded test bed are given in Table I, and the associated RF system outlined in Fig. 3. An earlier publication gives more details on the RF power systems at JET [4].

Table I: Specification of the RF test bed at JET

Max antenna size:	Ø2.1m by 1.4m deep
Base pressure:	$<5.10^{-7}$mbar (2,200 litre/sec turbo)
Temperature range:	20 - 450°C
Generator power:	2.5MW
Voltage limit:	55KV for 50msec pulses 50KV for 20sec pulses
Frequency range:	23 - 57MHz
Max. duty cycle:	30:1
Transmission lines:	30Ω, 9" lines with 3bar air
Diagnostics	
Up to 30 recorded thermocouples mounted on antenna.	
Residual Gas Analysis.	
Infra Red camera.	
Reflected power & vacuum pressure RF tripping.	
Mutiple Penning & Ion gauges.	

TEST PROCEDURE

A typical sequence of events during testing was:

- Set both transmission line branch lengths so T split is located at a high impedance point to maximise coupling.
- Set U length in one branch to give required phasing between current straps (i.e. monopole or dipole).
- Pump test vessel down to $<5.10^{-7}$mbar.
- Bake out up to 400°C, then reduce to 300°C.
- Multipactor condition over typically 4 hours.
- Adjust phase shifter in second branch to equalise voltage and phase between branches.
- Short pulse condition up to 55KV.
- Long pulse test up to 50KV.
- Repeat above sequence for all required test frequencies.

TEST RESULTS

The culmination of the test programme was the successful testing of the prototype antenna up to the limits of the pressurised transmission lines. It was subjected to a series of 50KV pulses of 20 sec duration at 30:1 duty cycle. This was successfully achieved at 35MHz with both monopole and dipole phasing between current straps. At other frequencies the coupling from the main transmission line into the separate branches limited the maximum voltage available at the antenna. Throughout the frequency range 23 - 55MHz, 20 sec duration pulses at 30:1 duty cycle were successfully run with monopole phasing at the maximum available voltage of 30 - 40KV.

The observations made during the RF test programme that led to design changes are detailed in Table II.

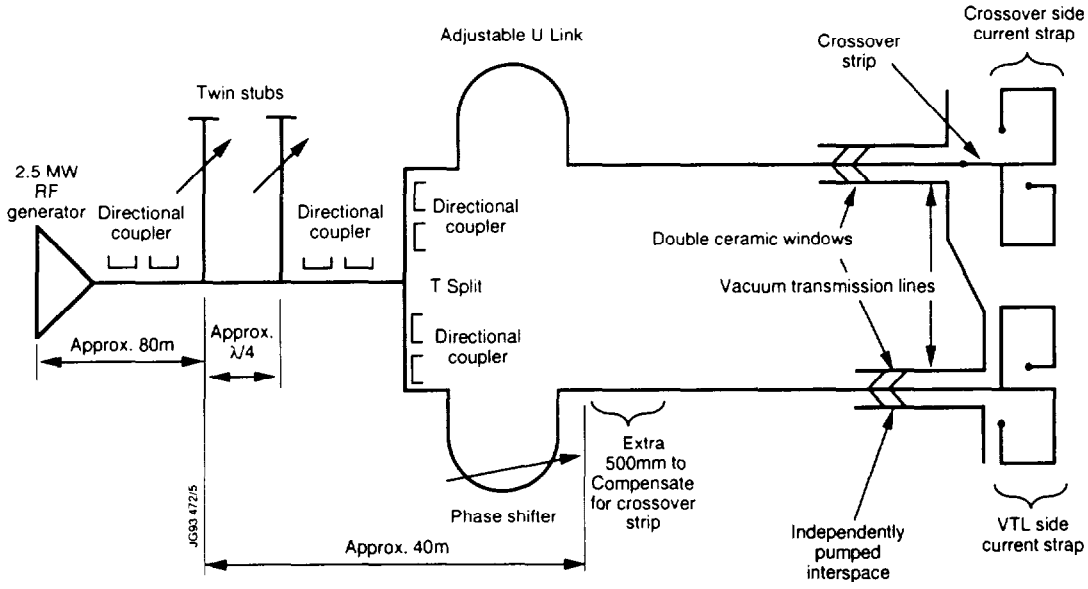

Fig 3: Schematic of the RF test bed at JET

Table II: Critical areas revealed during RF Testing.

Test Bed Observation	Enhancement made to torus antennae.
RF induced currents in the resistors can be up to twice the 35 amps rms calculated and measured at low power on the flat bed model. Displaced screen rods can also increase the current in their neighbours.	The Alumina substrate of the screen resistors was changed to Beryllia with a 30% increase in RF current capability.
The open side wall structure allows a significant flux to link around the rear of the antenna (up to 5% in the test bed). Induced currents in the support arms to the torus produced arcing in insulated joints.	Capacitively coupled earth straps were installed. The outside of the transmission lines were also shorted to the torus wall.
Arcing was observed between the crossover strip and housing at the tunnel (see Fig.2).	The crossover strip design was altered to reduce the max estimated electric field to less than 4KV/mm perpendicular to the magnetic field.
Tracking was observed on the inside of the cylindrical current strap support ceramic (see Fig.2).	The metallisation pattern on the ceramic surface was modified to reduce the field concentration at the edge of the metallisation.
Some spring energised RF joints between the housing and the current straps displayed excessive heating & arcing.	Successful operation of the seals was achieved with close dimensional control and inspection.

The more general observations made were:

- The current strap geometry defined on the flat bed model led to an approximately equal split in current between the upper and lower loops of the current straps at high power across the frequency range.
- The measured $\lambda/4$ resonances of the current strap loops for all the test assemblies occurred in the range 38 - 42MHz.
- Despite the absence of a magnetic field during testing of the prototype antenna, arcing between the strap and screen rods did not limit performance. However with the open circuit configuration possible in the Short Assembly the electric field in this region approached 5 KV/mm and arcing was observed. The design criteria used for A2 was a maximum of 4KV perpendicular to and 2KV parallel to the magnetic field.
- The maximum temperature rise observed during RF pulses was typically 100°C, occurring on the front faces of the housing side wall and septum where the magnetic flux compression is high. The lateral regions of the current straps exhibited similar temperature rises, dropping to typically half this in their central regions. All temperature rises were within design limits.
- The passive radiative cooling allowed a duty cycle of up to 20:1 at full power in the test bed. The limit was excessive heating of the current straps near their short circuit connections. JET operates at a maximum duty cycle of 60:1.
- The conductance of the Vacuum Transmission Lines, estimated to be 100litre/sec at the double ceramic windows (see Fig 3), was sufficient to ensure reliable operation in the test bed after RF conditioning, with no additional pumping.

THE CERAMIC RESISTORS

These resistors are connected in series with pairs of screen rods (as illustrated in Fig.4) to reduce disruption currents to manageable levels [1]. During operation, capacitive coupling between the current strap and the screen results in a current of typically 40A rms through each resistor. The tilting of the screen rods leads to inductive currents of similar magnitude. These currents add to give a maximum current towards the centre of the current strap loops of typically 70A rms at 50KV.

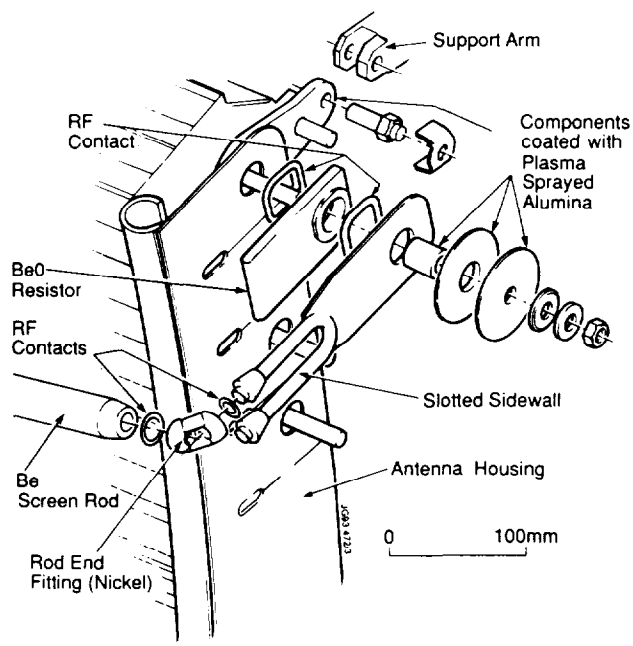

Fig 4: Exploded view of resistor assembly

Table III: Testing of screen resistors

Type of Test	Performance of torus parts	Required performance
RF Test Bed		
Up to 4 resistors form a short circuit in a 30Ω line, operating under vacuum at 300 - 600°C.	110A rms for 20sec pulses. (Temperature rise per pulse of typically 350°C)	70A rms for 20sec pulses.
Disruption Test Bed		
Modified lightning strike test facility subjects resistors to quasi sine-wave pulses.	1600A peak during sine-wave pulses of 13msec total duration. (1.7KJoule total deposited energy)	340A peak with a total deposited energy of 100Joules.

The resistors consist of a BeO substrate with approximately 6microns of electrolytic nickel plated on to a Molybdenum Manganese refractory metallisation of similar thickness, giving a resistance of 150mΩ at 300°C. After the Short Assembly tests indicated that the resistors were a critical item a development programme was initiated. A series of resistors was tested with regard to their performance during RF pulses and disruptions, as detailed in Table III. With changes in substrate and metallisation geometry, their performance in both tests was considerably improved as illustrated in Fig 5.

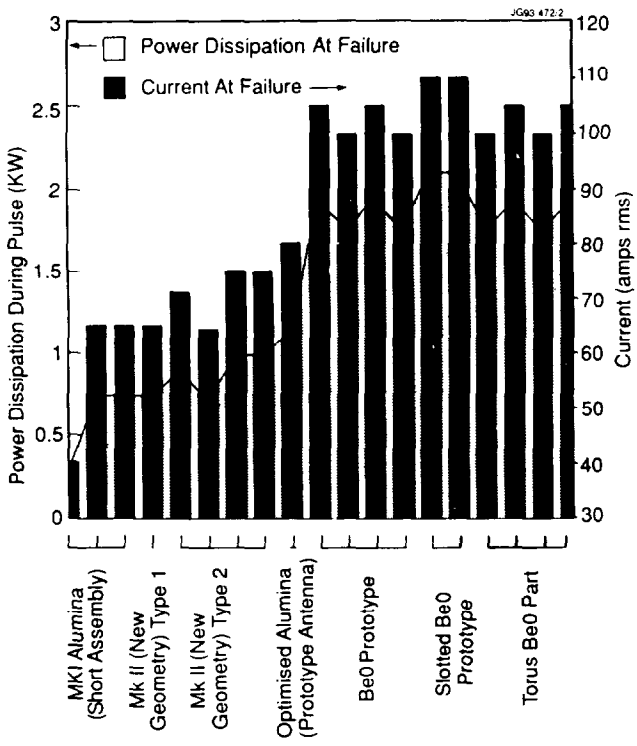

Fig 5: Development of the screen resistors

CONCLUSION

Reliable test bed operation of a prototype A2 antenna over a total of more than 350 pulses of 20sec duration has been demonstrated at:

- 50KV at 35MHz with repetitive 20 sec pulses at 30:1 duty cycle (monopole and dipole phasing).
- 30 - 40KV throughout the range 23-55MHz with repetitive 20 sec pulses at 30:1 duty cycle (monopole phasing). Voltage limited only by coupling into the transmission line branches.

The maximum permissible electric field specified in the A2 design brief of 2KV/mm *parallel to the magnetic field* appears to have been appropriate.

REFERENCES

[1] R Lobel, V Bhatnagar, J Jacquinot, A Kaye, H Panissie, P-H Rebut, "ICRF antenna for the JET pumped divertor configuration," 16th Symposium on Fusion Technology, London, 1990, Vol. 1, p73-78.

[2] A Kaye et al, "Present and Future JET ICRF Antennae," Fusion Engineering and Design, in press.

[3] P M Ryan, R H Goulding, V Bhatnagar, A Kaye, T Wade, "Electrical Characterisation of the JET A2 Antenna: Comparison of Model with Measurement, " Tenth Topical Conference on Radio Frequency Power in Plasmas", Boston, April 1993.

[4] T Wade et al, "Development of the JET ICRF Plant", Fusion Engineering and Design, in press.

Measurements and Calculations of Isotopic Exchange between Deuterium and Tritium and Their Implications to Neutral Beam Injection

D Ciric, A J Bickley, H P L de Esch, H D Falter.

JET Joint Undertaking, Abingdon, Oxon, OX14 3EA.

Measurements and Calculations of Isotopic Exchange between Deuterium and Tritium and their Implications to Neutral Beam Injection

D. Ciric, A. J. Bickley, H. P. L. de Esch and H. D. Falter
JET Joint Undertaking, Abingdon, Oxon. OX14 3EA, United Kingdom

ABSTRACT

The hydrogen isotope exchange in some beamline components of a tritium injector is analysed using the local mixing model. Various implantation and cleanup scenarios using tritium, deuterium and hydrogen beams are discussed. The model is also used to interpret D(t,n)α neutron measurements during the cleanup of beamline elements after the First Tritium Experiment (FTE) at JET.

INTRODUCTION

Tritium inventory in the beamline components of the tritium neutral beam injectors is important for the handling of those components after tritium injection and for tritium accountability. During the injection of tritium beams, large amounts of tritium will be implanted into beamline components (dumps, scrapers, calorimeters). Implanted tritium can be removed using deuterium cleanup pulses after tritium injection. A computer code based on the local mixing model [1] was developed to interpret hydrogen isotope exchange during hydrogen bombardment of actively cooled CuCrZr beam panels. The code was previously used to interpret hydrogen-deuterium exchange in the beam dump panels of the JET Neutral Beam Test Bed [2,3]. In this paper we present results of the computer simulation of tritium implantation and tritium recovery using deuterium and hydrogen beams.

II. EXPERIMENTAL RESULTS

In the First Tritium Experiment at JET [4], tritium was introduced into the plasma entirely by tritium beams. Two PINIs of one of the JET Neutral Injectors [5] (NIB 8) were operated with tritium gas. Beam history around the FTE, relevant for tritium implantation and subsequent cleanup of tritium from beamline components, is given in Table I. The estimated activities of the beamline components, assuming 100% implantation of energetic tritium during various phases of tritium operation, are summarised in Table II.

Table I
NIB 8 beam history around FTE.

Phase	T- beam commissioning	FTE	Cleanup phase 1	Cleanup phase 2
Beam	100% T	100% T	100% D	100% D
Beam type	deflected	synchronous	undeflected	deflected
Extr. voltage	78 kV	78 kV	55 kV	~80 kV
Extr. current	27 A	27 A	20 A	40 A
Time	1 s	6.7 s	30 s	144 s
Exposed component	calorimeter ion dumps	ion dumps scrapers	calorimeter	calorimeter ion dumps

Manuscript received October 11, 1993.

Table II
Tritium inventory in NIB 8 after FTE.

Component	Absorbed activity (Ci)
Calorimeter	10 ± 1
Ion dumps	60 ± 5
Box and duct scrapers	15 ± 3
TOTAL	85

Ion beam dumps and calorimeter were cleaned after the last tritium pulse by using deuterium beams. The progress of tritium recovery was monitored by measuring neutrons from the D(t,n)α reaction. One of the neutron counters from the torus diagnostic system was used for this measurement.

In the first cleanup phase, the calorimeter was cleaned within 30 beam seconds using undeflected 55 kV deuterium beams. In the second phase, the deflected ~80 kV deuterium beams were used to clean the dumps and the calorimeter. Measured neutron yield during the cleanup of beamline components is given in Fig. 1.

The tritium cleanup procedure by deuterium beams was also monitored by measurement of the activity of the gas regenerated from the injector cryopumps - ~70 Ci was recovered. Bearing in mind the uncertainties (~10%) which can be applied to both, the assumed total activity of the beamline components (Table II) and the measured activity of the tritium gas, we can conclude that essentially all of the implanted tritium was recovered. This also implies that the depletion of the implanted tritium through the diffusion at room temperature can be neglected, since the cleanup of the

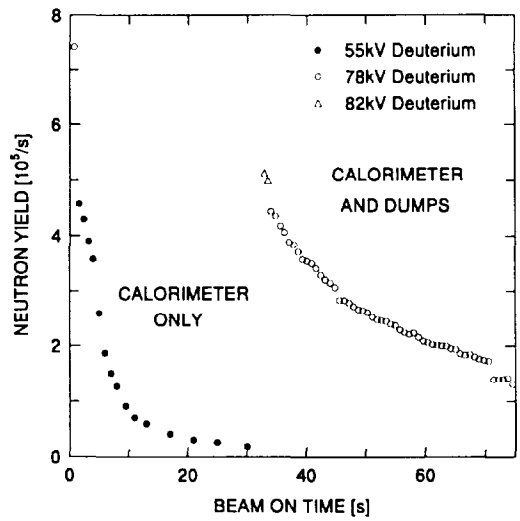

Fig. 1 Cleanup of the tritium injector with deuterium beams after the FTE using undeflected (solid symbols) and deflected beams (open symbols).

injector box using deuterium beams started two days after the FTE.

III. MODEL

The time evolution of the hydrogen isotope density inside a metallic (copper) target during the implantation of hydrogen, deuterium or tritium is calculated using the local mixing model [1]. Details of the calculations are described elsewhere [3], and only the basic assumptions are summarised here.

It is assumed that the local concentration of implanted hydrogen atoms is limited to a maximum value of n_{sat}, which is inversely proportional to the copper surface temperature [3]. The diffusion of implanted atoms is neglected and the only free parameter in the model is the saturation concentration.

Fast hydrogen atoms slow down in the host lattice and when they come to rest they are stored in a saturable trap. If the local concentration of hydrogen isotopes is below saturation level, the number of deposited hydrogen atoms can be determined from the corresponding range distributions [6]. If the incoming particle comes to rest within the saturated region, one implanted (trapped) atom is instantly released for each incoming atom without being trapped in the adjacent non-saturated region. In this case, the release rate equals the deposition rate and reflects the local implanted isotope mixture.

In the case of deuterium beams, neutrons are emitted in collisions of deuterium atoms with previously implanted tritium atoms. Slowing down of deuterium in copper is calculated using the stopping power formulas [7]. The total neutron yield can be calculated by using the total cross-section for the D(t,n)α reaction [8], the energy of the deuterium particles during the slowdown, and the calculated density distribution of implanted tritium atoms.

IV. TRITIUM RECOVERY AFTER THE FTE

For simplicity, only the cleanup of the calorimeter is considered, as the calorimeter was exposed to undeflected beams during the initial cleanup. This improves the accountability. It is assumed that the calorimeter panels were fully saturated with deuterium before tritium implantation, with deuterium to copper atomic ratio of 1:10 ($n_{sat} \cong 8.5\times10^{21}$ atoms/cm^3). This saturation concentration is lower than the one found in the literature [9], accounted for by the increase in temperature (~400°C) of the calorimeter panels exposed to energetic deuterium or tritium beams [3].

The calorimeter was exposed to tritium beams only during the commissioning phase. Charging and subsequent cleanup of the NIB 8 calorimeter after the FTE was simulated using beam parameters given in Table I. Incident particle densities required for the simulation were derived from the measured beam profiles.

The total neutron yield was calculated for the first phase of the cleanup process (55 kV deuterium beam). Since no attempt was made to derive total neutron count rates from measured values, the calculated neutron yield was normalised to experimental data. The result is shown in Fig. 2. The time evolution of the tritium density distribution inside the copper target during cleanup is given in Fig. 3. Note that the tritium saturation density was not reached during the charging of the calorimeter since the total tritium implantation time was only 1 second.

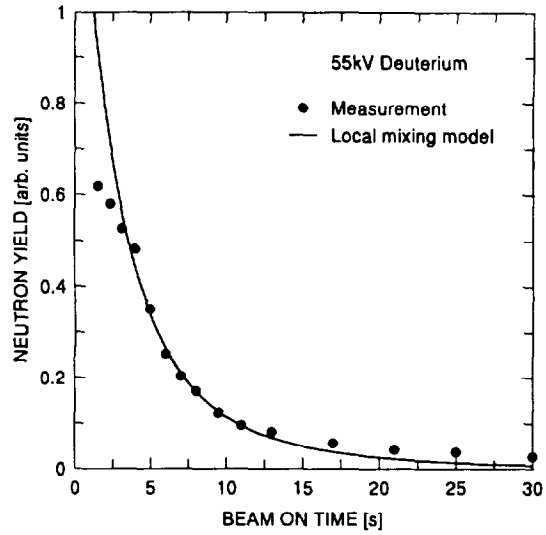

Fig. 2 Calculated and measured neutron yield during NIB 8 calorimeter cleanup after the FTE using 55 kV deuterium beams.

The fast initial decrease in the neutron yield can be explained by the efficient replacement of implanted tritium with deuterium around the mean projected range (Fig. 3). Tritium that was implanted deeper into the copper is removed very slowly due to the lower penetration depth of deuterium. The removal of deeply implanted tritium cannot be monitored using neutron detection, as decelerated deuterons do not have sufficient energy to produce a measurable neutron signal. At higher deuteron energies (78 kV), deeply implanted tritium is removed somewhat faster, but the amount of tritium retained in the copper target after 90 beam seconds is still ~5% of its initial value. We can expect that the amount of the retained

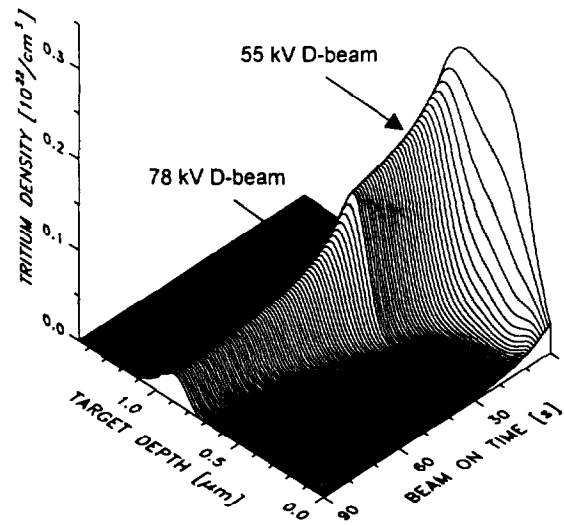

Fig. 3 Time evolution of calculated tritium density during calorimeter cleanup using 55 kV and 78 kV deuterium beams.

tritium in the injector ion dumps is also ~5%. Higher values can be expected for the box scrapers and the duct scrapers, as they are exposed to the lower beam densities, and are consequently cleaned with lower efficiency (see next section). This is in agreement with the difference between the measured activity of the recovered tritium gas and estimated implanted tritium activity.

Higher deuterium beam energies are required for the complete removal of implanted tritium. Note that the cleanup time is considerably longer than the implantation time.

V. LONG TERM TRITIUM OPERATION

The amount of tritium implanted into the beamline components during the active phase of JET will significantly exceed the values of the FTE. Different tritium implantation and cleanup scenarios were simulated using much longer implantation times.

The saturated hydrogen isotope concentration used in the simulation was n_{sat}= 8.5×10^{21} atoms/cm^3 (n_{sat}:n_{Cu}=1:10). In the simulation copper target was exposed to energetic tritium beams for a period of 100 seconds and the cleanup process using deuterium or hydrogen beams was simuleted for 1000 seconds. Incident particle densities were limited to the electrical equivalent of 20 mA/cm^2 perpendicular to the copper surface. This current density corresponds to a power density of 1.3 kW/cm^2 for 70 kV beams. The same incident particle density was used in the implantation and in the cleanup phase. Beams with extraction voltages in the range 60-80 kV, and with fixed species composition of 83%, 10%, and 7% (full, half and third energy) were considered.

Results are presented only for normal incidence beams. The variation of the angle of incidence has little effect on the amount of retained tritium if the flux of beam particles perpendicular to the surface is maintained constant.

The first considered case was the implantation of 70 kV tritium beams into copper and subsequent cleanup using 80 kV deuterium beams. Range distributions of tritium and

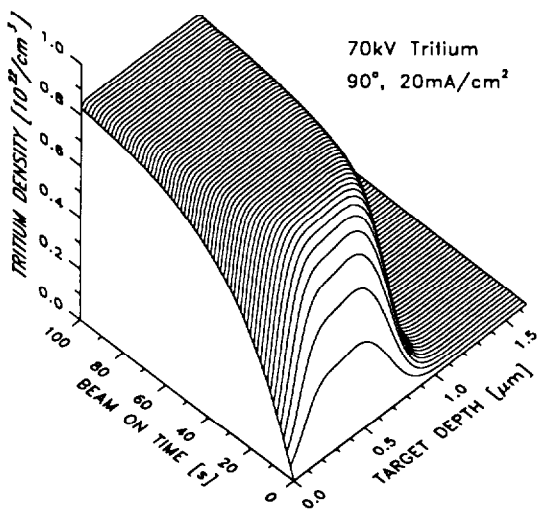

Fig. 4 Simulated time evolution of the tritium density distribution during implantation of 70 kV tritium beam into copper target.

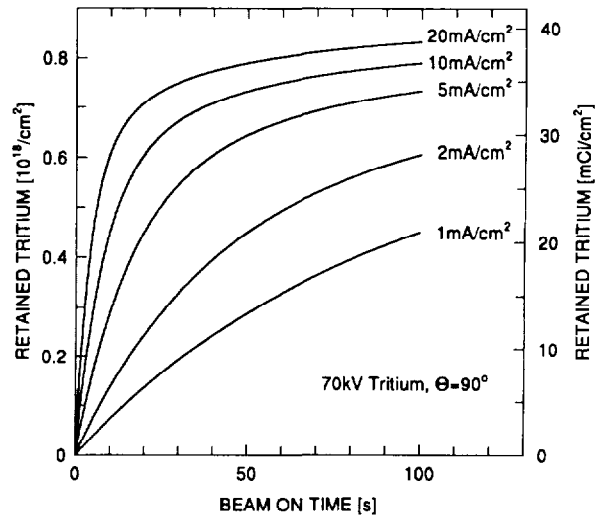

Fig. 5 The amount of retained tritium during tritium implantation into copper for different beam current densities.

deuterium in copper for those beam energies are quite similar, which should lead to efficient tritium cleanup.

The time evolution of tritium density distribution inside the copper target during implantation of 70 kV tritium beam at normal incidence is given in Fig. 4. Tritium saturation in the vicinity of the mean projected range is vary rapid. The saturated region extends gradually, and after 100 beam seconds the saturated region is roughly 1 μm deep.

For the lower incident particle densities, the saturation of the copper target is much slower, and only the region around the mean projected range will become fully saturated with tritium. Nevertheless, the amount of tritium retained in the target (i.e. the integral of tritium density along the total penetration depth) is still considerable (Fig. 5). This means that beamline elements which are not exposed to maximum beam particle densities will still contain a significant amount of tritium after the long tritium implantation. The amount of retained tritium is given per unit area. The corresponding activity is indicated on the right scale of the diagram (10^{18} atoms ~ 45 mCi).

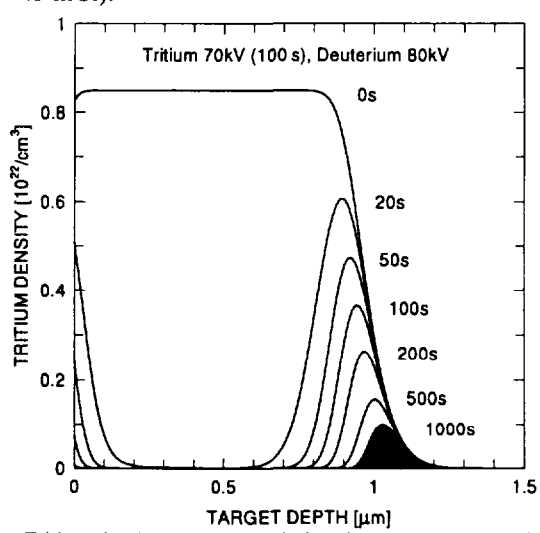

Fig. 6 Tritium density distribution during the cleanup phase using 80 kV deuterium beams at normal incidence, with current density of 20 mA/cm^2.

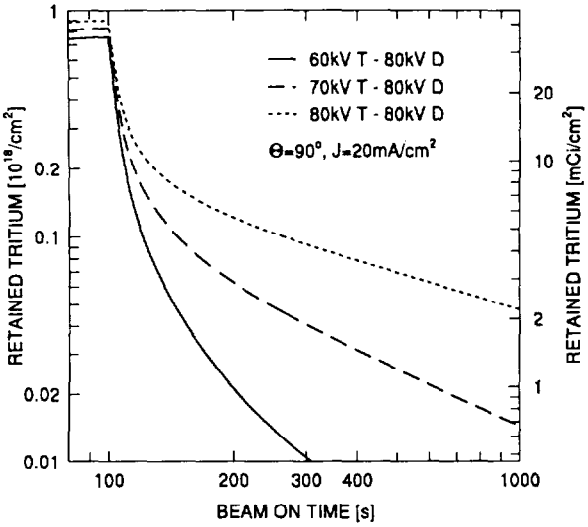

Fig. 7 The amount of retained tritium during the cleanup phase using 80 kV deuterium beams, after the implantation of tritium at 60, 70 and 80 kV for 100 s.

The cleanup process using 80 kV deuterium beams at normal incidence is illustrated in Fig. 6. Initially, tritium replacement with deuterium is very fast. The tritium removal rate decreases gradually, and after 1000 beam seconds the amount of retained tritium is roughly 1.5% of the initial value (shaded area in Fig. 6). It should be noted that the cleanup efficiency is lower for the lower beam particle densities - roughly 3% of the implanted tritium is retained for the beam particle densities equivalent to 1 mA/cm^2.

The cleanup efficiency can be significantly improved if the energy of the deuterium beam used for cleanup is higher than the energy of the tritium beam during implantation. This is demonstrated in Fig. 7, where 80 kV deuterium beam is used to clean the target which was previously saturated with tritium beams of 60, 70 and 80 kV. This implies that the tritium injection energies should be below the nominal maximum of the tritium injector (assumed here as 80 kV), to permit fast tritium recovery using deuterium beams with maximum energies.

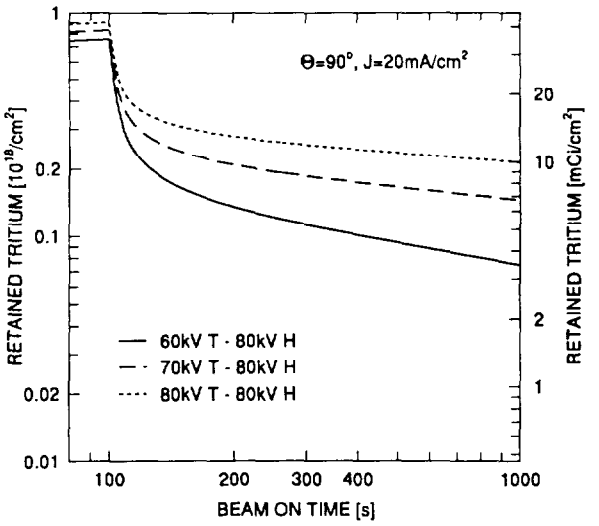

Fig. 8 The amount of retained tritium during cleanup using 80 kV hydrogen beams, after the implantation of tritium at 60, 70, and 80 kV for 100s.

Hydrogen beams are not suitable for cleanup purpose. Due to lower penetration of hydrogen, a considerable amount of tritium can be retained in the target. This is illustrated in Fig. 8, where 80 kV hydrogen beam is used to clean the target which was previously saturated with tritium beams of 60, 70 and 80 kV. Hydrogen beams of much higher energies are required for effective tritium cleanup. Another drawback in using hydrogen beams is the absence of neutrons for monitoring the cleanup process. Helium beams are unsuitable for similar reasons.

VI. CONCLUSIONS

The inventory of tritium in the beam injector can be well understood in the framework of the local mixing model. From the results obtained one can conclude that:

- the depletion of the implanted tritium by diffusion at room temperature is negligible compared to the cleanup with deuterium beams.
- hydrogen saturation densities of the order of 10^{22} cm^{-3} will be achieved during beam injection.
- the saturated region can be 1 μm deep (60-80 kV beams), leading to an activity of ~50 mCi/cm^2 after tritium implantation.
- implanted tritium can be efficiently removed using deuterium beams.
- deuterium beam energies used for cleanup should be roughly 20% higher than the tritium injection energies, to allow fast cleanup of deeply implanted tritium.
- hydrogen and helium beams are not suitable for the injector cleanup, unless significantly higher beam energies can be used.
- neutron detection is useful for monitoring the initial cleanup process.

REFERENCES

[1] G. Staudenmaier *et al.*, "Trapping of deuterium implanted in carbon and silicon: A calibration for particle-energy measurements in the plasma boundary of tokamaks", *J. Nucl. Mat.*, vol. 84, pp. 149-156, 1979.

[2] H. D. Falter, E. Thompson, D. Ciric and H. P. L. de Esch, "Implantation and desorption of tritium and tritium recovery from the JET neutral beam injectors", *J. Nucl. Mat.*, vol. 196-198, pp. 1131-1134, 1992.

[3] H. D. Falter *et al.*, "Hydrogen isotope exchange in the JET neutral beam injection system", in *Fusion Technology 1992*, vol. 1, C. Ferro, M. Gasparotto and H. Knoepfel, Eds., Amsterdam: North-Holland, 1993, pp. 481-485.

[4] The JET team, "Fusion energy production from a deuterium-tritium plasma in the JET tokamak", *Nucl. Fusion*, vol. 32, pp. 187-203, 1992.

[5] G. Duesing *et al.*, "Neutral beam injection system", *Fusion Technol.*, vol. 11, pp. 163-202, 1987.

[6] J. P. Biersack and L. G. Haggmark, "A Monte-Carlo computer program for transport of energetic ions in amorphous targets", *Nucl. Instr. and Meth.*, vol. 174, pp. 257-269, 1980.

[7] H. H. Andersen and J. F. Ziegler, *The stopping and ranges of ions in matter*, vol. 3, New York: Pergamon, 1977.

[8] H-S. Bosch, *Review of data and formulas for fusion cross-sections*, IPP I/252 , Garching: Max-Planck Institut für Plasma Physik, 1990.

[9] J. Kim, "D-D neutron and X-ray yields from high power deuterium beam injectors", *Nucl. Technology*, vol. 44, pp. 315-321, 1979.

Organic Cooling Fluids for the JET Toroidal and Divertor Field Coils.

M Cooke, P Butcher, M Huguet[1], J Last, C Sborchia[1].

JET Joint Undertaking, Abingdon, Oxon, OX14 3EA.
[1], ITER Naka Joint Work Site, Naka, Japan.

Organic Cooling Fluids for the JET Toroidal and Divertor Field Coils

M. Cooke, P. Butcher, M. Huguet*, J. Last, C. Sborchia*
JET Joint Undertaking, Abingdon, Oxon, OX14 3EA, UK
*ITER Naka Joint Work Site, Naka Japan

ABSTRACT

When the inter-turn electrical fault was found on the JET toroidal field coil 3.1 a series of studies were carried out to find an alternative cooling fluid to demineralised water with a high intrinsic electrical resistivity. The initial selection examined the physical characteristics of the fluids and ruled out all but three organic compounds. This paper describes the further tests and studies which were carried out to assess the performance and suitability of these organic cooling fluids. The plant implications including storage vessels, vent pipework, pump mechanical seals vapour detection scheme and leak detection are examined together with the waste management and the environmental aspects of using organic cooling fluids.

INTRODUCTION

The proposed change in the Toroidal Field coil cooling fluid for one with a high intrinsic electrical resistivity required the fluid to meet the needs of a high power electrical coil in a radiation environment. The fluid must fulfill the following parameters:

- High intrinsic electrical resistivity.
- Non-flammable, the open cup auto ignition temperature must be well in excess of 350°C. The vacuum vessel operates at this temperature and any risk of fire cannot be tolerated.
- The fluid must withstand the radiation level produced by the JET machine without breaking down, polymerisation or the formation of ions.
- Good heat transfer characteristics to avoid long pulse repetition times.
- The fluid shall be non-toxic and non-carcinogenic.
- The boiling point shall be in the range to give single phase flow at reasonable pressures.
- The viscosity and density shall be such that the existing pumping plant and heat exchangers can be retained.

COOLING FLUIDS

The table below lists the basic physical characteristics of the fluids considered.

When the control parameters are applied to each fluid the conventional heat transfer fluids (silicone liquids, glycols, synthetic oil and mineral oil) are ruled out because of the possibility of fire and auto ignition of a fluid spill on a hot vacuum vessel.

TABLE 1: CHARACTERISTICS OF HEAT TRANSFER FLUIDS

	Density Kg/l	Boiling Point °C	Auto Ignition Temp °C	Viscosity Cst	Thermal Conductivity W/m.k
Water	1	100	-	0.88	0.598
CFC113	1.55	47.7	-	0.41	0.064
C_6F_{14}	1.682	58.2	-	0.39	0.0653
C_2Cl_4	1.62	121	-	0.5	0.06
Glycol	1.113	200	180	20	0.16
HCFC 141b	1.236	32	550	0.35	0.104
Mineral Oil	0.88	190	150	16	0.147
Silicone	0.92	200	62	3	0.105

The non CFC replacement refrigerant for Trichlorotrifluroroethane CCl_2F-$CClF_2$ (CFC113), namely HCFC 141b, is an aggressive solvent which would not pass the compatibility tests and the vapour is flammable.

The fluids considered suitable for further testing were the three organic cooling fluids C_6F_{14} perfluorocarbon, CFC113 and C_2Cl_4 perchloroethylene.

COMPATIBILITY STUDIES

All fluids under consideration were subjected to tests for compatibility with the materials which are part of the Toroidal Field cooling loop. The materials tested included, brazed copper joint, EPDM hose, Hypalon hose, epoxy glass, nitrile gaskets and viton gaskets for which the following tests were carried out:

- Absorption and physical dimension change.
- Extraction and change in weight.
- Electrical properties of residue fluid.
- Chemical properties of residue fluid.

The tests with perchloroethylene showed that there was a much larger extraction and absorption than the other fluids and the epoxy glass samples cracked and delaminated (see Fig. 1). It was concluded that any contact of the perchloroethylene with the TF coil insulation could cause serious damage and this fluid was for this reason considered to be not suitable.

The results of the studies with CFC113 showed that the original EPDM hose material had a greater absorption than the Hyperlon hose. It was therefore recommended that the hose material be changed from EPDM to Hyperlon. The results of absorption, extraction and electrical properties of all samples with CFC113 were acceptable and the fluid was considered to be compatible. The results with C_6F_{14} indicated that the loss tangent was adversely effected when in contact with epoxy glass, hyperlon hose and the brazed copper joint. The resistivity was however only slightly lower than the original stock fluid.

Fig. 1: Compatibility of Epoxy Glass with Perchloroethylene

IRRADIATION STUDIES

Samples of the three organic fluids were γ irradiated to the equivalent dose of the active phase of JET 1.5Mrad for C_6F_{14} 1Mrad for CFC113 and 0.73Mrad for perchloroethylene. The difference in levels is due to a weighting factor which has been applied for the elemental composition of each fluid.

The samples were tested under two separate conditions. The first tests were carried out with sealed glass containers, with air above the fluid and with and without copper pieces present. The second tests were carried out with sealed glass containers with nitrogen above the fluid and with copper pieces present. In addition the samples were subjected to much higher radiation levels i.e. 60Mrads to check for signs of breakdown or polymerisation.

After irradiation the samples were checked for signs of polymerisation, the formation of copper, chlorine or fluorine ions, the composition of the breakdown gases or compounds and any change in physical properties i.e. viscosity, thermal conductivity resistivity.

TABLE 2: IRRADIATION RESULTS

Fluid	With Cu	Irrad time/ mins	dose rate/ kGy/h	Dose/ kGy	[F-]/ µg/g	[Cl-]/ µg/g	[Cu]/ µg/g
Samples Sealed With Air							
C_6F_{14}	Yes	9850	3.45	906.20	260	<1	<=0.005
C_6F_{14}	Yes	340	2.45	22.21	110	<1	0.006
C_6F_{14}	No	9850	2.76	724.96	280	15	<0.005
C_6F_{14}	No	340	2.47	22.39	130	<1	<0.005
C_2Cl_4	Yes	28	2.45	1.83	2	5	5.3
C_2Cl_4	Yes	170	2.45	11.11	<1	130	n.m
C_2Cl_4	No	28	2.47	1.84	2	130	<0.005
C_2Cl_4	No	170	2.47	11.20	<1	200	<0.005
CFC113	Yes	9850	2.47	648.79	110	100	0.62
CFC113	Yes	242	2.45	15.81	110	70	0.15
CFC113	No	9850	2.74	719.71	130	70	<0.005
CFC113	No	242	2.47	15.94	110	100	<0.005
Samples Sealed With Nitrogen							
CFC113	Yes	180	3.04	9.12	4	20	<0.002
C_6F_{14}	Yes	180	3.04	9.12	3	0.5	<0.002
C_2Cl_4	Yes	180	3.52	10.56	2	15	1.4

The analysis of the results indicated the following:

- None of the fluids broke down even when the samples were subjected to the higher level 60Mrads.
- Polymerisation did not occur with either CFC113 or C_6F_{14} however small signs of precipitation or polymerisation did occur with perchloroethylene. This was thought to be due to the stabiliser compound added to the fluid.
- With air or oxygen above the sample there were signs of copper oxide forming on the copper samples. This observation reinforced the decision to use nitrogen as the pressurisation gas in vessels and pipework.
- The irradiation did not effect the viscosity, thermal conductivity or resistivity of the fluids.
- There were no measurable quantities of copper chlorine or fluorine ions as a consequence of the irradiation.
- Without the presence of oxygen or water the breakdown products take the form of free radical carbon, chlorine or fluorine atoms.

ACTIVATION CALCULATIONS

The activation of the three organic fluids was calculated using a neutron flux model of the JET machine. The calculations allowed for the quantity of fluid within the coils during a ten second energy pulse, a total neutron production of 10^{24} neutrons for the whole D-T operation phase and 10^{20} neutrons for D-D operation.

During the non-active phase of the machine access to the cooling plant for maintenance of the equipment in the basement will not require any controls from Health Physics. Unless there is a leak of coolant then the area around the leak will be a controlled area.

The basement plant room will be equipped with γ monitors and in the active phase access will normally be allowed 24 hours after the last pulse when the radiation level due to the activation of CFC113 would be 10µSv/h or for C_6F_{14} 14µSv/h. In the event of a leak or other emergency, access immediately after a pulse can be considered for short durations only (controlled entry) since the dose rate would be 160mSv/h with CFC113 or 560mSv/h with C_6F_{14}.

A sample of CFC113 was taken at the end of the last operating campaign and the radioactivity measured. The results showed a reduced activity compared with the calculations by a factor 4.4. Measurements of β emission were also made on the inside surface of the stainless steel pipework to assess the plating out of activity on the oxide surface layer. The measurements indicated that 25% of the activity was plated out on the surface of the pipework.

A test was carried out to find what proportion of the activity would be held in the molecular sieve of the system drier. A test rig was manufactured including a small drier with the same molecular sieve materials as the system drier. The active fluid was circulated in the test rig for a time corresponding to a year of operation. The results indicated a reduction in activity by a factor of 4.7.

A further experiment was carried to see if the activation products P^{32} and S^{35} etc.would remain on the floor of the

TABLE 3: PREDICTED, ACTIVATION AND HALF LIFE

Isotope	Production Reaction	1/2-Life	Gamma Rays (MeV)	Activity at Shutdown (Bq/g)		Gamma-Ray Dose-rate (μSv/h)		Activity at Shutdown (Bq/g)		Gamma-ray Dose-rate (μSv/h)		Activity at Shutdown (Bq/g)		Gamma-ray Dose-rate (μSv/h)	
				CFC113				Perfluorocarbon C_6F_{14}				Perchloroethylene C_2Cl_4			
				D-T	D-D	D-T	D-D	D-T	D-D	D-T	D-D	D-T	D-D	D-T	D-D
Be^{10}	$C^{13}(n,d)$	2.5×10^6y	-	1.5, -3	-	-	-	4.7, -3	-	-	-	1.2, -3	-	-	-
C^{14}	$C^{13}(n,\gamma)$	5.7×10^3y	-	3.3, -3	6.7, -7	-	-	1.0, -2	2.1, -6	-	-	2.6, -3	5.4, -7	-	-
F^{18}	$F^{19}(n,2n)$	110m	0.51	4.3, 5	-	1.2, 5	-	2.0, 6	-	5.6, 5	-	-	-	-	-
P^{32}	$Cl^{35}(n,2n)$	14.3d	-	6.4, 5	2.0	-	-					6.9, 5	1.8	-	-
P^{33}	$Cl^{37}(n,na)$	25d	-	3.4, 3	-	-	-					3.8, 3	-	-	-
S^{35}	$Cl^{35}(n,p)$	88d	-	1.1, 6	1.7, 2	-	-					1.2, 6	1.8, 2	-	-
Cl^{36}	$Cl^{35}(n,\gamma)$	3.1×10^5y	0.51	6.4, 1	6.7, -3	-	-					6.9, 1	7.2, 3	-	-
Cl^{38}	$Cl^{37}(n,\gamma)$	37m	2.1	1.0, 5	2.1, 1	4.3, 4	8.4					1.1, 5	2.3, 1	4.6, 4	9.4

Note: 1.5, -3 = 1.5×10^{-3}

Torus Hall when evaporation occurred of any CFC113 spill. A small quantity of CFC113 was heated in a flask and then recondensed in a liquid N_2 cold trap. After total evaporation the results showed that the level of S^{35} was reduced by a factor 4. The result confirmed that the radioactive activation products would not become airborne.

COOLING PERFORMANCE

The predicted cooling performance of water CFC113 and , C_6F_{14} for a typical high energy TF pulse (67kA current 12 second flat top, energy 106 10^9A^2s) are shown below together with the actual curves for demineralised water and CFC113 cooling.

The CFC113 cooling flow rate is less than that for water. This was brought about by the necessity to keep the absorbed power the same when the fluid was changed and the pump impeller was ground to the new pump duty point.

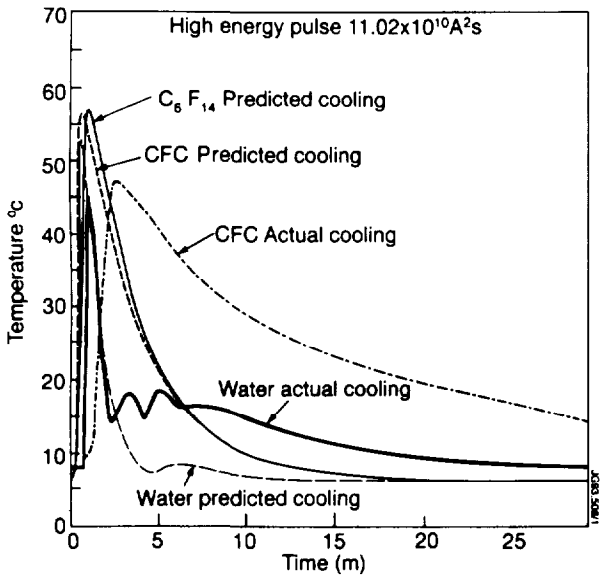

Predicted and Actual Cooling Curves

PLANT CONSIDERATIONS

The use of an organic fluid necessitated mechanical design changes to ensure a totally sealed closed loop system with storage vessels, drainage vessel and expansion tank. The vent pipe from each vessel and the crown distribution pipes on the top of the machine are linked together to ensure the transfer of vapour during any draining or filling operation without any release to the atmosphere.

To give the maximum integrity to the system, all valves were kept to a minimum and the pipework was fully welded. The most vulnerable item, the hoses connecting the manifolds to the coils, were changed to "Hyperlon" material after the compatibility tests indicated that EPDM was not suitable and connected with hydraulic screw connectors in preference to the Rafix push-on connectors. The shaft seals on the main circulating pumps were changed to a double carbon silicon carbide seal with the interspace filled with a heat transfer oil. The oil has a pressure 1 bar gauge greater than the pump discharge pressure to ensure no leakage of CFC113 to the plant room atmosphere. The individual pumps for the divertor coils are magnetically coupled sealess units and the control valves have bellows shaft seals to reduce further the possibility of a leak.

The control system was designed with relay logic and the supplies connected to a uninterruptible power supply. Should a leak occur at a hose or joint the system automatically drains into the storage vessels. The drainage sequence is initiated by either a very low level switch in the expansion vessel or an individual CFC113 reading above 2000ppm on the analyser panel. The liquid from the spill would be collected in the floor drainage system and then pumped to a separate storage vessel. After a clean up operation the vapour remaining would be released to the atmosphere. However a cryogenic trap in the Torus Hall cell and basement ventilation discharge duct, is currently under design for installation during the next shutdown. When commissioned any CFC113 vapour from a spill together with the atmospheric water vapour would be condensed and piped to a storage vessel.

ENVIRONMENTAL ASPECTS

All organic fluids have an impact on the environment either as a greenhouse gas or are ozone depleting.

The production of CFC chemicals has been the subject of world wide discussions and recommendation for many years because of the ozone depletion properties. The current recommendations follow the Montreal, London and Copenhagen protocols which state that production should stop by the year 2000. Recent EEC directives have brought this date forward to 1997 and the UK has declared an earlier date of 1st January 1994. Although production will cease all existing stocks and user applications are considered in environmental terms to have been released into the atmosphere.

The fluids considered are all greenhouse gases and because of their inert nature remain in the atmosphere for many years. The lifetime in the atmosphere for CFC113 is 111 years and for C_6F_{14} perfluorocarbon is up to 2000 years. There are no recommendations or legislation on the use of chemicals that are greenhouse gases. However, the recent proposal by the EEC to introduce a carbon tax to reduce greenhouse gas emission and also the fact that global warming and greenhouse gases was on the agenda of the Earth summit does mean it will become a major environmental issue. Some major chemical manufacturers no longer produce perfluorocarbons because of the global warming potential.

WASTE MANAGEMENT

At the completion of the active phase all fluid will be drained from the coils and pipework into the main $63m^3$ storage vessel. Assuming the neutron production will be 10^{22} neutrons and allowing a plating out factor of 10 the CFC113 would contain two prominent isotopes Cl^{36} at a level of 6.4×10^{-3}Bq g^{-1}, half life 3×10^5 years and S^{35} at a level of 1.1×10^3Bq g^{-1}, half life 88 days.

The activity prohibits the re-use of the fluid as a feed stock for a different compound and the final waste management route will be disposal by high temperature incineration. In order to achieve the activation level at which the disposal company has a license to operate of 11Bq g^{-1} it will be necessary to store the fluid on site for approximately two years. This delay would not occur with the use of the perfluorocarbon C_6F_{14} as the activation level is below 11Bq g^{-1} in a matter of hours.

FLUID SELECTION

The compatibility studies showed that perchloroethylene was not a suitable fluid because of the high extraction and eventual cracking of epoxy glass. Also there were signs of polymerisation of this fluid when irradiated.

The remaining two fluids which were studied in detail CFC113 and C_6F_{14} have similar physical properties, radiation tolerance, and heat transfer abilities. They both have an impact on the environment although there is no current legislation on the future use of perfluorocarbon compounds there is however a limit on the manufacture of CFC compounds of the 1st January 1994.

The activation products of CFC113 have a much longer half live than C_6F_{14} and the concern of an activated CFC vapour release to the atmosphere must be accomondated in the plant design. Perfluorocarbon has a higher storage tank surface radiation dose rate than CFC113 which may restrict immediate access to the plant room in the event of a fault. The purchase cost of CFC113 was £1 kg^{-1} when supplied to JET for the non-active phase. The cost to change to perfluorocarbon C_6F_{14} for the active phase would be an additional £1.3×10^6 assuming the circuit volume was reduced to $38m^3$ with pipework size changes and route modifications and the current cost of C_6F_{14} of £20 kg^{-1}.

The final selection was made for the active phase to use CFC113 for which there is now operational experience and install the necessary plant modifications to condense any activated vapour that may be released.

CONCLUSIONS

The use of CFC113 as a coolant for the TF coils has shown that reasonable cooling efficiency has been achieved with a fluid with a high instrinsic electrical resistivity. There have been no operational restrictions with the new coolant and an interpulse time of between 15 to 25 minutes has been achieved for standard pulses. For high energy pulses 106.10^9 A^2s current of 67kA and a 12 second flat top a interpulse time of 24 minutes was maintained for consecutive pulses. This interpulse time is very similar to that for demineralised water since the cooldown time for high energy pulses is determined by the capacity and control sequence of the chiller plant on the primary site water rather than the thermal properties of TF coolants.

REFERENCES

[1] J. Last et al., JET TF Coil Fault Detection Diagnosis and Prevention, Proc. 16th SOFT, London, UK.

[2] A. Watts and D.S.L. Slim, Study of the Compatibility of Various Materials with 113, Tetrachloroethylene and Perfluorocarbon, Rhône-Poulene Chemicals, Bristol, February, April 1990, January and November 1992, .

[3] M.C. Kent and H.E. Sims, Radiolysis of Chloro and Fluorocarbons, Potential Coolant for JET AEA Reactor Services, Harwell.

[4] O.N. Jarvis, private communication.

[5] A.F. Avery and K.G. Greenhouse, Activation of Cooling Fluid in the Toroidal Coils of JET AEA Reactor Services, Winfrith, December 1991.

[6] B.H. Baxter, private communication. British Aerospace Defence, Member United Nations Environmental Protection Coatings and Adhesives Technical Options Committee, April 1992.

The New Control Scheme for the JET Plasma Position and Current Control System

M Garribba, R Litunovsky, P Noll, S Puppin.

JET Joint Undertaking, Abingdon, Oxon, OX14 3EA.

The New Control Scheme for the JET Plasma Position and Current Control System

M. Garribba, R. Litunovsky, P. Noll, S. Puppin
JET Joint Undertaking, Abingdon, Oxfordshire, OX14 3EA

ABSTRACT

The new setup for the Plasma Position and Current Control (PPCC) to be implemented in the next JET operational campaign is described. A decoupling control scheme is used because of the strong coupling between the coils introduced by the new divertor coils and magnetic configuration [1]. A general discussion of the method applied with results of simulations is presented. Effects of modelling errors and operational limits are discussed.

CONTROLLER DERIVATION

The controller is based on the eigenvalue allocation technique typical of the multivariable control synthesis. The control is performed on the nine power amplifiers [2] that supply the JET Poloidal Field (PF) system. The feedback quantities can be chosen from a set of plasma-wall gaps and PF currents such that a set of nine quantities is always controlled. The approach taken is to have as many actuators as degrees of freedom in the system, so that the controller can be uniquely derived from the open loop model.

The first step for deriving a controller is to define an open loop model of the plant. This can be obtained by writing the following two non linear equations:

$$\bar{X} = \bar{X}\left(\bar{I}_t, \beta_P, l_i, \psi_c\right) \tag{1}$$

$$\frac{d}{dt}\left(\bar{M}\left(\psi_c, \bar{X}, \beta_p, l_i\right)\bar{I}_t\right) + \bar{R}\,\bar{I}_t = \bar{V}_t \tag{2}$$

Equation (1) expresses the plasma force balance by means of the array of the chosen plasma shape parameters as functions of the PF equilibrium currents, the iron core magnetisation status ψ_C, the plasma current profile, parametrised by the internal inductance l_i and the poloidal beta. Equation (2) establishes the differential equation describing the evolution of the PF currents including the plasma current. The arrow indicates matrices and arrays.

The first equation can be linearised around any equilibrium position or trajectory for small variations of the independent quantities. The execution of the time derivation in (2) yields a *modified and reduced system.* The plasma current is excluded from the PF coils currents set, which represent the state variables, because it is a secondary current and the inductance matrix of the PF system is *modified* by the presence of the plasma. The variation of the shape parameters δX can be written highlighting the part depending on the PF currents and the other terms in (1) which will be treated as external perturbations:

$$\delta\bar{X} = I_p^{-1}\,\bar{B}_s\,\delta\bar{I}_{PF} + \bar{G}\,\delta\begin{bmatrix} l_i \\ \beta_p \end{bmatrix} + \bar{d}\,\psi_c \tag{3}$$

The matrices B_S and G, and the array d represent the variation of the plasma shape for a variation of the PF coil currents, the profile parameters and the iron saturation state respectively.

The matrix B_S is also *reduced* by eliminating the plasma current from the PF set. The following equation defines it:

$$\bar{B}_s = \bar{B}_{PF} - \frac{1}{\bar{L}_p}\bar{b}_p\,\bar{m}_{pi} \qquad \bar{b}_p = \frac{\partial\bar{X}}{\partial I_p} I_p$$
$$\bar{B}_{PF} = \frac{\partial\bar{X}}{\partial\bar{I}_{PF}} I_p \tag{4}$$

where L_p is the plasma inductance, m_{pi} is the array of mutual inductances between the PF coils and the plasma (first row of M in (2), excluding L_p) and I_p is the plasma current. The tilde denotes *modified* inductances defined in a way similar to the matrices below.

Equation (2) can be rewritten:

$$\bar{M}_s\dot{\bar{I}}_{PF} + \bar{R}\,\bar{I}_{PF} = \bar{V}_{PF} - f\left(\psi_c, \beta_p, l_i\right) \tag{5}$$

As in equation (3) the unknown variation in the profile parameters and in the iron core saturation state are treated as disturbances expressed by the function f.

The matrix of coil inductances M_{PF} is *modified* by the shape variation giving:

$$\bar{\bar{M}}_{PF} = \bar{M}_{PF} + \frac{\partial\bar{m}_{ip}}{\partial\bar{X}}\bar{B}_{PF} \tag{6}$$

m_{ip} is the first column of M in (1) excluding L_p.

The elimination of the plasma current from the state variables yields:

$$\bar{M}_s = \bar{\bar{M}}_{PF} - \frac{1}{\bar{L}_p}\bar{\bar{m}}_{ip}\,\bar{\bar{m}}_{pi} \tag{7}$$

The plasma current variation can be expressed as the linear combination of the PF coil currents if the resistance is assumed to be zero.

$$\delta I_p = -\frac{1}{\bar{L}_p}\bar{\bar{m}}_{pi}\,\delta\bar{I}_{PF} \tag{8}$$

Equations (3), (5) and (8) are the final form of the open loop system for control design. If the time responses of the actuators are negligible compared with the desired closed loop time constants the model derived is suitable for the controller calculation.

The chosen form of the controller is:

$$\bar{K} = \bar{E}\,\bar{C} \tag{9}$$

C is a diagonal matrix whose elements are desired eigenvalues of each loop and E is the decoupling matrix.

The controller is applied on a set Y defined by a linear space transformation T from the space of the PF coil currents (state variables) into the space of the actual quantities to be controlled: plasma current, some plasma-wall gaps X_S and the remaining PF currents I_S.

$$\delta\bar{Y}=\delta\begin{bmatrix} I_p \\ \bar{X}_s \\ \bar{I}_s \end{bmatrix}=\begin{bmatrix} -\frac{1}{\tilde{L}_p}\tilde{m}_{pi} \\ I_p^{-1}\bar{B}_s\text{rows} \\ \text{unity matrix rows} \end{bmatrix}\delta\bar{I}_{PF}=\bar{T}\delta\bar{I}_{PF} \qquad (10)$$

Ignoring the PF coils resistances R in (5) and the disturbance terms in (3) and (5), it is easy to see that the final form for the controller matrix K is:

$$\bar{K}=\bar{M}_s\bar{T}^{-1}\bar{C}=\bar{E}\bar{C} \qquad (11)$$

A controller of this form diagonalises the overall closed loop system and imposes the closed loop eigenvalues of the matrix C.

The voltage to be applied to the PF coils is therefore:

$$\bar{V}_{PF}=\bar{R}\bar{I}_{PF}+\bar{K}\left(\bar{Y}_{ref}-\bar{Y}\right) \qquad (12)$$

where the resistive term is applied as a positive feedback term to suppress the effect of the finite coil resistances.

DESIGN APPROXIMATIONS

The inductance matrix M_S is quite insensitive in JET to the plasma shape and the *modification terms in* (6) are always small compared with the real coil coupling terms.

Moreover the vacuum vessel toroidal eddy currents are not included in the open loop model because the chosen closed loop time constants are slower than the vessel response time (≈ 3-5ms).

The vertical stabilisation is decoupled from the shape control on the different time scale used by the two systems (0.5 ms for the vertical stabilisation). The shape control assumes the plasma already vertically stabilised.

It is important to ensure that the system stability is not affected by the variation of the plasma current profile or by a shape change in the actual plant (B matrix change). An example of this is given in Table I, where the closed loop eigenvalues for an ideal situation are compared with the ones obtained with varied l_i and β_p. This problem has been addressed extensively by simulation using the equilibrium code PROTEUS [3].

Table I

Comparison of the closed loop eigenvalues (s^{-1}) for reference (l_i= 0.9, β_p = 0.2) and real plasmas with β_p = 0.2 l_i = 1.1 (Case I) and β_p = 1.1 and l_i = 0.9 (Case II)

Controlled Quantity	Design Eigenvalue	Case I	Case II
Plasma Current	3.3	3.3	3.3
Outer Gap	50	34	36
Centroid Height	10	9	12
Inner Gap	20	17	15
Shaping Current	10	10	10
D1-coil Current	10	10	10
X-point Radius	100	94	68
X-point Height	10	11	13
D4-coil Current	10	10	10

The steady state errors are almost eliminated by choosing to apply a positive feedback using the PF coils resistances (12). In JET this is possible and not dangerous given the time constants of the coils are several seconds long, and therefore the positive feedback is a small fraction of the overall feedback gain. The only source of steady state errors left is the plasma loop voltage itself. A loop voltage of 0.1 volt produces a steady state error of order 10kA in the plasma current and few millimetres in the controlled gaps.

The alternative to the positive feedback is to introduce integral control. This technique poses the problem of how to deal with a loop saturation propagating to the other loops.

The PF generator-converter system which drives the Ohmic Heating (OH) circuit in JET [2] is a slow system with an equivalent first order time constant of 50ms or more. This violates the hypothesis on the short response time of the actuators. The problem is solvable in two ways. The first one [4], [5] is the classical technique of series connecting two state space described systems. This method has the marked disadvantage of increasing unnecessarily the order of the overall system without solving the problem of the varying characteristics of the generator [6]. The second method consists of simply preceding the generator loop (after the controller loop) with the inverse transfer function of the generator itself, using a cancellation technique. This method has been preferred for its simplicity and the generator compensation is included in the simulations. The command voltage for the PF generator therefore goes through a compensating PID controller [4] after the decoupling process.

CONTROLLER OPTIMISATION

The controller has been simulated in the JET FAT and SLIM configurations [1]. The design procedure followed allocate freely the closed loop system eigenvalues and does not take into account the voltage and current limitations of the power supplies.

These limitations can be included in a controller design by means of methods like the LQR regulator [4], [5]. However the LQR controller matrix would be obtained by a complex manipulation of the open loop system matrices M_S and B_S with two weight matrices Q_1 and Q_2 representing the voltage and current limitations and not directly the closed loop time constants of the system. It is therefore, at this stage, preferred to implement a controller whose elements represent a product of well known quantities like the PF coils inductance matrix and the coil to plasma boundary sensitivity matrix B_S.

The result of the full allocation technique used is that , due to the very different time constants requested in the system behaviour (see Table I), it is quite easy to get a voltage saturation in circuits which produce field components not appropriate to control a certain gap.

A typical example is the outer gap control. This is controlled most effectively by the vertical field. Moreover the time constant of this control is only 20ms. It is appropriate in the control matrix to set to zero the terms

which would ask the sources of radial field to help in the control action. These cancellations do not alter significantly the eigenvalue structure of the closed loop system and achieve the same effect of the LQR controller in demanding minimum power from the amplifiers.

The other example worth noting is the plasma current control. In this case it turns out that the full row of the decoupling matrix K (excluding the diagonal term) can be suppressed advantageously. This means that the PF generator controls only the plasma current, while the error on the plasma current is fed to all the amplifiers. The suppression of these terms is particularly significant during the X-point sweeping because of the very reduced energy extraction from the generator.

The controller includes also the facility to feedback the plasma-outer wall gap on the ICRH coupling resistance or on the LH reflection coefficient. In the case of the ICRH feedback the coupling resistance error is transformed to an outer-gap demand waveform which can operate between two preset limits: a minimum and a maximum distance from the wall. The limits are tracked if they are reached. A hysteresis mechanism avoids the possibility of bouncing between ICRH feedback and limit tracking.

OPERATIONAL LIMITS

The operation modes of the controller have been subject to extensive studies using the PROTEUS code. These studies comprise the optimisation of the choice of the control set Y and the parameters range which can be covered in terms of variations of plasma current profile and currents in the PF coils.

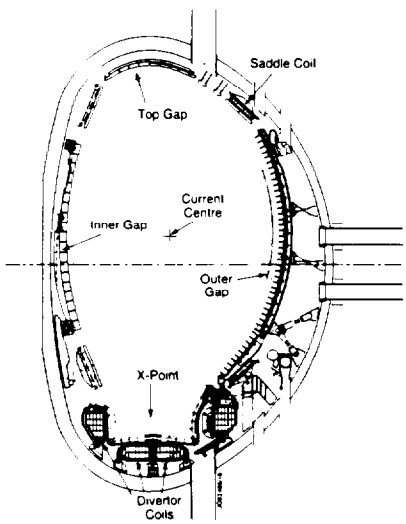

Fig. 1 Plasma FAT configuration and the JET vessel.

The choice of the control set Y to be included in the control loop is quite important. The gaps have to be selected such as the matrix T in equation (10) is far from being singular. In addition there is the need to guarantee that large variations in the plasma current profile parameters do not lead to a wall contact between the controlled points.

The control set illustrated in the Table I is considered the optimum set for the control of the FAT configuration shown in Fig. 1. The control scheme is based on the on-line measurement of the plasma boundary distances from the wall and the X-point position using the XLOC algorithm [7]. This is a substantial change from the previous control system based on flux differences which could not directly control the boundary of a detached plasma [2].

In the simplest operation mode the plasma current, the outer gap and the inner gap at the machine mid plane, and the plasma current centroid vertical position (ZP) are included in the control loop. The X-point position is in this case left in open loop, while the divertor currents are controlled to be proportional to the plasma current (fig. 1). If β_p increases from 0.2 to 1.1 the plasma shape is mildly deformed near to the upper saddle coils. The X-point is moved radially inwards by order 6cm and vertically 1cm. Substantial peaking of the plasma current profile (l_i above 1.2) at high plasma current (5MA) leads to a fast rise in the current of the PFX amplifier which produces a strong quadrupolar field by producing a difference current in the primary inductor coils [2]. A strong increase in l_i can lead in any case to plasma-wall contact in the top part of the vessel.

Fast changes in β_p can cause transient plasma current errors up to 300kA for a β_p rate of change of $0.5s^{-1}$ in 1s.

Operation is improved by excluding the direct control of the divertor currents D2 and D3 [1] and including the couple of parameters X-point radius and X-point height (RX, ZX) or strike point radius , X-point height (RS, ZX). Simulations show that higher non linearities are present in the control of RS rather than RX. A current feedforward could be applied in this case. A decoupling matrix should be used to avoid reintroducing crosstalk.

In the choice of the control set the top gap is preferred to ZP when a full size plasma is obtained. The plasma current rise would on the contrary be preferably performed using the control of ZP.

Current saturation in the PF circuits is particularly dangerous for those loops which are in gap control. They correspond to losing a degree of freedom in the system and lead very soon (200-300ms) to instability. The control mode in such cases must be switched to current control of the circuit which has saturated. The direct control of the gap mostly affected by this circuit is abandoned. It can be resumed when the gap error changes its sign. The voltage limitations in the amplifiers on the contrary are not dangerous because they represent only a limitation in the speed of the response.

SIMULATIONS

Two simulations are presented here. The first one shows the sweeping of the X-point radius at a frequency of 4Hz with the setup shown in Table I for a FAT plasma configuration. The simulation is carried out on a time interval of 2s for a requested RX amplitude of 10cm. The model used for the simulation includes also a mismatch between the matrices used for the controller calculation (M_S and B_S at the nominal β_p = 0.2 and l_i = 0.9) and the one used in the plasma model (β_p = 0.2 and l_i = 1.1). It is worth noting that the time constant on the RX loop is chosen 10ms in order to cover the third harmonic of the triangular demand at 4Hz. The time constant on the ZX loop is chosen 100ms in order to let the divertor coils act as passive stabiliser for the vertical stabilisation. The compensated model of the PF generator is also included.

The uncontrolled quantities top gap and outer top gap are also shown to for comparison with the other feedback controlled gaps.

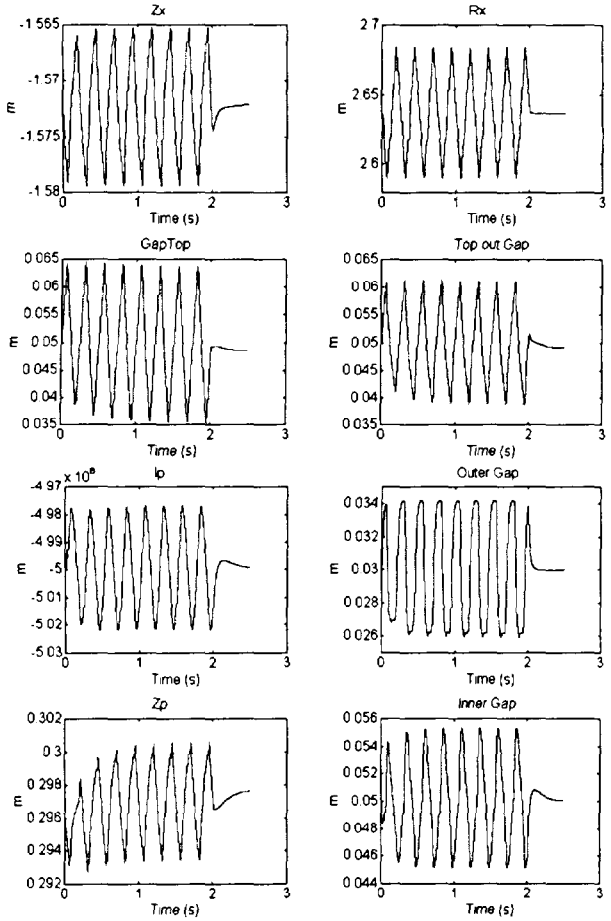

Fig.2 Simulation of X-point Sweeping with 4Hz triangular reference.

The second simulation shows a step applied to the radial position control with and without the cancellation in the terms of the matrix K. Here the different behaviour of ZP and the inner gap when their principal actuators are not excited by the gap demand is highlighted. The voltages in both cases are also shown. The continuos line represents the case with no cancellations and the dotted line the case with cancellations.

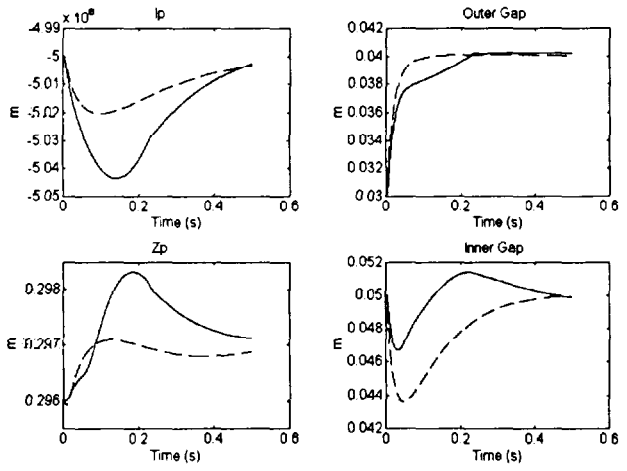

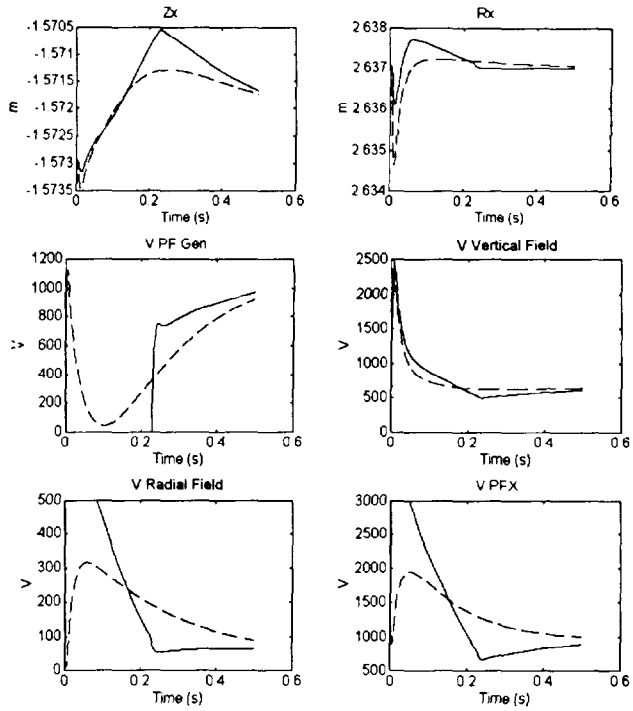

Fig. 3 Simulation of an 1cm external demand in the outer gap

CONCLUSIONS

We have presented a general method for the application of a non-interacting multivariable controller in a Tokamak. The introduction of gap control will allow a straightforward implementation of different operating scenarios for the JET divertor operation. The possibility of easily changing the operating mode will provide flexibility during the commissioning. The control scheme described represents a substantial improvement of the plasma shape control in JET by allowing a direct control of the plasma boundary at different locations and the inclusion of a number of PF coil currents in a multivariable decoupled scheme.

REFERENCES

[1] J. Last, P. Barabaschi, E. Bertolini, M. Garribba, M. Huguet, P. Noll, P. H. Rebut, C. Sborchia, The JET divertor magnetic configuration and coil design, Fusion Technology Proceedings of XVI SOFT, London 1990, pp. 1614-1618.

[2] E. Bertolini, P. L. Mondino, P. Noll The JET Magnet Power Supplies and Plasma Control Systems, Fusion Technology, January 1987, Vol 11, Number 1, pp.71-119

[3] R. Albanese, J. Blum, O. de Barbieri, Numerical Studies of the Next European Torus via PROTEUS Code, Proc. of XII Conference on Numerical Simulation of Plasmas, S. Francisco 1987.

[4] F. Franklin, G. Powell, M. Workman, Digital Control of Dynamic Systems, Addison-Wesley1990, pp. 238-322, pp. 430-441.

[5] G. Marchesini, E. Fornasini, Appunti di Teoria dei Sistemi, Progetto Padova, 1985.

[6] P. Silvestrin, Digital Control of the Plasma Current in JET, Phd Thesis, 1985.

[7] D. O'Brien, J. J. Ellis J. Lingertat, Local Expansion Method for Fast Boundary Identification at JET, Nuclear Fusion 33, 467 (1993).

Installation and Inactive Commissioning of the JET Active Gas Handling System (AGHS)

J L Hemmerich, A C Bell, P Boucquey, C Caldwell-Nichols, P Chuilon, F Delvart, B Grieveson, R Haange, G Jones, R Lässer, M Laveyry, J Lupo, J Mart, P Milverton, J-L Salanave, L Serio, N Skinner, R Stagg, K D Walker, J Yorkshades, A Konstantellos[1], E Küssel[2].

JET Joint Undertaking, Abingdon, Oxon, OX14 3EA.
[1] EEC DG XII, Brussels, Belgium.
[2] KFA Jülich, Germany.

Installation and Inactive Commissioning of the JET Active Gas Handling System (AGHS)

J L Hemmerich, A C Bell, P Boucquey, C Caldwell-Nichols, P Chuilon, F Delvart, B Grieveson, R Haange, G Jones, R Lässer, M Laveyry, J Lupo, J Mart, P Milverton, J-L Salanave, L Serio, N Skinner, R Stagg, K D Walker, J Yorkshades, A Konstantellos[1], E Küssel[2]
JET Joint Undertaking, Abingdon, Oxon, OX14 3EA
[1]EEC DG XII, Brussels, Belgium
[2]KFA Jülich, FRG

ABSTRACT

The installation of all AGHS subsystems in compliance with a strict Quality Assurance Programme[1] was completed in 1993. Installation was followed by end-to-end commissioning of signal and control loop connections to the Distributed Control System (DCS)[2]. Plant layout and function are described and results of process tests with hydrogen, deuterium and other test gases are presented. These tests have revealed some minor deficiencies on the subsystems for Cryogenic Distillation, Exhaust Detritiation and Impurity Processing which have been or are in the process of being resolved prior to commissioning with tritium, initially 3g of T_2, due to start in 1994.

Some recent developments are presented:

- adiabatic calorimetry on Uranium Beds (U-beds) in the AGHS Hydrogen Isotope Storage Assemblies (HISA) permitting *in situ* measurement of tritium inventory;
- isothermal calorimetry for accurate input and tritium purity measurement with high resolution and repeatability;
- a novel regeneration method for the molecular sieve dryers of the Exhaust Detritiation System together with a method to demonstrate the expected improved performance by reliable humidity measurement to dewpoints of -100°C or lower.

INTRODUCTION

The JET AGHS was designed for the JET tritium operations phase to handle a daily throughput of up to 5 moles of T_2 together with 15 moles of D_2 and 150 moles of H_2. JET torus operation will result in a variety of mixtures of these hydrogen isotopes together with additions of ^4He as the main D-T fusion reaction product and impurities resulting from plasma-wall interaction. The impurities consist mainly of tritiated water Q_2O and tritiated hydrocarbons C_xQ_y, in particular methane CQ_4, where Q_y stands for any combination of the hydrogen isotopes HDT. The AGHS receives these mixtures and produces pure T_2 and D_2 for recycling to the torus. The main aim of these operations is to minimise the release of tritium to the environment and to avoid production of tritiated waste.

I AGHS CONFIGURATION AND COMMISSIONING STATUS

Fig 1 presents the AGHS plant layout with the main interconnections between subsystems. The present status of each subsystem is indicated by percentage numbers:

- the left hand number indicates the degree of completion of installation, including the completion of statutory leak and pressure tests;
- the middle number indicates the state of completion of end-to-end signal and control loop tests;
- the right hand number indicates the state of process commissioning without tritium.

A more detailed account is given in the following.

A Cryogenic Forevacuum (CF)

The CF system[3] uses a combination of 77K coldtraps, 77K adsorbers, 4K cryocondensation, 4K cryosorption and 20K distillation to pump all gases arising from torus operations and to separate them into pure Q_2 mixtures and impurities (Q_2O, C_xQ_y, ^4He). Process installation and control connections are complete. First cryogenics tests with LN_2 and LHe have been successfully completed, process tests with gas mixtures to measure pumping speeds and separation efficiency are in progress.

B Impurity Processing (IP)

The IP system[4] receives impurity mixtures (Q_2O, C_xQ_y, ^4He) mainly from CF with occasional inputs from the Mechanical Forevacuum system (MF) during torus wall conditioning by glow discharge cleaning with ^4He and gas samples after analysis in the analytical glove box (AN). IP processes impurity mixtures in ^4He carrier gas with O_2 addition by catalytic recombination to Q_2O, collection of Q_2O on a 160K coldtrap, subsequent reduction of Q_2O on hot iron beds and collection of Q_2 on U-beds. Q_2 is transferred to Intermediate Storage (IS) for subsequent isotopic separation, detritiated impurities (mainly CO_2 in ^4He carrier) are vented to stack via MF and Exhaust Detritiation (ED). The IP system is fully installed and tested. A deficiency in processing speed (only 20% of the intended mass flow rate through the catalytic

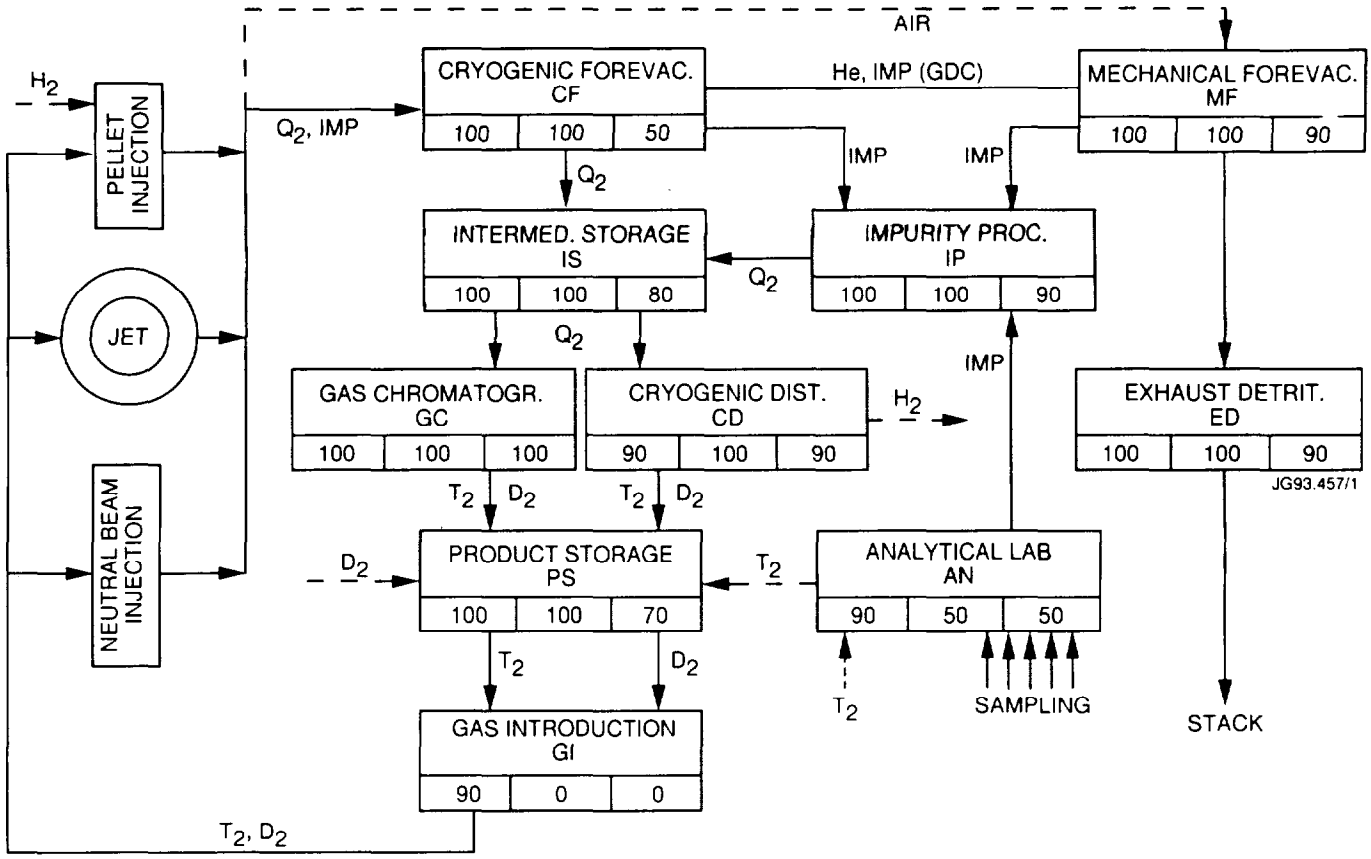

Fig 1 Overall AGHS flow diagram. The numbers indicate (in percent from left to right) the completion status of installation, control system connection and process testing with H_2 and D_2.

recombiner) can either be accommodated due to the fact that the actual amount of impurities produced in torus operation is now expected to be only 10 to 20% of the original design value or by replacing the recombiner module with a design comprising sinter filters of larger surface area.

C Intermediate Storage (IS)

The IS system uses four U-beds[5] with a maximum of 27 moles each sorption capacity for Q_2 to receive Q_2 mixtures from CF and IP at low pressures and to supply Q_2 at a constant pressure of 140kPa to the subsequent isotope separation system. The U-beds have been activated showing the full expected sorption capacity and reliable control at constant temperature as well as at constant pressure. Operating in the constant pressure mode (feedback control of heater via pressure signal), the bed temperature is monitored simultaneously and, upon reaching a maximum temperature ($T_{max} \approx 800K$) with the delivery pressure starting to droop, the U-bed is known to be nearly empty. Another U-bed with sufficient Q_2 inventory is then selected for delivery.

D Cryogenic Distillation (CD)

The CD system[6] comprises of three distillation columns with the necessary recirculating streams through catalytic equibrators at room temperature to separate the full AGHS design throughput (see introduction). Difficulties were encountered with the pumps driving the recirculating streams: transpiration pumps proposed by JET[5] built with metal sinter filters were found to cease operation when pumping H_2/D_2 mixtures rather than pure isotopes. This was found to be due to isotopic enrichment of the less volatile (D_2) species on the high pressure (heated) side of the sinter filter leading to a rise in boiling point and, eventually, to loss of the full heating power by thermal conduction to the low pressure outer side containing liquid at lower D_2 concentration. The problem was resolved by replacing the transpiration pumps with conventional hydrostatic syphon pumps, which however, will lead to a slight increase of T_2 inventory of CD in full operation (from ~30g T_2 to ~33g T_2). The performance for H/D separation was found satisfactory: H_2 purity at top of Column 1 was 99.9995% (with D_2 at or below the detection limit of the analytic equipment used) and D_2 purity at the bottom of Column 3 was 99.97%. A more detailed account of these tests will be given later[7]. In the meantime, further

tests have shown that use of transpiration pumps built with low thermal conductivity ceramic sinter filters could provide superior performance in pumping isotopic mixtures at minimum liquid inventories[8].

E Gas Chromatographic Separation (GC)

The GC system is fully installed and commissioned for separation of H/D mixtures. A detailed account on design, function and performance will be given at this conference[9].

F Product Storage (PS)

The PS system comprises one HISA with 4 U-beds (maximum capacity 7.5 moles Q_2) for T_2 storage and one HISA with 4 U-beds (maximum capacity 27 moles Q_2) for D_2 storage together with assay tanks for T_2 (100ℓ vol) and D_2 (600ℓ vol) for PVT inventory measurements. A recirculating system comprising a 15m^3/h Normetex and a metal bellows pump serves to remove ^{3}He arising from T_2 decay which would otherwise prevent T_2 sorption on U-beds due to its blanketing effect.

The system is fully installed, U-beds have been activated with D_2 and tested for temperature/pressure control.

G Gas Introduction (GI)

The GI system distributes T_2 and D_2 from PS to the various users. It contains calibrated volumes permitting to account by the PVT method for gases delivered to eight individual user lines, which are presently terminated in a valve box near the torus.

The system is installed but will not be included in tritium tests pending installation of all final user lines to torus, neutral beam and pellet injectors.

H Analytical Laboratory (AN)

The AN system serves three major purposes:

- analysis of process gases through a variety of sampling lines from several subsystems (IP, IS, GC, CD, MF, GI) using an analytic gas chromatography system[10] and omegatron[11] and quadrupole mass spectrometers;

- continuous monitoring of CD product purity, mainly T content in H_2 via an ionisation chamber, H_2 and D_2 purity via comparison to pure H_2 and D_2 reference gases in dedicated thermal conductivity detectors. A method for tritium purity monitoring by a calorimetric method is under development (see chapter "Recent Developments");

- tritium make-up, ie connection of and transfer from small transportable U-beds containing up to 5g T_2 to PS or IS depending on the result of a purity measurement. Tritium inventory received will be assessed by the PVT method in the PS-T_2 assay tank and the purity analysed in AN or (see chapter "new developments") by isothermal calorimetry of the transport bed as received.

The AN glovebox is fully installed, the omegatron mass spectrometer has been extensively tested with H_2, HD, D_2, ^{3}He and ^{4}He, the GC system has been extensively tested with all specified test gas mixtures including small amounts of tritiated species[10]. Integrated system tests are in progress.

I Mechanical Forevacuum (MF)

The MF system comprises one Normetex pump of 600m^{3}h^{-1} and two Normetex pumps of 150m^{3}h^{-1} nominal pumping speed. This system will be used for torus roughing, discharging to Exhaust Detritiation (ED) and for ^{4}He pumping (including tritiated impurities) during torus glow discharge cleaning, discharging to IP for recovery of tritium. The system has been fully installed and tested with ^{4}He and N_2. Another part of the MF system, an on-line analytical station, is foreseen to measure tritium concentration (based on the experience gained in the JET First Tritium Experiment[12]) in gas batches arriving from the torus systems and to detect the pressure of combustible mixtures by a PVT method prior to compression by CF to exclude the hazard of explosive mixtures. The method employed measures the pressure of a gas sample at 77K in a 1ℓ volume at the (low) delivery pressure before and after heating an internal platinum filament to 600°C. Due to the negligible vapour pressure of Q_2O at 77K, each O_2 molecule recombining with $2Q_2$ molecules will lead to a pressure drop after recombination, eg for 1% O_2 in Q_2 the pressure will drop by 3%. Mixtures with excessive O_2 content can then be processed differently using activated charcoal adsorbers in CF[3]. This detection system is installed and ready for testing.

J Exhaust Detritiation (ED)

The main purpose of ED[13, 14] is to prevent major tritium emissions in case of torus systems up-to-air accidents and during torus maintenance operations which require venting to atmospheric pressure and opening for access. Its throughput of 500m^{3}h^{-1} was designed to maintain air inflow at a speed of $\geq$1ms^{-1} into a torus main horizontal port (remote handling access) at continuous duty. The system comprises a catalytic recombiner for Q_2 at 150°C, CQ_4 at 500°C and three subsequent molecular sieve dryers collecting the resulting Q_2O, alternating in adsorption, regeneration and standby. Q_2O is collected in a 5m^3 holding tank, the disposal route depending on tritium concentration. The system was installed and commissioned in 1991/92[14] including tests for CH_4 combustion efficiency: recombiner temperatures were gradually raised in steps of 10°C. At each step a 1 minute pulse of 1% methane was added to the once-through air flow of 500m^{3}h^{-1} and the ED outlet analysed by gas chromatography[10] immediately after the methane pulse. CH_4 combustion started at ~270°C recombiner temperature. At 350°C recombiner temperature combustion was virtually complete (99.7%). At the design recombiner temperature of 500°C, the design value (detritiation factor DF $\geq$1000) is well achieved (CH_4 below detection limit of ~100ppm). Only tritiated methane with its much lower detection limit would allow accurate measurements at design conditions.

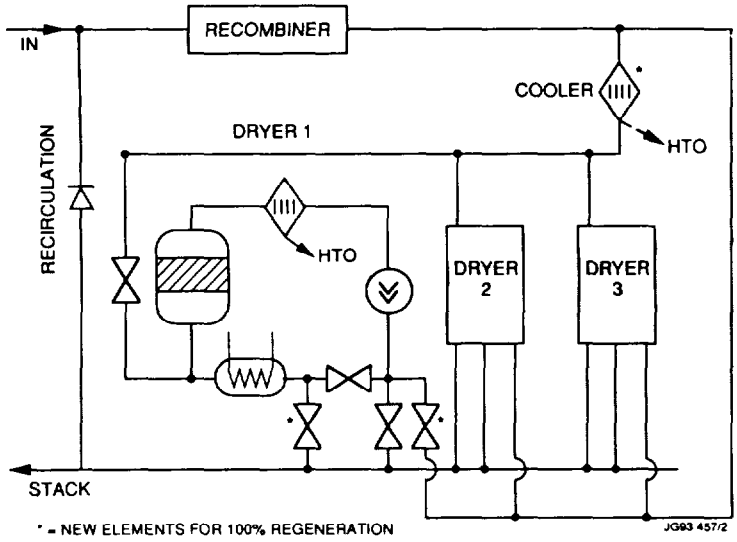

Fig 2 Exhaust Detritiation system after addition of new components.

The molecular sieve dryers reached their design value of outlet dewpoint -60°C, corresponding to a humidity concentration of ≤10ppm (vol), again to achieve DF ≥1000 for inlet humidities in the order of 10000ppm (vol).

A subsequent analysis[15] showed that a major improvement in dryer performance is possible: the present regeneration method leaves ~3% Q_2O (by weight) on the molecular sieve; by "borrowing" a flow of dry air from the systems outlet manifold during the final phase of regeneration, this residual humidity can be shifted to an additional cooler and the adsorbing dryer to produce a fully regenerated molecular sieve with a potential outlet dewpoint ≤-100°C, ie outlet humidity ≤0.01ppm (vol). These modifications have recently been implemented and recommissioning of the system is in progress. The flow diagram of the modified system is shown in Fig 2, the additional components (valves, lines, cooler) are highlighted by asterisks.

II RECENT DEVELOPMENTS

A Hygrometry

The demonstration of the expected enhanced performance of the modified ED system will require reliable measurements of dewpoints to ≤-100°C (apart from using undesirably large amounts of tritium). Our experience has shown that manufacturers' claims for sensitivity and accuracy of humidity sensors in this very low dewpoint range have to be treated with caution. To overcome this problem, we have developed a humidity generator ("Hygrostat"[16]) permitting sensor calibration *in situ*. This device is based on the principle that air or other gases are recirculated through a counterflow heat exchanger and a heavy isothermal copper block with large internal surface area -copper wool- saturated with H_2O in form of ice. The recirculated air contains humidity in equilibrium with the surface temperature, the dewpoint is directly obtained by measuring the block temperature. This device is schematically shown in Fig 3. The humidity sensor is either connected to the process, measuring its humidity with valves

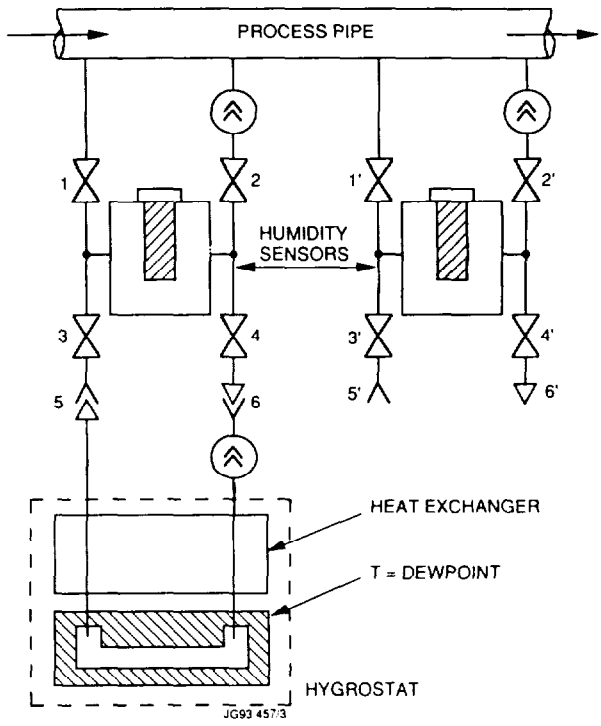

Fig 3 Schematic of humidity sensors in the Exhaust Detritiation system with on-line calibration facility.

1 & 2 open or to the Hygrostat for calibration with valves 3 & 4 open. The mobile calibration device can be connected to other process sensors in different plant locations via couplings 5 & 6. Employing this method will permit us to optimise plant operation prior to tritium commissioning.

B Adiabatic Calorimetry

The JET U-beds[5] are typically arranged in groups of four in secondary containments under high vacuum[17] (pressure ≤1 x 10^{-6}mbar). As a result, their ideal thermal insulation permits tritium inventory measurement by adiabatic calorimetry. Tests with ohmic heating (10W, corresponding to ~30g T_2) have shown that tritium inventories of 30g T_2 can be measured with 1% accuracy. The accuracy and repeatability are typically limited by fluctuations and drift of the ambient temperature. We are presently working on a method to compensate for external temperature fluctuations by suitable data analysis procedures (probably Fourier transform) with the expectation of improving the repeatability by one order of magnitude (30g T_2 to ±0.1%). Results will be published after completion of these further tests.

C Isothermal Calorimetry

In 1992 we started to test a commercially available thermoelectric calorimeter[a] for the purpose of tritium

[a] Model CR.-100-SP, Manufacturer: ITI, Delmar, Ca

inventory measurements on as-received transport U-beds, containing up to 5g T_2. The repeatability limit of this device was found to be ±3mW corresponding to ±3.7TBq (±100Cie). For a 5g T_2 inventory with 1.62W decay heat, this accuracy of ±0.2% is satisfactory in view of the accuracy (±0.3%) to which the decay heat of tritium is known[18]. The basic elegance and simplicity of this method induced us to consider further applications, for example: given a known amount of gas (by PVT method), its decay heat output measured calorimetrically will give its tritium content and hence could be used to measure tritium concentration in mixtures with other hydrogen isotopes. Ideally, this should enable us to measure on-line tritium purity from isotope separation systems, in particular CD. Clearly, the sample size required is inversely proportional to the repeatability of the calorimeter in absolute terms.

Realising that the repeatability of calorimetric measurements is directly related to the temperature stability of its environment (the originally measured repeatability of ±3mW was achieved by using an industrial thermostat with a temperature stability of $\pm 0.02 K h^{-1}$), we developed a novel temperature stabilisation method[19], which improved the repeatability of the same calorimeter to ~ ±10μW. A sample of ~50cm^3 at room temperature and atmospheric pressure would be sufficient to measure tritium purity to ±0.3%. The further development of this method will be reported after completion of present tests.

The development of calorimetry had the prime aims of improving the accuracy of tritium measurement and of measuring the tritium discharged from U-beds in the configuration used in the first Tritium Experiment. It should be noted that the accuracy of tritium accounting within a fusion fuel cycle is determined by the precision of measurement or assessment of bound tritium, particularly in the tokamak walls. Uncertainties of the order of grams are likely and this, rather than the precision of inventory measurement in individual components, will determine the feasibility and value of "safeguards" accounting.

SUMMARY

The JET AGHS is now fully installed and most subsystems have been or are being commissioned with hydrogen, deuterium and other test gases.

The present phase will be completed by the end of 1993, to be followed by a short assessment of H/D results and subsequent start of commissioning with tritium in 1994. With the major part of tritium-related process monitors (ionisation chambers) already satisfactorily tested and used during the JET First Tritium Experiment[12], we expect no major problems during tritium commissioning.

REFERENCES

1 P Chuilon, A C Bell, J L Hemmerich "Experience in the Installation Programme of the JET Active Gas Handling System" Fus Tech 21, 359 (1992)

2 A Konstantellos, J L Hemmerich, A C Bell, J Mart, J Yorkshades, K Walker, N Skinner, G Jones, F Delvart "The JET Active Gas Handling Plant Process Control System" Fus Tech 21, 365 (1992)

3 E Küssel, G Gowman, J L Hemmerich, K Walker, "The Cryogenic Forevacuum System for the JET Active Gas Handling Plant" Fus Tech 14, 552 (1988)

4 J L Hemmerich, A Dombra, C Gordon, E Groskopfs, A Konstantellos, "The Impurity Processing Loop for the JET Active Gas Handling Plant" Fus Tech 14, 557 (1988)

5 J L Hemmerich, A Dombra, J Gowman, E Groskopfs, R Haange, A Konstantellos, E Küssel, R Lässer, P Milverton, K Walker, K Walter "Key Components of the JET Active Gas Handling System - Experimental Programme and Test Results" Fus Eng Des 11, 93 (1989)

6 D Ulrich, P Chromec "Process and Safety Aspects of the Cryogenic Distillation System to Process Hydrogen Isotope Feeds at JET" Fus Tech 21, 891 (1992)

7 P Boucquey et al "JET AGHS Cryodistillation Commissioning without Tritium" to be published

8 J L Hemmerich, P Milverton "Ceramic Transpiration Pumps for Recirculation/Recycle Loops in Cryodistillation Systems" UK Patent Application 9310463.6 (1993)

9 R Lässer, et al "Protium-Deuterium Separation with the Preparative Gas Chromatographic System at JET", this conference

10 R Lässer, B Grieveson, J L Hemmerich, R Stagg, T Dowhyluk, K Torr, R Massey, P Chambers "The Gas Chromatographic Analysis System in the JET Active Gas Handling Plant" Rev Sci Instr 64 (9) Sept 1993

11 H Gentsch "Inertes Zyklotronresonanz-Massenspektrometer (Omegatron)" Vakuum Technik, Heft 6/7, p 224 (1987)

12 M Huguet et al "Technical Aspects of the First JET Tritium Experiment" Fus Eng Des 19, 121-178 (1992)

13 A H Dombra, M E P Wykes, J L Hemmerich, R Haange, A C Bell "Exhaust Detritiation System for JET" Proc 15th Symp Fus Tech Utrecht 1988, p 1301, Fusion Technology 1988, Elsevier Science Publishers (1989)

14 D P Wong, J L Hemmerich, J J Monahan "The Exhaust Detritiation System for the JET Active Gas Handling Plant - Engineering, Construction, Installation and First Commissioning Results" Fus Tech 21, 572 (1992)

15 J L Hemmerich "A Systematic Approach to the Design of a Large-Scale Detritiation System for Controlled Thermonuclear Fusion Experiments" Fus Tech 24, 137 (1993)

16 J L Hemmerich, P Milverton "Hygrostat - A Calibration Device for Humidity Sensors" UK Patent Application 9310464.4 (1993)

17 P R Ballantyne, A C Bell, J L Hemmerich "The Design Features of Secondary Containments for the JET Active Gas Handling System and their Role in mitigating both Chronic and Accidental Releases" Fus Tech 21, 483 (1992)

18 P C Souers "Hydrogen Properties for Fusion Energy", Univ of Cal Press, Berkeley and Los Angeles, CA (1986)

19 J L Hemmerich, L Serio, P Milverton "Thermostatic Method and Device" UK Patent Application 9315687.5 (1993)

Protium–Deuterium Separation with the Preparative Gas Chromatographic System at JET

R Lässer, F Botter[1], J L Hemmerich, M Laveyry, J Lupo, P Milverton, R Stagg, S Tistchenko[1], K D Walker, J Yorkshades.

JET Joint Undertaking, Abingdon, Oxon, OX14 3EA.
[1] Commissariat a l'Energie Atomique-Centre de Saclay–DTA/CEREM/DTM/SERC, 91191–Gif sur Yvette Cedex, France.

PROTIUM-DEUTERIUM SEPARATION WITH THE PREPARATIVE GAS CHROMATOGRAPHIC SYSTEM AT JET

R Lässer, F Botter*, J L Hemmerich, M Laveyry, J Lupo, P Milverton, R Stagg, S Tistchenko*, K D Walker, J Yorkshades
JET Joint Undertaking, Abingdon, Oxfordshire OX14 3EA, United Kingdom,
*Commissariat a l'Energie Atomique-Centre de Saclay-DTA/CEREM/DTM/SERC,91191 - Gif sur Yvette Cedex (France)

ABSTRACT

The design of the preparative gas chromatographic (GC) hydrogen isotope separation system at JET, the process of displacement chromatography and the results of the commissioning phase with inactive gas mixtures of protium and deuterium are presented. The GC system meets fully the specifications for isotope separation. Protium and deuterium concentrations in the Pd filled column can be calculated by means of a simple program which simulates the gas chromatographic process.

INTRODUCTION

During the tritium operation phase of JET the hydrogen isotopes (deuterium (D) and tritium (T)) will be injected into the torus. In the Active Gas Handling (AGH) plant[1-3] the exhaust gases (mainly unburnt hydrogen, helium ash and impurities (hydrocarbons, water, etc) will be collected, purified, isotopically separated into pure D_2, T_2 streams and recycled to the torus.

In the AGH plant two isotopic separation systems will be used: i) Gas Chromatographic (GC) system[4] for a maximum daily gas feed of 30g tritium and 60g deuterium and ii) Cryogenic Distillation (CD) system[5, 6] for a maximum gas feed of 30g tritium, 60g deuterium and 300g protium (the latter being used as driver gas for high velocity tritium or deuterium targets).

This paper presents the design of the GC system with the incorporated safety measures and commissioning results obtained with inactive gas mixtures. In addition, a computational method will be sketched which allows the simulation of the hydrogen isotope separation system.

I PRINCIPLE OF HYDROGEN ISOTOPE SEPARATION

For hydrogen isotope separation, differences in the physical properties of the isotopes between two phases (CD: liquid-vapour, GC: gas-packing material) are exploited. The following packing materials have been used for gas chromatographic hydrogen isotope separation: molecular sieve or alumina at around 77K or metal hydrides in the temperature range between 250 and 800K.

At JET it was decided to use palladium as the packing material due to its unique properties in connection with hydrogen: a) high diffusion coefficient; b) high isotope separation factor; c) high isotope exchange rate; d) equilibrium pressures in an easily accessible range for temperatures between 270 and 450K; e) catalytic surfaces not easily poisoned even in the presence of high level of impurities (there are no stable oxides in the presence of hydrogen); f) absorbed hydrogen can easily be desorbed at moderate temperatures of about 500K. The isotope separation factor S_{DH} (defined as the ratio of the D and H concentrations in the gas phase divided by the ratio of the D and H concentrations in the metal hydride phase) in the β-palladium hydride (PdQ_r, Q=H, D, T) phase is large due to the fact that the equilibrium partial pressure of the heavier hydrogen isotope is greater than that of the lighter one at equal conditions. The potential well for the vibrating hydrogen atom in β-PdQ_r is much broader and flatter than the corresponding well for the hydrogen molecule[7]. The ground state vibrational energies in the β-PdQ_r are thus smaller than in the gas phase. Therefore, more energy is gained during the absorption of a protium atom than of a deuterium atom. This favours the absorption of light hydrogen atoms in comparison to heavier ones and, if a hydrogen isotope mixture is forced through a Pd packed column, the heaviest hydrogen isotope tritium will exit before deuterium and protium.

II THE PREPARATIVE GC SYSTEM AT JET

Fig 1 shows a simplified flow diagram of the JET preparative GC system. A separation cycle can be divided into 5 steps: a) injection of the hydrogen isotope mixture to be separated into the evacuated or preferably helium filled column; b) displacement of the hydrogen mixture via the eluant gas (mainly pure protium (H)) supplied from one of the uranium (U) beds (U-bed 3 or U-bed 4), which is heated to about 700 K; c) observation of the pure product streams T_2, D_2 and of the interfractions (He + T_2), (T_2 + TD + D_2), (D_2 + DH + H_2) and switching of the corresponding valves V12, V13 to pure

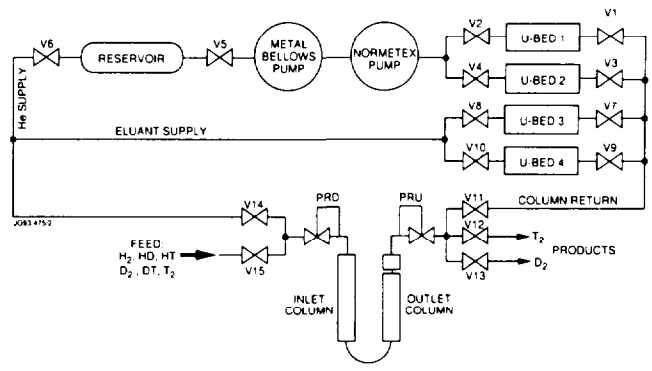

Fig 1 Simplified flow diagram of the GC system: U-bed means uranium bed, V valve, PRD (PRU) down (up) stream pressure regulator

tritium and deuterium product lines; d) evacuation and heating of the column to desorb the eluant H_2 and its absorption in a cold U-bed (U-bed 4 or U-bed 3) and e) circulation of helium through the columns via Normetex- and metal bellows pumps for efficient removal of eluant, its gettering in U-bed 1 or U-bed 2 and storage of helium in the reservoir.

Fig 2 presents the protium and deuterium concentrations of the gas phase inside the Pd filled column after partial injection of a 40 vol% H/ 60 vol% D mixture, after partial eluant

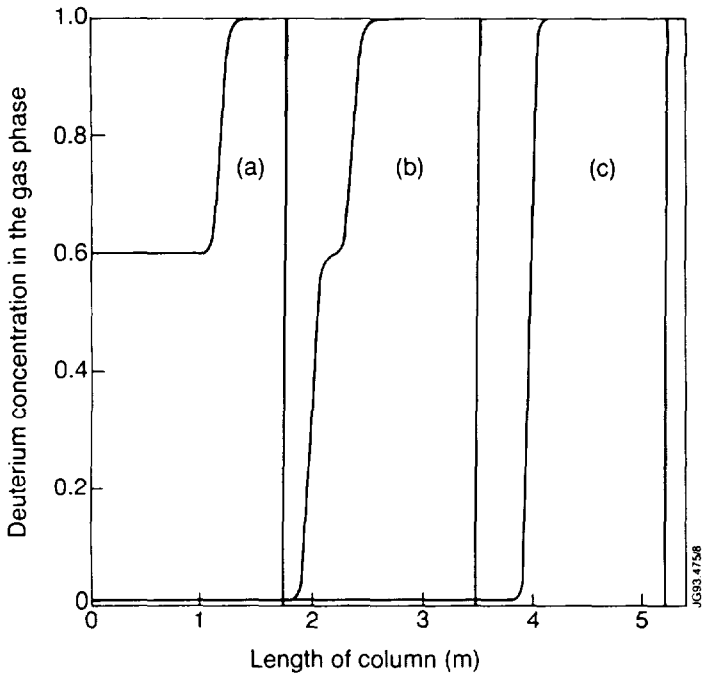

Fig 2 Calculated deuterium (x_D) and protium ($1-x_D$) concentrations in the gas phase inside the Pd packed column with 150 barℓ hydrogen capacity after: a) partial injection of a 60 barℓ, 40 vol% H/ 60 vol% D gas mixture, b) partial displacement with 99 vol% H/ 1 vol% D eluant and c) almost full separation

displacement and after almost full displacement. Isotope separation and enrichment of deuterium in the gas phase already partially occurs during injection.

III DESCRIPTION OF SELECTED PARTS OF THE GC SYSTEM

The columns (total length: 5.4m, inner diameter: 34mm) were packed with material supplied by CEA, France. The main characteristics of the packing[8] are: 18 weight% palladium deposited on porous α-Al_2O_3, capacities: 27.5 (15.7) barcm^3 hydrogen per 1cm^3 (1g) of Pd-packing.

Four columns (every column consists of an inlet and an outlet column, which are connected via a pigtail at the bottom) are mounted inside a large secondary containment (4.5m height by 1.2m diameter) which is divided by a bulkhead into two closed volumes. The upper volume contains the valves, diagnostics, feedthroughs and process connections to the columns and is filled with He. The lower volume is evacuated to avoid heat losses due to thermal convection. The heating and cooling of the columns is done with a special high temperature oil which flows around the columns between two further concentric tubes. A 1mm gap between the column tube and the inner oil tube is only open to the upper volume at the top, where the inner oil tube is welded to a penetration flange in the bulkhead. At the bottom, the column tube and the inner oil tube are connected. This design assures that movement of the column heads with all connecting pipes at the top of the columns in the upper volume due to thermal expansion is minimised and that direct permeation from the process gas into the oil circuit is excluded. The other parts of the columns are hanging freely in the lower volume, where the oil connections are made via flexible metal hoses. Thus, the columns are not subjected to thermal stresses during temperature cycling.

The uranium beds are of the standard JET AGH plant design[2]. Each bed contains 18 moles uranium and can store up to 27 moles hydrogen gas (640 barℓ).

IV DIAGNOSTICS CONNECTED TO THE COLUMN HEADS

The connections to the external gas loops are made via 44 x 44 x 290mm^3 stainless steel blocks mounted to the top of the inlet and outlet columns. These blocks (a cross section of an outlet head block is shown in Fig 3) function as manifolds (4mm diameter bores for the gas flow) with a total

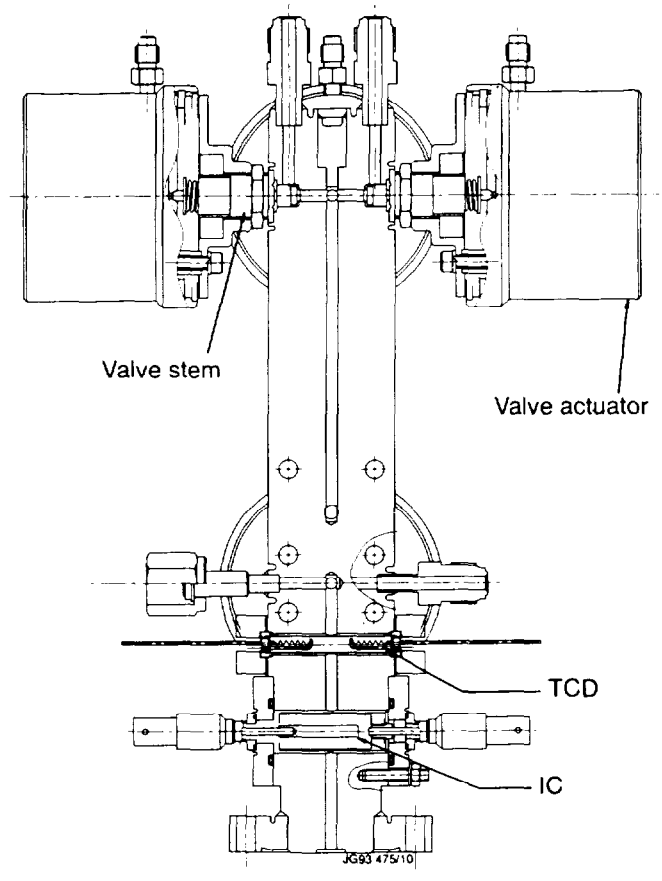

Fig 3 Cross section of outlet head showing katharometer (TCD), ionisation chamber (IC), valves and valve actuators

dead volume (<30cm^3) and contain valve seats (only the valve stems were purchased from Nupro[a] and welded to the block), pressure gauges, flow meters, ionisation chambers (IC) and thermal conductivity detectors (TCD or katharometers) to characterise the separation process and support down and up stream pressure regulators and JET all metal valve actuators.

A Katharometer

The TCD consists of 4 matched rhenium tungsten filaments with two placed in the process gas and two in a reference gas. To avoid damage and cooling due to the large flows of up to 6 L/min, the filaments were shielded from the main gas flow by a stainless steel cylinder of 0.15mm wall thickness. One small inlet hole and two exit holes divert a small flow past the filaments. The fairly small and linear flow dependence of the katharometer signal is plotted in Fig 4 for pure protium and deuterium and allows the characterisation of the product purity at different flows. The TCD signal of a separated gas mixture can be seen in Fig 5.

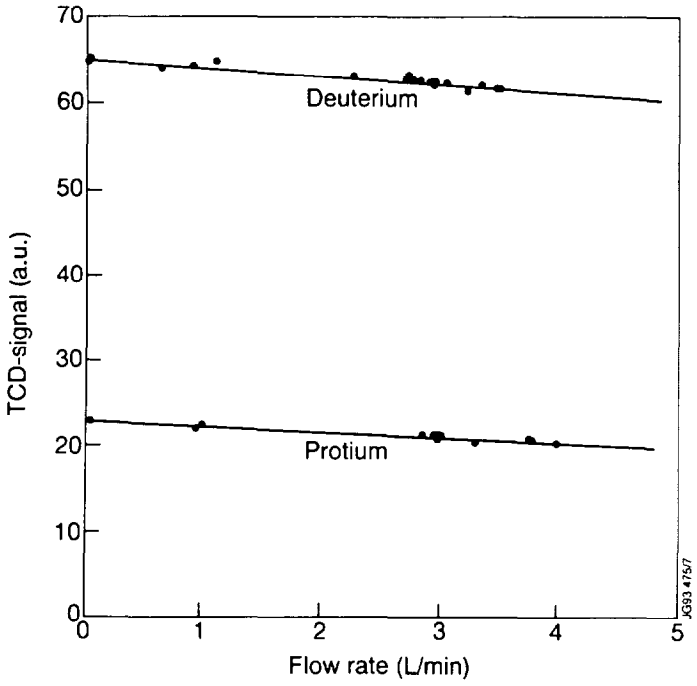

Fig 4 Katharometer (TCD) signal for deuterium and protium as a function of flow rate through the column

B Batch Fill Monitor

Two metal sheathed thermocouples (outside diameter: 0.5mm) were connected to the inlet column tube at half height in the 1mm gap mentioned above to detect the arrival of the hydrogen front in the Pd packing via the exothermal absorption heat created. The increase of this temperature (see Fig 5) can be used as a trigger to switch from gas mixture supply to eluant injection. The thermocouples show also a small temperature rise when the deuterium/protium front arrives because the heat created by the absorption of protium is higher than for deuterium.

C Thermopile

Near the exit of every column a thermopile consisting of 12 sheathed thermocouples (0.5mm outer diameter) with insulated junctions is mounted. The thermocouple tips are in direct contact with the packing to achieve a fast response. The thermopile gives a signal during the time needed by the hydrogen to pass from the lower six to the upper six junctions, which are 6cm apart. See Fig 5.

D Down and Up Stream Pressure Regulators

All metal down and up stream pressure regulators[2] hold the pressures at the column inlet and outlet at preselected values and allow to adjust the flow rate through the column via the selected pressure drop.

V RESULTS OF ISOTOPE SEPARATION RUNS WITH THE GC SYSTEM

The following gas mixtures were studied: 50 vol% H/ 50 vol% D; 70 vol% H/ 30 vol% D; 90 vol% H/ 10 vol% D; and 98 vol% H/ 2 vol% D. The injected gas amounts were varied between 4 and 104 barℓ. Flow rates between 0.5 and 5 L/min were used. During separation the oil temperature was kept constant at about 320K. D_2 purity better than 99.5 vol% was achieved in all separation runs with a good choice of parameters. If the columns were prefilled with helium, helium concentrations below 0.2 vol% were found in the first sections of the D_2 product. Flow rate variations between 0 and 10

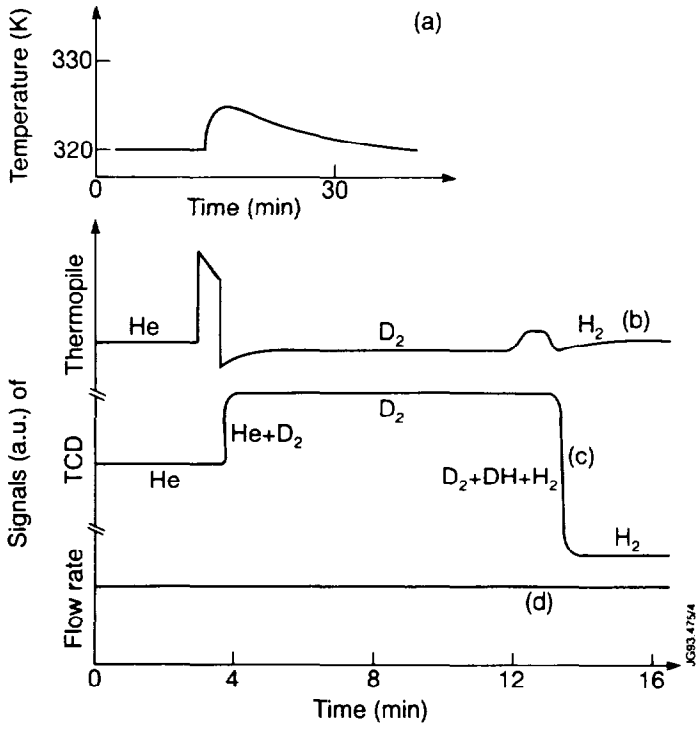

Fig 5 Signals of a) batch fill monitor; b) thermopile; c) katharometer (TCD); d) flow meter measured during an isotope separation run

[a] Nupro Company, Ohio 44094

L/min seemed not to upset the separation process. Also temperature changes of +/- 10K had no observable influence on the separation quality (this is not too surprising because every separation process itself creates temperature gradients due to the exothermic heat generated during absorption). Sharp transitions from helium to deuterium and from deuterium to protium were observed in the gas streams exiting the columns. Minor differences in the sharpness of the transitions were observed between the four columns and are probably caused by different batches of the Pd packing. The size of the (D_2 + DH + H_2) interfractions varied between 0.3 to 0.6 barℓ for the 4 columns and is independent of the HD amount in the injected gas mixture. The independence is a consequence of the atomic solubility of hydrogen in metals and gives pure protium, deuterium and tritium products at the expense of the interfractions HD, HT and DT.

VI CONTROL SYSTEM

The separation runs were performed fully automatically with a distributed control system[9]. Gas mixtures were delivered from Intermediate Storage (IS) and the pure D2 stream sent to Product Storage (PS). IS and PS are two further subsystems of the AGH plant[3].

VII SIMULATION

A simple program was developed which allows the simulation of the separation in the Pd packing. The T, D, and H concentrations in the column during the separation and of the products as well as maximum amounts of gas mixtures to be separated can be calculated.

The column is subdivided into many equal cells. A gas amount of the mixture to be separated or of the eluant gas equal to the gas amount in the gas phase of the first cell is injected into the column and all other gas batches in the gas phase are displaced to the next cell. After calculation of the new isotopic equilibrium in the cells between the new H, D, T concentrations in the gas phase and the previous ones in the Pd by means of the isotope separation factor, the next injection and displacement can be performed. Simulation results are shown for the injection of 60 barℓ of a 40 vol% H/ 60 vol% D mixture in Fig 2.

VIII SAFETY

The GC system was designed to withstand all pressures occurring during normal and abnormal conditions and to achieve He leak rates with no detectable He leak in the 10×10^{-10}mbarℓ/s range. Only tritium compatible construction material is used in the process lines. All primary containments are surrounded by secondary containments[10].

Hardwired interlocks are provided for the most critical components, eg heaters, pumps, etc.

Software interlocks are used to stop actions or raise alarms in case of faulty or unsafe conditions.

IX CONCLUSION

The inactive commissioning phase of the preparative GC system shows that the GC system meets its specification for isotope separation to 100 percent. This displacement chromatography seems to be very robust and not sensitive to changes of most separation parameters such as flow, temperature, etc. The final step will be the test of the performance with gas mixtures containing tritium.

REFERENCES

[1] R Haange, J L Hemmerich, A C Bell, C Caldwell-Nichols E Groskopfs, A Konstantellos, E Küssel, M Tschudin, K Walter "General Overview of Active Gas Handling System at JET" Fus Tech 14, 461 (1988)

[2] J L Hemmerich, A Dombra, J Gowman, E Groskopfs, R Haange, A Konstantellos, E Küssel, R Lässer, P Milverton, K Walker, K Walter "Key Components of the JET Active Gas Handling System - Experimental Programme and Test Results" Fus Eng Des 11, 93 (1989)

[3] J L Hemmerich, A C Bell, P Boucquey, C Caldwell-Nichols, P Chuilon, F Delvart, B Grieveson, R Haange, G Jones, R Lässer, M Laveyry, J Lupo, J Mart, P Milverton, J-L Salanave, L Serio, N Skinner, R Stagg, K D Walker, J Yorkshades, A Konstantellos, E Küssel "Installation and Final Commissioning of the JET Active Gas Handling System (AGHS)" this conference

[4] F Botter, J Gowman, J L Hemmerich, B Hircq, R Lässer, D Leger, S Tistchenko, M Tschudin "The Gas Chromatographic Isotope Separation System for the JET Active Gas Handling System" Fus Tech 14, 562 (1988)

[5] D Ulrich, P Chromec "Process and Safety Aspects of the Cryogenic Distillation System to Process Hydrogen Isotope Feeds at JET" Fus Tech 21, 891 (1992)

[6] P Boucquey et al "JET AGHS Cryodistillation Commissioning without Tritium" to be published

[7] R Lässer "Tritium and Helium-3 in Metals" Springer Series in Materials Science 9, 1-159 (1989)

[8] F Botter, S Tistchenko, B Hircq "Separation of Hydrogen Isotopes by Displacement Gas Chromatography" Proc 16th Symp Fus Tech London 1990, p 713, FUSION TECHNOLOGY 1990, Elsevier Science Publishers (1991)

[9] A Konstantellos, J L Hemmerich, A C Bell, J Mart, J Yorkshades, K D Walker, N Skinner, G Jones, F Delvart "The JET Active Gas Handling Plant Process Control System" Fus Tech 21, 365 (1992)

[10] P R Ballantyne, A C Bell, J L Hemmerich "The Design Features of Secondary Containments for the JET Active Gas Handling System and their Role in mitigating both Chronic and Accidental Releases" Fus Tech 21, 483 (1993)

A New Coil Protection System for the Divertor Configuration at JET

V Marchese, J R Last, G Sannazzaro, L Scibile, J van Veen.

JET Joint Undertaking, Abingdon, Oxon, OX14 3EA.

A New Coil Protection System for the Divertor Configuration at JET

V. Marchese, J.R. Last, G. Sannazzaro, L. Scibile, J. van Veen
JET Joint Undertaking, Abingdon, Oxfordshire, OX14 3EA

ABSTRACT

The paper describes a new Coil Protection System (CPS) which is planned to be installed at JET before the next experimental campaign with a pumped divertor. The protection system will make circuit equation integration, computations of forces on and stress in the coils and check current and voltage levels and coil heating effects in real time. If acceptable values for any of these parameters are exceeded, the pulse will be terminated. A fully digital implementation of the algorithms is being designed using a high performance Digital Signal Processor (DSP). A programme has been written for convenient off-line calculation and checks of model parameters with JET data.

1. INTRODUCTION

The new CPS will detect electrical faults and protect the coils against mechanical or thermal overstressing due to operation outside safe limits. The motivation for the new CPS comes mainly from the newly installed divertor coils [1]. The existing short circuit detectors for toroidal and poloidal coils, based on voltage comparison between coil subassemblies and ampere-turn measurements (Rogowski), are not feasible for the divertor coils because each one is different and there is no space to install current and voltage transducers in the vacuum vessel. In order to make the system completely independent from the control system, new voltage and current transducers have been installed in most of the circuits. The voltage measurements are used for overvoltage protection and also as inputs to the poloidal and toroidal circuit models. The circuit inductance and resistance matrices are preset on the basis of the magnetic configuration. The poloidal field model includes a correction to take into account the variation of the plasma with time and the effect of the iron core whilst unsaturated. The computed currents are compared with the measured currents. A large difference would indicate a possible fault, an open circuit or a configuration error and would terminate the pulse.

The radial and vertical forces on the outer poloidal coils P2, P3 and P4 [2] and the vertical forces on the divertor coils are computed via coil flux loops and ampere-turns. Since vertical flux loops have not been fitted on the divertor coils because of lack of space, the radial forces acting on these coils will be computed analytically. The tensile and shear stress of each coil, assuming a uniform distribution, is computed as a linear combination of vertical force, radial force and I^2t. The coefficients are determined by mechanical analysis. The detection of some possible faults specific to the magnetising coil P1 will also be implemented in the new system [3].

A simplified model will be used to estimate the temperatures of the epoxy insulation and copper windings of the divertor coils. The inputs to the model are the vessel temperature, the coils case temperature, the coil currents, the coolant flow and the coolant inlet and outlet temperatures.

2. FAULT DETECTION ALGORITHMS

2.1 POLOIDAL CIRCUIT

The poloidal field (PF) includes up to n=10 independent circuits and up to m=22 coil elements as listed in Table 1.

TABLE 1: Poloidal Circuit and Coil Elements

Circuit		Coil Elements	Power Supply
1	P1End	P1EU, P1EL, P3MU, P3ML	PFGC
2	P1 Centre	P1CU, P1CL	PFX
3	Radial Field	P2UIR, P2LIR, P3UR, P3LR	FRFA
4	Shaping Field	P2UOS, P2LOS, P2UIS, P2LIS P3US, P3LS	PSFA
5	Upper Vertical Field	P4UV	VFA1
6	Lower Vertical Field	P4LV	VFA2
7	Divertor Field 1	D1	PDFA1
8	Divertor Field 2	D2	PDFA2
9	Divertor Field 3	D3	PDFA3
10	Divertor Field 4	D4	PDFA4

Legend: E=End, M=Magnetising, C=Central, I=Inner, L=Lower, O=Outer, R=Radial, S=Shaping

The circuit equations, in presence of a stationary plasma - Ip - (i.e., plasma centre in fixed position) are:

$$L_\theta \cdot \frac{dI_\theta}{dt} + R_\theta \cdot I_\theta = U_\theta$$

$$U_\theta = V_\theta - \left|L_{1p}\ L_{2p}\ \ldots L_{np}\right|^T \cdot \frac{dIp}{dt} \qquad (1)$$

where:

V_θ (n) - vector of the input voltages, I_θ (n) - vector of the computed PF circuit currents, L_θ (n×n) - circuit inductance matrix, R_θ (n×n) - circuit resistance matrix, L_{ip} - mutual inductance of the "i-th" circuit with the plasma.

The system inductance matrix, when the iron core is saturated, is computed as $C \cdot \Lambda \cdot C^T$ where "C(n×m)" is the configuration matrix and "Λ(m×m)" is the coil single turn inductance matrix. The direction of the currents in each coil element is specified in the configuration matrix by means of the sign of the relevant number of turns (n_i). The currents are assumed to be positive when flowing in anticlockwise as seen from the top of the machine.

The unsaturated state of the iron core has been modelled, as first approximation, by adding to each element (i, j) of the inductance matrix, the contributions $N_i \cdot N_j \cdot L_o$, with $L_o = 10\mu H$ and N_i total number of turns in "i-th" circuit. The iron core is assumed to be saturated when the total ampere-turns of the poloidal system, (absolute value), exceeds 230 kAt. An improved model of the iron core based on the use of the limb flux loops will be defined at a later stage.

The plasma current derivative is calculated as the difference between the vessel un-integrated Rogowski coil signal and the divertor current derivatives:

$$\frac{dIp}{dt} = \oint \frac{dH}{dt} dl - \sum_{i=7,10} \frac{dI_\theta(i)}{dt} \qquad (2)$$

The small contribution of the vessel toroidal current is neglected. The divertor current derivatives are measured with pick-up coils designed at JET.

The smallest time constant of the system, in the usual configuration, is of the order of 100ms and therefore an integration time of 10ms appears to be adequate. The trapezoidal formula will be used as integration method.

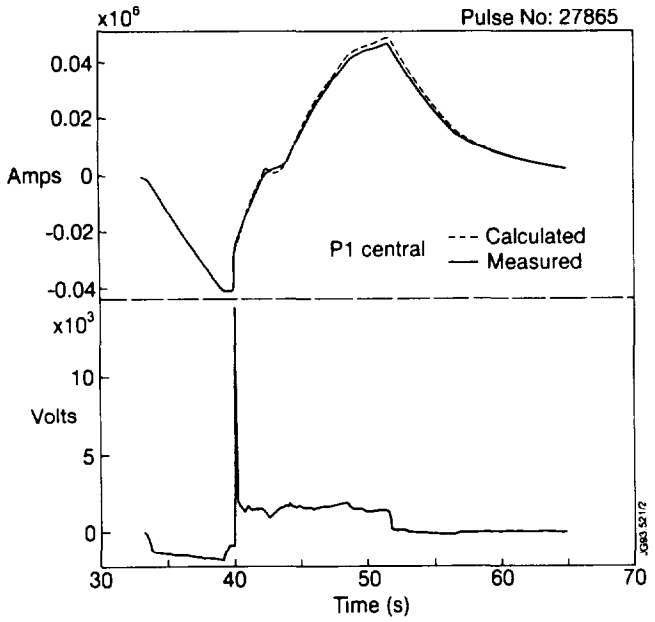

Fig. 1: PF Model-Comparison with JET data

Two sets of matrices of the associated sampled system will be used, the first for the unsaturated and the second for the saturated core case. The model outputs have been compared with JET experimental data (Pulse 27865) with good results (see Fig. 1).

2.2 TOROIDAL CIRCUIT

The toroidal field (TF) circuit includes the configuration for the "ripple" experiment. In this configuration the 32 D-shaped TF coils have been split into two sets. The odd coils (TC1) are fed from the Toroidal Flywheel Generator & Converter (TFGC) and even coils (TC2) are fed from two thyristor converter units (Static Unit 1 & 2) connected in series. Two first order, time varying, differential equations represent with sufficient accuracy the current transient in the two sets of coils:

$$L_\phi \cdot \frac{dI_\phi}{dt} + R_\phi(t) \cdot I_\phi = V_\phi \qquad (3)$$

where V_ϕ is the vector of the input voltages, I_ϕ is the vector of the computed TF currents, R_ϕ is the circuit resistance matrix (diagonal) L_ϕ is the circuit inductance matrix (symmetric). R_ϕ is a function of the temperature of the copper which, for the TF coils, changes considerably during a pulse. This is taken into account with the following equations:

$$R_\phi(t) = R_\phi(0) + \beta \cdot \int_0^t I_\phi^2(\xi) d\xi \qquad (4)$$

The model has been tested on a 67kA pulse and has shown a very good agreement with the experimental data (see Fig. 2). The resistance of the entire TF coil before the pulse was 60mΩ and the coefficient β =1.18e-13. The total self inductance was assumed to be constant at 0.64H.

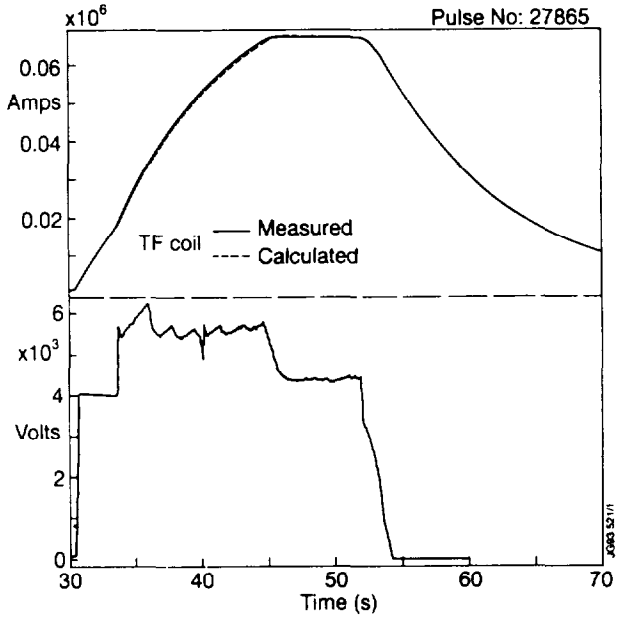

Fig. 2: TF Model-Comparison with JET data

Since the two time constants of the load are in the order of 5 seconds, the 10ms integration time as used for the PF model is more than adequate. Assuming the input voltage is constant over each time step, the circuit equations (3) and (4) will be integrated recursively using the Euler integration formula, thus avoiding matrix inversion at each step.

2.3 FORCES AND STRESSES

The stress parameters considered are the copper tensile stress (σ) and the insulation shear stress (τ). These are given by equations of the form

$$\sigma = aF_r + bF_z + cT$$
$$\tau = dF_r + eF_z + fT \qquad (5)$$

where Fr and Fz are the radial and vertical forces per unit length acting on a coil, T is the temperature of the coil (computed from the energy dissipated), a, b, c, d, e and f are

coefficient related to the coil and obtained by mechanical analysis.

The radial and vertical forces acting on each coil element are given by equations of the form:

$$F_r = nI\,B_z$$
$$F_z = nI\,B_r \qquad (6)$$

where n is the number of turns on the coil, I is the current in the coil and B_z and B_r the measured fields crossing the coil. The total vertical force transmitted to the vacuum vessel by the divertor coils is the sum of the forces acting on the 4 coils

The vertical field at the divertor coils is not measured but will be estimated as a linear combination of the ampere-turns of all coils and the plasma current. The contribution of coil P1 can be neglected since almost all the flux is confined within the iron core.

The protection system also detects operation faults in the P1 circuit such as separating forces between coils [3] and inductive effects during disruptions.

2.4 *DIVERTOR COIL THERMAL MODEL*

During operation the temperature of the vessel is maintained at about 300 °C. This means that as long as the vessel is hot, the divertor coil cooling has to be continual.

In order to keep the epoxy resin in the main body of the coil below its glass transition temperature (about 75 °C) with some safety factor (say 25%) the temperature of the epoxy should be kept always below 60 °C. This is achieved into two ways:

- Limiting the maximum I^2t on the basis of the initial temperature of the coolant before the pulse
- Monitoring the coil case temperature during baking of the vessel.

The average epoxy and copper temperatures of the divertor coils will be estimated by considering heat inputs by radiation and conduction and by ohmic heating and cooling by Freon coolant. The inputs to the model are the vessel temperature (T_v), the Freon coolant flow rate (qf), the coil case temperature (T_c) and the coolant inlet and outlet temperatures (T_{in} and T_{out}).

In order to reduce the thermal stresses between turns, the temperature difference (T_{out} - T_{in}) has to be maintained below 20°C. This is achieved by recirculating the hot coolant from the outlet to the inlet circuit [4] and checked by CPS.

3. PROTECTIVE ACTIONS

The block diagram shown in Fig.3 summarises all the fault detection algorithms. Hardware faults within the protection system itself are not shown. Measurements or computed quantities are compared with suitable thresholds. If a threshold is exceeded an alarm is generated and protective actions are taken.

The circuit currents, the forces and the stresses on PF and divertor coils are computed only during "Pulse On", whilst the remaining quantities are monitored continuously.

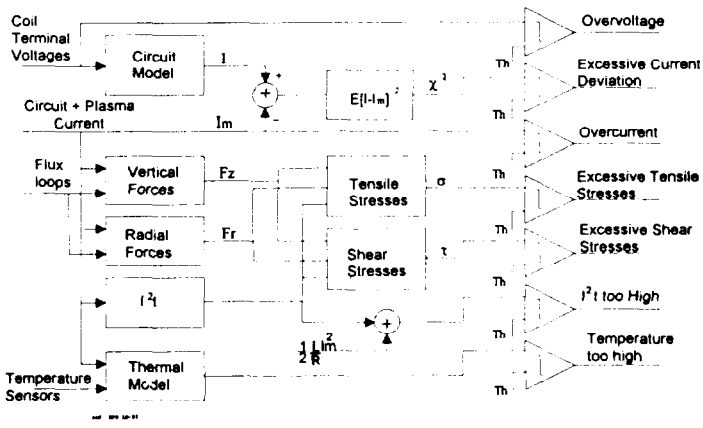

Fig. 3 Fault Detection Algorithms

A contribution $(L / 2R)I_m^2$ is added to the I^2t to take into account the residual magnetic energy of the coil. The thresholds for the I^2t limits on the divertor coils will be computed as functions of the initial temperature of the coolant as follows:

$$\left(I^2t\right)_{max} = 0.46\left(60^\circ - T_{start}\right)\cdot 10^9 \qquad (7)$$

Similar equations will be used also for the TF coil I^2t protection.

The new protection system will be interfaced with the following JET devices:

- PF and TF Power Supplies
- PF Crowbar
- Pulse Termination Network (PTN)
- Central Interlock and Safety System (CISS)
- Control and Data Acquisition System (CODAS)

Two fail-safe commands are sent individually to the PF and TF power supplies: a Voltage Off (VOF) and a Circuit Breaker Open (CBO) command (see Table 2).

The PF crowbar is closed if the "average" current of the magnetising coil P1, defined as $(N_1I_1+N_2I_2)/(N_1+N_2)$, exceeds the nominal value of 40kA by 10%.

These commands are backed-up by the actions performed via PTN and CISS. Two actions are required of PTN: the Slow. Pulse Termination (SPT) and the Fast Pulse Termination (FPT). The SPT is defined as a controlled termination of the pulse (e.g. few seconds), via the Plasma Position & Current Controller (PPCC), and a staggered switching OFF of the plasma additional heating (ICRH, LHCD and NBI) thus avoiding disruptions. The FPT instead will remove the voltage from the coils and the additional heating as quickly as possible (e.g., it takes about 300ms to de-excite PFGC and TFGC). The actions required via CISS are Inhibit Pulse (IP) and Emergency Shutdown (ES).

All the alarms and statuses of the system will be transmitted to CODAS. Some protective actions that need to be implemented in a time of the order of a few minutes are left to the operator in the control room. For example, the switching off of the baking in case of an un-recoverable failure of the cooling system of one of the divertor coils when the vessel is hot (350°C).

TABLE 2: CPS Protective Actions

Circuit	Fault Detection Algorithm	Protective Actions					
		PS VOF	PS CBO	PTN SPT	PTN FPT	CISS IP	CISS ES
PF	Over voltage	x			x		x
	Excessive Current Deviation	x			x		x
	Overcurrent 5%	x			x		x
	10%		x		x		x
	I^2t too high	x			x		x
	Excessive Shear Stresses	x			x		x
	Excessive Tensile Stresses	x			x		x
	Temper-ature too high			x		x	
TF	Over-voltage	x		x			x
	Excessive Current Deviation	x		x			x
	Overcurrent 5%	x		x			x
	10%		x	x			x
	I^2t too high	x		x			x

4. IMPLEMENTATION

The heart of the system is a VME crate (see Fig. 4). Most of the modules are standard components and others have been designed by JET and manufactured by outside companies.

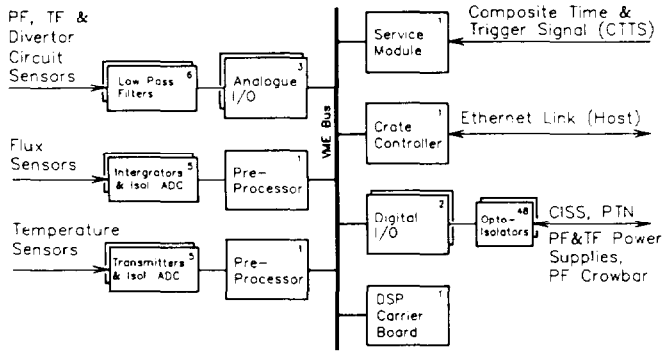

Fig. 4: CPS Hardware Configuration

The Service Module performs the function of synchronising all the internal timers to the Central Timing System by decoding the CTTS signal. This is an encoded signal containing a 1MHz clock, trigger signals and pulse parameters. It also performs subsidiary functions such as air-flow monitoring and checking the VME crate power supply for healthy status.

The VME crate is interfaced with the host computer by means of an Ethernet link via the Crate Controller fitted with a Motorola 68040 processor clocked at 33MHz.

The Digital I/O is a standard board, fitted with a security watch-dog mechanism, which directly interfaces the VME bus. It provides 40 inputs and 32 outputs isolated in groups of 8 channels. The galvanic isolation of each channel with the outside world is performed with standard opto-isolators operating at 24V.

The DSP carrier board can accommodate up to two TIM modules each containing a Texas Instrument TMS320 C40 parallel DSP clocked at 40MHz. This incorporates a powerful floating-point processor and will be used to perform most of the fault detection algorithms described previously. The external interfaces also include two RS232 serial ports and the daisy-chained JTAG port for the two TIM modules.

The Analogue I/O card contains a 12 bit Analogue to Digital Converter (ADC) capable of sampling rates of up to 320kHz. The input multiplexers will be configured to provide 16 differential channels of analogue input all sampled at the maximum frequency of 10kHz.

The Pre-processor board contains a Motorola 68030 processor and it can handle up to 64 channels of analogue signals sampled at the maximum frequency of 10kHz. The Pre-processor will be used to perform drift compensation of the integrators, and conversion to engineering units.

The Software is being developed in two different environments: a PC based development system, with OS/2, for the DSP, and a X-Terminal, Operating under UNIX, for the 68k family processors.

The development and testing of the DSP software is based on the TMS320 Software Development Tools provided by Texas Instruments. The software is loaded into the C40 processor via the front panel JTAG connector. The majority of the code is written in 'C'.

Similar tools are available on X-Terminal for the 68k series processor running VxWorks. The software for the 68k family processors, including the communication with the host computer is common for most of the VME applications in JET. The X-Terminal is also used for the man-machine interface in the remote control room.

System simulations, calculations and comparison with the experimental data are performed with a dedicated computer code. The code will be used also for sensitivity analysis and as a convenient off-line simulator for the Coil Protection System.

REFERENCES

[1] E. Bertolini and the JET team, "JET Development Towards Pumped Divertor Operations", this conference.

[2] M. Huguet et al, "The JET Machine: Design, Construction and Operation of Major Systems", Fusion Technology, January 1987.

[3] P.L. Mondino et al, "The PF System Enhancement in JET to produce plasma currents up to 7MA with material limiters and up to 4MA with magnetic separatrix: a report on electrical study", 12th SOFE conference, Monterey, U.S.A., 1987.

[4] J.R. Last et al, "The JET Divertor Magnetic Configurations and Coil Design", 16th SOFT Conference, London, 1990.

Development of Beryllium-Carbide Fibre Reinforced Beryylium for Fusion Applications

A T Peacock, W J Haws[1], M A Pick.

JET Joint Undertaking, Abingdon, Oxon, OX14 3EA.
[1] Brush Wellman Inc, 17876 St Clair Avenue, Cleveland, OH 44110, USA.

Development of Beryllium-Carbide Fibre Reinforced Beryllium for Fusion Applications

A T Peacock, W J Haws*, M A Pick,
JET Joint Undertaking, Abingdon, Oxon OX14 4DD UK
*Brush Wellman Inc, 17876 St Clair Avenue, Cleveland, OH 44110, USA

ABSTRACT

Be-Be_2C composite materials have been produced via two routes. The first produces a two dimensional composite with woven carbon cloth converted to the Be_2C fibres and infiltrated with molten Be with the assistance of a wetting agent. A number of wetting agents with low atomic number were tried, the best being silicon, either in metallic form or as polydimethylsiloxane. The second composite has a three dimensional structure, again with Be as the matrix but with random Be_2C fibres, produced by hot pressing a mixture of Be powder with 0.25 inch Be_2C fibres; no wetting agent was used. Some fibre agglomeration was observed with resulting porosity and the component had a density of 93% of theoretical. The room temperature thermal conductivity of the second composite was 84W/mk, slightly less than would be expected by a rule of mixtures, possibly due to the porosity.

I INTRODUCTION

Beryllium metal has many distinct advantages as a plasma facing material of a fusion reactor. Beryllium has thermal and mechanical properties which make it superior to graphite for removing heat in steady state. A major advantage of beryllium is the effect it has on the plasma purity which is due to the gettering of oxygen. Hydrogen tends to be bound only weakly by beryllium resulting in reduced tritium inventories in the wall. The main disadvantage of beryllium is its low melting point, 1289^0C. Beryllium plasma facing components exposed to disruptions and other off-normal effects can lose their shape and integrity by local melting. The idea behind the present work was to create a fibre reinforced beryllium material which ideally could withstand thermal shocks without losing its shape and combine the best properties of carbon-carbon fibre composites and beryllium.

Previous work had shown that carbon fibres could be converted to Be_2C fibres in the presence of beryllium. In fact, because of the exothermic nature of the reaction it is difficult to stop the reaction. The present work is aimed at incorporating these fibres into a Be matrix.

II EXPERIMENTAL PROCEDURE

A. Liquid Metal Infiltration

Previous attempts to infiltrate a woven carbon fibre cloth (Goodfellow LS98429 M L E) with molten beryllium resulted in little or no infiltration of the cloth. The lack of infiltration appeared to be due to poor wetting of the cloth. Five different elements/compounds were chosen to modify the surface tension of the molten metal or carbon cloth to promote infiltration.

These surface tension modifiers were polydimethylsiloxane (PDMS), silicon, boron oxide, lithium oxide, and lithium silicate. The surface tension modifiers were usually applied to the surface of the metal. Early experiments showed that this was more effective than applying the surface tension modifiers to the carbon cloth. The surface tension modifiers were fine (325 mesh) powders except for the PDMS which was a liquid. The powders were dispersed in either water or acetone and applied to the metal and for INF1 and INF3 also to the cloth..

Infiltration was carried out at 1500°C for all but the first experiment. Two forms of cloth were used in the infiltration experiments, the as-received carbon cloth (Goodfellow LS98429 M L E) and Be_2C cloth which was made by acting carbon fibre cloth with beryllium vapour. The experimental details of the fourteen experiments are presented in Table 1.

A piece of solid beryllium was placed on top of a single layer of cloth (either carbon or Be_2C) in a covered beryllium oxide crucible. These materials were heated in a vacuum furnace to the specified temperature and held at temperature for the specified hold time. The specimens were removed from the furnace and examined as to the degree of infiltration both visually and metallographically.

A multi-layer infiltrated part (INF-12) was produced using 31 layers of carbon cloth and 32 layers of beryllium. The diameter of the cloth and beryllium layers was 1.5 inches. The thickness of the beryllium layers was calculated based on the weight and apparent density of the carbon fibre cloth. The top and bottom beryllium pieces were 0.022 inch thick and the internal beryllium pieces were 0.044 inch thick. The theoretical volume percent of Be_2C in this experiment was 16.6%. The conditions for this experiment were silicon coated on the beryllium, carbon cloth input, and 1500°C for 5 hours. Two additional experiments were performed to evaluate the effect of the silicon addition on infiltration of carbon cloth

TABLE 1

List of experimental conditions/results of infiltration experiment

Specimen I.D.	Cloth Type	Surface Tension Modifier	Percent[1] (%)	Infiltration Temperature (°C)	Infiltration Time (hours)	Comments
INF-1	Be_2C	PDMS	1.1	1300	1	No infiltration
INF-2	Be_2C	Si	1.3	1500	1	No infiltration
INF-3	Be_2C	Si	2.6	1500	1	No infiltration
INF-4/11	C	Si	2.0	1500	5	Excellent infiltration
INF-5	C	B_2O_3	3.5	1500	5	Some infiltration
INF-6	Be_2C	B_2O_3	7.7	1500	5	Less infiltration than INF-5
INF-7/8	C/Be_2C	Li_20	0.2/0.3	1500	5	No infiltration
INF-9	C	Li_2SiO_3	1.2	1500	5	Some infiltration
INF-10	Be_2C	Li_2SiO_3	8.6	1500	5	No infiltration
INF-12	C	Si	18.2	1500	5	Excellent infiltration, density about 70%
INF-13	C	Si	1.3	1500	5	Infiltration, but not as good as INF-4, and INF-12
INF-14	C	None	N/A	1500	5	No infiltration

[1] expressed as a weight percent addition based on the weight of the Be metal

input. These experiments were performed as single layer experiments.

B. Blended Fibre Composite

An alternative approach to produce a Be-Be_2C composite is to consolidate a blend of beryllium powder and Be_2C fibres cut to 1/4 inch long. The Be_2C fibres were prepared by reacting carbon fibre cloth with beryllium vapour. The Be_2C fibre cloth was cut into 1/4 inch long lengths and separated by hand to individual fibres. The cut Be_2C fibres were blended with beryllium powder with 30 volume percent fibres. This blend was consolidated by vacuum hot press at 1100°C for 4 hours at 1000 psi.

The consolidated part evaluated by density measurement, micro structural examination and thermal conductivity.

III RESULTS

A. Liquid Metal Infiltration

The results of the infiltration experiments are presented in Table 1. The first three experiments (INF-1 to INF-3) were performed with Be_2C cloth with PDMS or silicon as the wetting agent. Infiltration did not occur for any of these conditions.

The surface of the cloth had a slight metallic look and there was a cavity in the beryllium piece. Metallographic examination showed some metallic Be near the surface but according to the micro structure no wetting of Be_2C fibres or infiltration occurred. INF-3 showed small beaded up metallic spheres. These turned out to be silicon that had agglomerated during the infiltration cycle.

For the next experiment (INF-4), the input material was changed from Be_2C cloth to carbon cloth. Silicon powder was coated onto the beryllium and excellent infiltration occurred at 1500°C along with conversion of the carbon cloth to Be_2C cloth. A photograph of the reaction products is shown in Fig 1.

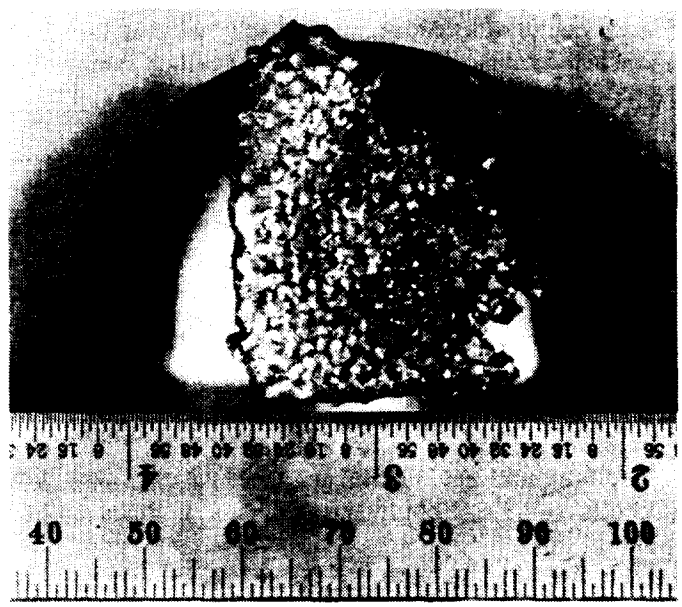

Fig 1

The photomicrographs in Fig 2 illustrate the quality of the infiltration of the cloth. Excellent wetting of the carbide fibres with very little porosity was observed.

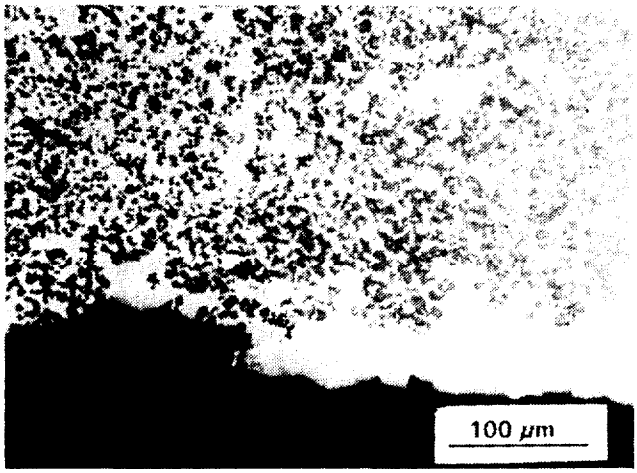

Fig 2

The next six experiments (INF-5 to INF-10) were performed to evaluate the effect of the other three surface tension modifiers (B_2O_3, Li_2O, and Li_2SiO_3) using both carbon cloth and the Be_2C cloth input. The only significant amount of infiltration was observed for the B_2O_3 surface tension modifier (INF-5 and INF-6), but did not compare in quality to INF-4. Some infiltration was observed for the B_2O_3 surface tension modifier with the carbon cloth and even less infiltration with the Be_2C cloth. The photomicrographs in Fig 3 illustrates the degree of infiltration for the B_2O_3 surface tension modifier.

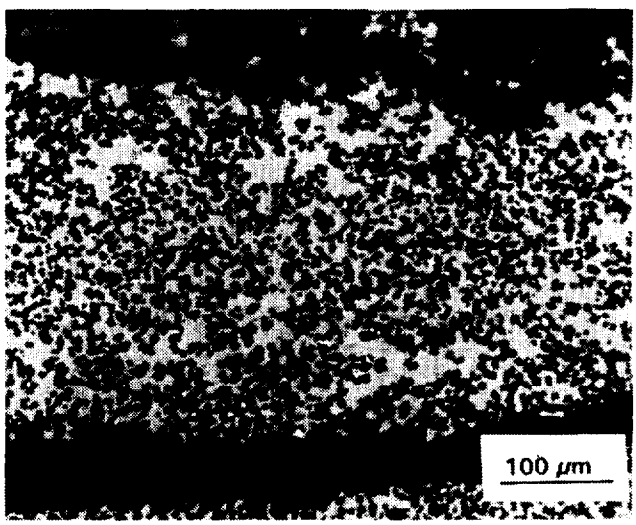

Fig 3

Good infiltration was observed in many areas but several areas contained poor infiltration. Fine porosity was also observed in most areas. Several cracks were also observed. Some infiltration was observed for the Li_2Si0_3 surface tension modifier only with the carbon cloth input. The photomicrographs in Fig 4 illustrates the degree of infiltration for the Li_2Si0_3 surface tension modifier. There is more fine porosity present along with a very coarse porosity or lack of infiltration.

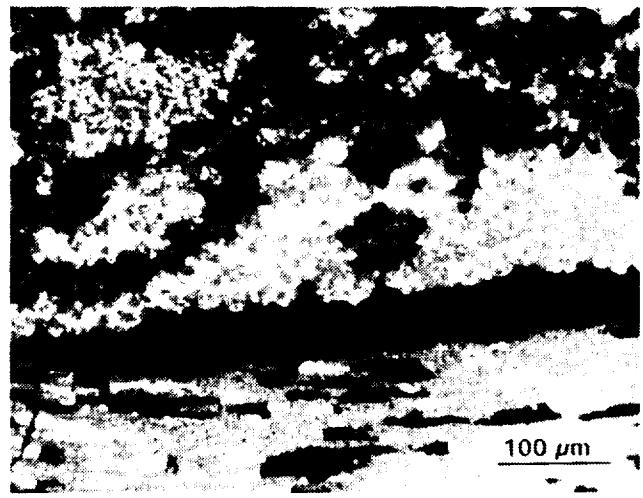

Fig 4

The best infiltration occurred using silicon coated on the beryllium and carbon cloth input (INF-4). This experiment was repeated (INF-11) with similar results.

A multi-layer infiltrated part (INF-12) was produced using 31 layers of carbon cloth and 32 layers of beryllium coated with Si. Excellent infiltration occurred with this piece but full density was not achieved. The cloth layers were in contact with the walls of the crucible and friction could have prevented densification. The density was calculated to be 1.379 g/cc from the dimensions and mass of the part. Theoretical density was estimated at 2.004 g/cc. The percent of theoretical density was 68.8%. This part is shown in the photograph in Fig 5.

Fig 5

Two additional experiments were performed to evaluate the effect of the silicon addition on infiltration of carbon cloth input. No infiltration was evident on the carbon cloth with no silicon addition compared to the cloth with the silicon addition. Infiltration of INF-13 was not as good as that of INF-4, INF-11 or INF-12. One possible explanation is the lower amount of silicon addition in the INF-13 experiment.

B. Blended Fibre Composite

The Be/Be_2C blend was made by blending 76.30 grams of Be with 43.13 grams of Be_2C cut fibres for 1 hour. There was some agglomeration of the Be_2C fibre bundles evident after blending. The blend was loaded into the graphite hot press die and consolidated at 1100°C for 4 hours at 1000 psi. Density was determined after pressing from mass/volume measurements to be 1.89 g/cc or 93.1% of theoretical density (2.03 g/cc). The photomicrographs in Fig 6 illustrate the typical micro structure. There appears to be good bonding between the Be and Be_2C. There is some porosity present mostly associated with the agglomerated fibres. Even though there was agglomeration of the Be_2C fibres many areas contained uniform distribution of Be_2C.

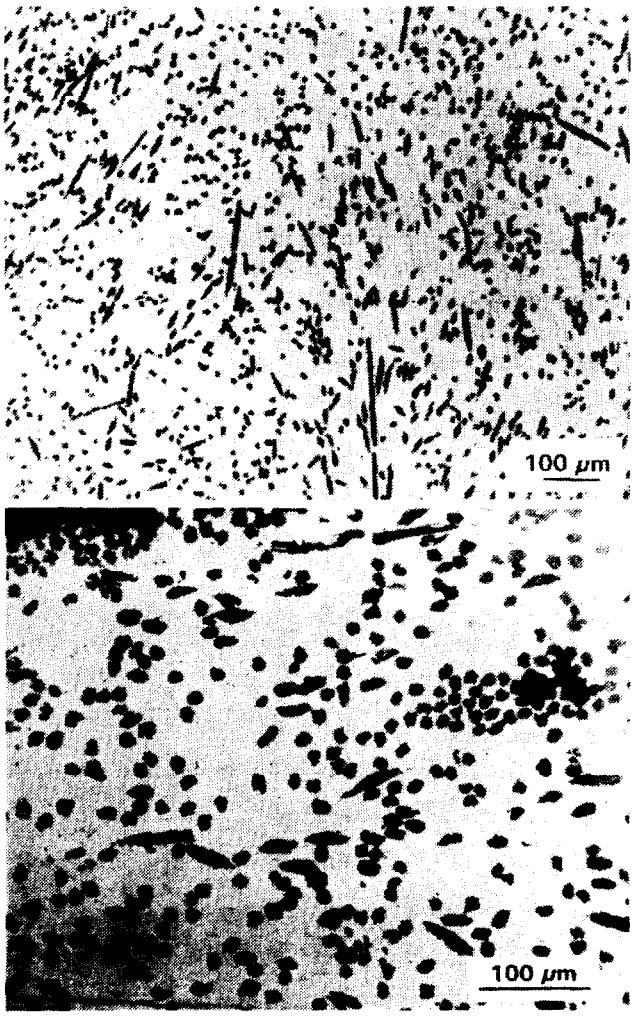

Fig 6

Specimens from this pressing were prepared for specific heat and thermal diffusivity measurements. These measurements were performed by Professor Hasselman at Virginia Polytechnic Institute and State University. The specific heat was measured from 25°C to 700°C and ranged from 1.64 J/g°C to 2.97 J/g°C. The thermal diffusivity was measured from room temperature up to 1000°C and ranged from 0.2810 cm^2/s to 0.05 cm^2/s. Thermal conductivity was calculated over the temperature range 25°C to 1000°C from measured density, specific heat, and thermal diffusivity. The value for specific heat is extrapolated from 750°C to 1000°C using a constant value taken at 700°C. These values are presented in in Fig 7. The room temperature value for thermal conductivity was 84.3 W/mK. This value may be on the low side due to porosity present in the specimen. Consolidation at higher temperatures and pressures may improve the thermal conductivity.

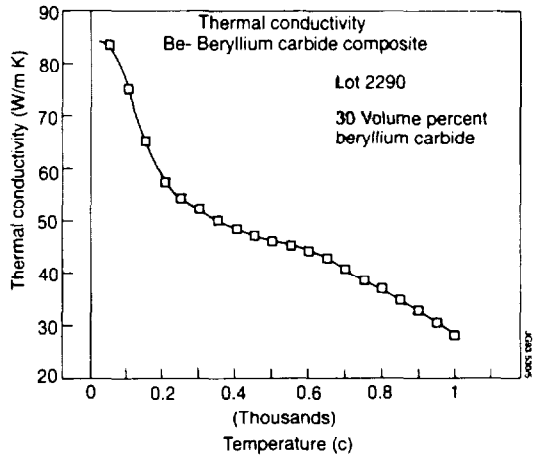

Fig 7

IV CONCLUSIONS

1. Successful infiltration of a woven carbon cloth by molten Be was achieved with Silicon as a surface tension modifier.
2. Silicon was the best surface tension modifier attempted for promoting infiltration.
3. Infiltration was most effective using a carbon cloth precursor instead of beryllium carbide cloth. The exothermic reaction which occurs to form the Be_2C when molten beryllium contacts the carbon cloth assists the infiltration process.
4. The combination of silicon as a surface tension modifier and a carbon cloth precursor was shown to be necessary for successful infiltration.
5. Boron oxide and lithium silicate also improved wetting but were not as effective as silicon.
6. Lithium oxide was not effective as a wetting agent.
7. The blended Be_2C cut fibre/beryllium powder process was successful in producing a consolidated composite with randomly oriented fibres. Room temperature thermal conductivity was 84.3 W/mK.

The New First Wall Configuration of JET

M A Pick, H Altmann, P Andrew, G Celentano, C Froger, J Graham, F Hurd, G Israel, P Lomas, B Macklin, E Martin, R Middleton, P Miele, R Mohanti, P Noll, W J Parsons, A T Peacock, L Rossi, C Sborchia, S M Scott, J Tait.

JET Joint Undertaking, Abingdon, Oxon, OX14 3EA.

The New First Wall Configuration of JET

M A Pick, H Altmann, P Andrew, G Celentano, C Froger, J Graham, F Hurd, G Israel, P Lomas, B Macklin, E Martin, R Middleton, P Miele, R Mohanti, P Noll, W J Parsons, A T Peacock, L Rossi, C Sborchia, S M Scott, J Tait,
JET Joint Undertaking, Abingdon, Oxon OX14 4DD, UK

ABSTRACT

The installation of the pumped divertor into the JET machine during 1992-1993 includes a total refurbishing of most of the in-vessel components and a new first wall configuration. The paper describes the new components, and the requirements which were implemented in the design. These include the requirements related to normal plasma operation and off-normal effects such as disruptions as well as those related to installation and alignment.

INTRODUCTION

At the end of 1992, the experimental phase of JET concluded as planned and the longest and most complex shutdown yet undertaken was started. This shutdown is being used to install all the new components of the pumped divertor and will lead to a totally transformed interior of the JET vessel. The new single null x-point pumped divertor configuration of JET should allow progress towards extended high power operation with 40MW additional heating using neutral beams and ICRF power. The control of disruptions using the new saddle coils will also be studied. The main aim of the new configuration is to study and demonstrate effective methods of impurity control in operating conditions close to those of ITER [1].

THE SHUTDOWN

The installation of the new components must be performed to very high accuracy and quality requirements within the confined space of the vessel and taking into account safety restrictions when working in a beryllium, tritium and radiation environment. For this reason the design of each component was optimised to take installation into account. Each installation work package was defined in detail, analysed in terms of its impact and dependence on all other on-going and planned work, i.e. interface checks, and then recorded. Each of these installation packages including the use of all tools and jigs must be practised, planned and organised in great detail before being implemented in order to ensure that the work is performed effectively, quickly and easily.

The shutdown consists of three major stages:

Stage 1: Preparation of vessel for new installation consisting of complete strip-out of vessel, decontamination and installation of all lower bosses and supports required for divertor coil build.

Stage 2: Manufacture and assembly of the four divertor coils and casings inside the vacuum vessel.

Stage 3: Installation and alignment of all new divertor and first wall components and diagnostic systems.

Vessel Decontamination

After many years of operation the JET vacuum vessel wall was covered in layers of carbon, beryllium, and metal from accidental melting of components. This layer contained tritium from D-D reactions and, in particular, from the recent Preliminary Tritium Experiment. The layer had to be removed before any new attachments could be welded onto the vessel wall. It was clear from the outset that in order to maintain the proposed time table it was necessary to clean the vessel of beryllium and tritium to a level at which it was not necessary for in-vessel workers to wear pressurised plastic suits. Although no such cleaning exercise had been done previously nor was it known to have been done elsewhere the shutdown plans did envisage such a cleaning.

Many techniques were studied for effectiveness, their safety aspects and their possible effect on future plasma operations. Some techniques were tried out in mock-up experiments. The method finally chosen consisted of water blasting the vessel at high pressure with boron carbide abrasive grit. This method proved highly effective, fast, and had the added advantage that any residual material would not be expected to be detrimental to plasma operations. The cleaning was accomplished in one week and resulted in a vessel in which the air borne beryllium levels and tritium levels are below the limits of detection or so low that work can be performed in the vessel without requiring any form of respiratory protection, Fig 1 [2].

Fig 1 The JET vessel after removal of all in-vessel components and after decontamination

THE MAIN COMPONENTS

The main new components to be installed in the vessel during the present shutdown are: the divertor coils, cryopump, gas baffles, divertor modules themselves, antennae, lower hybrid system, saddle coils, inner wall guard limiters and outer wall poloidal limiters. Fig 2 shows a CAD drawing of the in-vessel configuration after the shutdown.

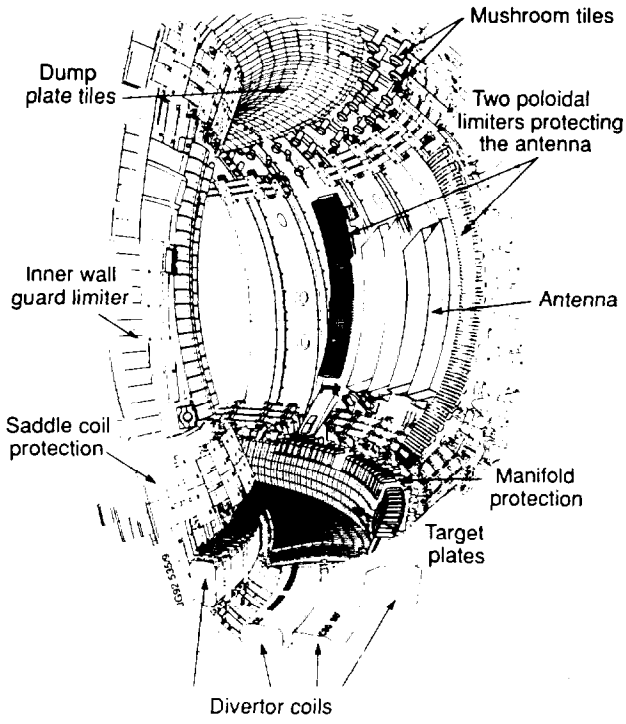

Fig 2 CAD drawing of the new first wall configuration of JET

Design Requirements

A number of design requirements, which have evolved as a result of experience during the operation of JET, have been included in the new components. Some of these requirements are a consequence of the damage to first wall protection which was caused by the interaction of so-called "halo" currents with the magnetic field. Tiles and their supports had been torn off the wall [3]. Measurements with instrumented tiles at strategic positions of the first wall of JET confirmed findings at DIII-D that the magnitude of the total halo current is generally limited to less than 20% of the maximum plasma current [4]. More recently modelling of the evolving vertical disruptions has confirmed the location and expected magnitude of the forces on the first wall components [5]. The increased understanding in the cause and magnitude of forces on the first wall components has led to two main consequences for the design. 1) A consistent system of insulating and earthing the components via earth straps which aims to direct the halo currents to the wall of the vessel by the most direct route so as to minimise the forces on the components. 2) In-vessel components and their attachments are designed to withstand the expected maximum forces caused by halo currents and to ensure that the forces exerted on the components are directed towards the wall and do not pull the components away from the wall into the plasma. A model of the evolution of the plasma configuration during vertical instabilities leading to vertical disruptions was used to check the efficacy of the in-vessel configuration against damage [6]. An important point considered in the design was the requirement that no metal components be exposed to high heat fluxes during disruptions. The new components are optimised for ease and speed of installation and removal and they include strategically located small "optical targets" to be used for alignment purposes during installation.

The heart of the new configuration is the divertor which consists of the four coils, the cryopump and associated baffles, and the water cooled divertor modules carrying the target plate tiles. It is the divertor target plate which is the main power handling component in the new configuration. However, both the inner wall guard limiters, designed to protect the inner wall, and the outer wall poloidal limiters, designed to protect the antennae and the outer wall, are able to handle a limited amount of conducted power so that they can be used as limiters for low power start-up plasmas and for controlled ramp down at the end of discharges. The poloidal limiters are able to handle 10MW of conducted power for 3-6 seconds and the guard limiters can take the same power for approximately 1-2 seconds depending on the scrape-off-layer thickness and the q value.. All the protection tiles in the vessel including those on the dump plates on the top of the vessel are either carbon fibre reinforced carbon (CFC) or fine grain graphite. Four re-designed beryllium evaporators allow a thin layer of beryllium to be deposited on all the plasma facing surfaces [7].

The divertor coils have been described in detail by Tesini et al. [8], the cryopump and baffles by Obert et al. [9], and descriptions of the design and operation of the saddle coils are given in [10, 11].

Divertor Target

The Mark I divertor target consists of inertially cooled tiles of either CFC or beryllium precisely aligned on a water cooled inconel support structure. Tiles of both materials are being prepared for installation but the more forgiving CFC tiles will be installed first. The support structure is made up of forty eight U-shaped modules each consisting of four beams which carry the tiles, Fig. 3. The beams have deep drilled water cooling channels. The modules are clamped down on to short sections of toroidal rails welded onto pads attached to the coil casings.

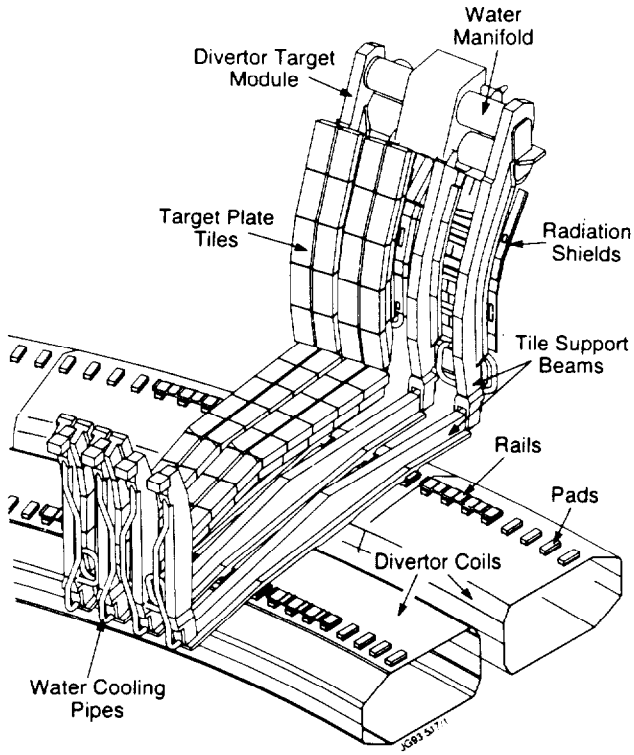

Fig 3 Target plate support structure module and interface between beams and divertor coils

TILE DESIGN AND TILE ALIGNMENT

The power handling capability of in-vessel components depends both on the design of the plasma facing components i.e. the tiles, and the precision with which they are aligned. These two features are not independent. Fig. 4 schematically shows the design of the inner wall guard limiter tiles, the poloidal limiter tiles and the divertor target plate tiles. These tiles exhibit rather complicated shapes and chamfers all of which have the objective of maximising the power load which the tiles can carry whilst allowing for a certain degree of misalignment of one tile relative to the next without exposing tile edges. It is the exposed tile edges, where power directed along field lines impinges at a near normal direction, which lead to hot spots and consequently to carbon blooms or the melting of beryllium. In order to maximise the thermal conductivity away from the hot tile surface the guard limiter and target plate tiles are made of material with carbon fibres lined up along planes normal to the thermally loaded surface. The poloidal limiter tiles consist mainly of re-machined fine grain graphite former belt limiter tiles. Areas of highest heat flux will be fitted with new CFC tiles.

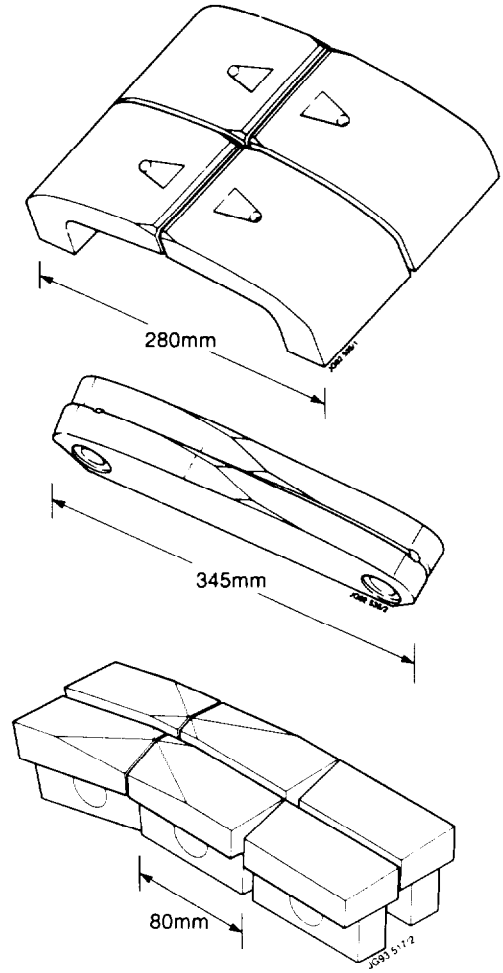

Fig 4 Schematic drawing showing, from top to bottom, inner wall guard limiter tiles, outer wall poloidal limiter tiles, divertor target tiles

The alignment precision of the tiles depends on the alignment of the tile support structure, the tolerances of the tile attachment holes and all attachment features (which are part of the design). These have been carefully analysed for the limiters and divertor target and the results are reflected in the design of the tiles which must take into account the worst expected misalignment. In the case of the target, however, the positional accuracy of the pads on the divertor coils, Fig 3, after curing is an unknown element and must therefore be assumed to have a large error. Together with the build up of tolerances of the attachments the expected misalignment of the tiles is such that the required design of the tiles would render the power handling capability of the target unacceptably small.

Better alignment of the target at installation is therefore an absolute requirement. The target plate tiles have been designed assuming the vertical step from one rail to the next never exceeds 0.6mm. The design depends on taking in-situ measurements of the vertical, radial and toroidal position, as well as radial slope of each of the pads, on which the rails rest. The rails, which are welded onto the pads, will be machined to suit the as built coils and the measured pad details. The positional tolerances of the divertor tiles are therefore reduced to the manufacturing and assembly tolerances of the modules and tiles, and the installation tolerances of the rails onto the pads. These positional tolerances, together with the angles of incidence of the field lines for a variety of plasma configurations determine the design of the tiles. Fig. 5 shows the calculated angles of incidence of virtually all the plasma configurations likely to be run on the horizontal target plate of the divertor. The open circles indicate the position of the separatrix, the open triangles and full circles represent field lines one and five centimetres into the scrape-off layer at the mid-plane respectively. The lines in the figure represent the acceptable angles of incidence resulting from chosen target plate tile design assuming different installation tolerances of the rails. Any misalignments greater than about ± 0.2mm will cause tile edges to be exposed in at least some of the envisaged plasma configurations. It is now clear, however, that an installation tolerance of better than ± 0.15 mm will be achieved. Assuming 10 MW of conducted power per divertor leg the resulting power handling capability of the target plate is between 0.5 and 1 second depending on the plasma configuration. Sweeping the separatrix across the target increases the power handling capability by a factor of 4 - 5.

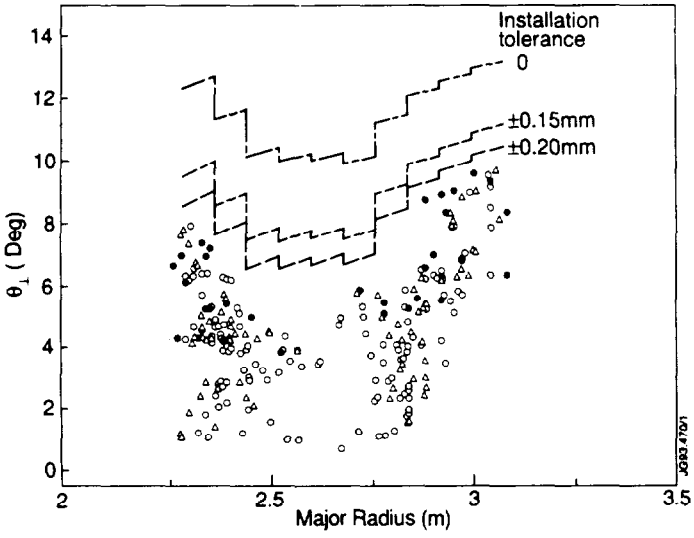

Fig 5 Angles of incidence of plasma field lines for divertor plasma configurations and results of tile design, (see text)

Method of Alignment

Using two electronic theodolites linked to a PC and a software package called ECDS (Electronic Coordinate Determination System) the coordinates of 184 uniquely identified targets welded onto the vacuum vessel wall were determined to +/- 0.30mm. A reference coordinate frame based on that data allows the use of the theodolites to accurately position any in-vessel component fitted with targets to that accuracy. The database of target coordinates can be transferred to the CATIA CAD system used for all designs at JET and has allowed a comparison to be made between the nominal and actual target positions. This in turn allows for a very useful comparison between the nominal and as built dimensions of the JET vacuum vessel.

REFERENCES

[1] E Bertolini, ibid

[2] S Scott, et al., unpublished

[3] M A Pick, P Noll, P Barabaschi, F B Marcus, L Rossi, 'Evidence of halo currents in JET', 14th Symp. on Fusion Eng., San Diego, USA, October 1991, Vol. 1, pp 187 - 190.

[4] E J Strait, et al., 'Observation of poloidal current flow to the vacuum vessel wall during vertical instabilities in the DIII-D tokamak', Nucl. Fusion, 1991, vol. 31, pp 527 - 534.

[5] P Noll, P Barabaschi, G Sannazzaro, C Sborchia, 'Electromagnetic forces during JET divertor operation', unpublished.

[6] L Rossi, et al., 'The new first wall protection at JET', Proc. 17th Symp.. on Fusion Tech. 1992, C Farro, M Gasparotto, N Knoepfer, Eds

[7] A. Peacock, et al., 'Operational experience with the JET beryllium evaporators', Proc. 16th Symp. on Fusion Tech. 1990, B.E. Keen, M. Huguet, R. Hemsworth, Eds., pp 468 - 472.

[8] A. Tesini, et al., ibid

[9] W. Obert, et al., 'JET pumped divertor cryopump', Proc. 16th Symp. on Fusion Tech. 1990, B.E. Keen, M. Huguet, R. Hemsworth, Eds., pp. 488 - 492.

[10] M. A. Pick et al., 'Integrated engineering design of new in-vessel components in JET,' Proc. 15th Symp. on Fusion Tech. 1988

[11] A. W. Morris et al., 'Feedback stabilization of disruption precursors in a tokamak', Phys. Rev. Lett. Vol. 64 (1990) pp 1254 - 1257

Design of the M=2, N=1 Tearing Mode Control System for JET

A Santagiustina, S Ali Arshad, G Bosia, M Browne,
D J Campbell, G D'Antona, G Fishpool, G F Neill.

JET Joint Undertaking, Abingdon, Oxon, OX14 3EA.

Design of the M=2, N=1 Tearing Mode Control System for JET

A. Santagiustina, S. Ali Arshad, G. Bosia, M. Browne, D. J. Campbell,
G. D`Antona, G. Fishpool, G. F. Neill.
Jet Joint Undertaking, Abingdon, Oxon, OX14 3EA, UK

ABSTRACT

This paper describes a new control system being installed at JET, which is designed to stabilise the m=2, n=1 tearing modes by magnetic feedback. After reviewing the principles of the stabilisation, the results of the system analysis are presented. The uncertainty, complexity and variability of the plasma model suggest the use of a flexible digital controller. To obtain fast responses a processor formed by a cluster of four TMS320C40`s will be used.

I. INTRODUCTION

In large tokamaks, it is necessary to avoid major disruptions and the consequent large electromechanical and thermal stresses on the first wall components. In JET disruptions are usually preceded by a growing m=2, n=1 tearing mode: a magnetic island near the q=2 surface, rotating at frequencies between 0.1 and 10 kHz. When the island reaches a certain amplitude (~1 mT of field perturbation at the wall) it stops rotating, grows more rapidly and finally, occupying a significant fraction of the total plasma section, leads to a disruption. In the attempt to avoid or delay disruptions, a new system, the Disruption Feedback Stabilisation System (DFSS), has been designed to stabilise the m=2, n=1 mode.

Experiments performed in DITE [1] suggest that stabilisation of tearing mode is possible under certain plasma conditions. It is our plan to study and try to extend these stabilisation limits in JET.

II. THE DISRUPTION FEEDBACK STABILISATION SYSTEM

The JET DFSS (Fig. 1) consists of a set of eight Saddle Coils [2], installed inside the vacuum vessel, fed by four 4.5 MVA amplifiers [3] called DFAS (output current up to 3kA for f=0-1 kHz; 3/f (kA/kHz) for f=1-10kHz). The arrangement of the Saddle Coils, each of which covers one quadrant of the vessel, is such as to excite primarily an m=2, n=1 magnetic structure in the plasma (~0.1-1 mT), to counteract that of the mode instability. The position and amplitude of the internal mhd mode are determined by a set of four poloidal field pick-up coils, mounted near the torus mid plane to minimise direct pickup from the Saddle Coils. The loop is closed through the Disruption Feedback Controller (DFC) that produces the required references to the amplifiers.

III. THE PHYSICS PRINCIPLES

In cylindrical geometry, the equation describing the tearing mode magnetic field in terms of helical flux ψ [4], is :

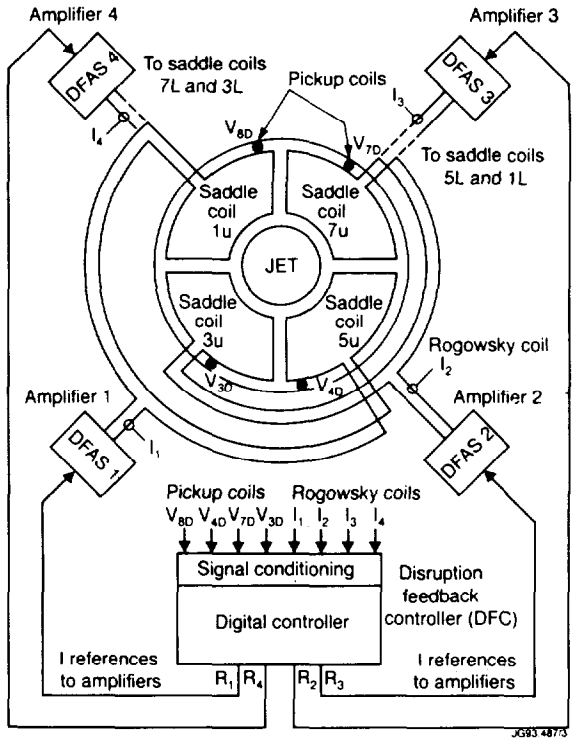

Fig. 1 JET Disruption Feedback Stabilisation System.

$$\nabla^2\psi = \frac{\mu_0 j'_0}{B_\theta (1-q\, n/m)}\psi. \qquad (1)$$

Where, j'_0 is the plasma current gradient, B_θ is the poloidal field and q is the safety factor. The mode perturbed radial field is $B_r = -i\,\psi\, m/r$.

Equation (1) describes the shape of ψ but its value shall be derived from the diffusion equation of ψ at the resonant surface $r=r_s$ (q=2):

$$d\psi_{rs}/dt \cong 3.32\ \eta\ \Delta'/(\mu_0\, w)\ \ \psi_{rs}. \qquad (2)$$

w is the island width (function of ψ_{rs}), η is the plasma resistivity at r_s, Δ' is the normalised jump of the ψ gradient at the resonant surface [4] : $\Delta' = \partial\psi/\partial r\ /\ \psi\ |\,|_{rs}$.

The effect of an external helical feedback field on the mode free evolution can be seen in Fig. 2 in the tenuous plasma approximation (no plasma for $r>r_s$). The vacuum feedback flux ψ_{ev} is screened at the $r=r_s$ surface by a plasma current sheet that prevents fast field penetration. The resulting flux ψ_{ep} is a solution of equation (1) and modifies ψ and Δ', generating, for sufficiently high feedback gains, stable modes ($\Delta'<0$).

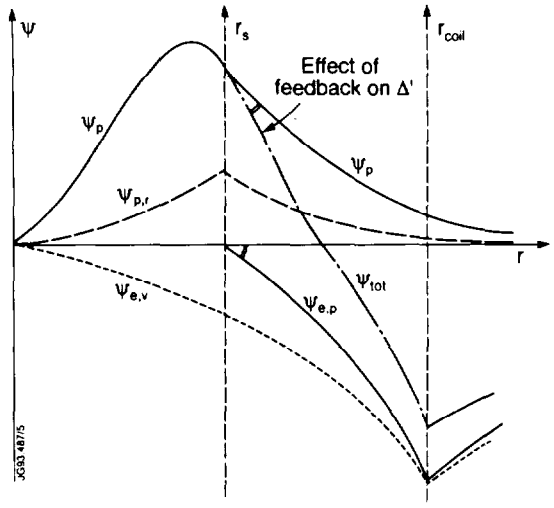

Fig. 2 Effect of an external feedback flux on Δ`(tenuous plasma).
Total flux ≡ $\psi_{tot} = \psi_p + \psi_{ep}$ = Plasma alone + External flux.
External flux ≡ $\psi_{ep} = \psi_{ev} + \psi_{pr}$ = Vacuum flux + Plasma response.

IV. A SIMPLIFIED DFSS MODEL

A. *Mode Growth Equation*

From the theory of tearing modes in the cylindrical, tenuous plasma approximation, and far from island saturation, a linearized model can be derived that describes the evolution of the perturbation b of the mode radial field at $r=r_s$ ($B=B^0+b$) as a function of the perturbed direct component b_{ed} of the vacuum external helical radial field ($B_{ed} = B_{ed}^0 + b_{ed}$) at $r=r_s$:

$$db/dt = \gamma\, b + b_{ed}/T_* , \qquad (3)$$

$\gamma \cong 3.32\, \eta\Delta'_0/\mu_0 w_0$ ($10 - 10^4$ s^{-1}), instability growth rate, $T_* \cong 0.3\, \mu_0 w_0 r_s/4\eta$ (0.1-100 ms), island penetration time. Equation (3) is valid around the equilibrium condition : $B_{ed}^0 = -B^0 \Delta'_0 r_s/4$.

B. *Mode rotation equation*

The mode rotation can be described by the equations :

$$J\, d\Omega/dt = - B\, B_{eq} V_{rs}/\mu_0 - k_v(\Omega - \Omega_*) \qquad (4)$$
$$d\vartheta/dt = \Omega .$$

Where Ω is the mode toroidal angular speed, ϑ is the mode toroidal phase, B_{eq} is the external field in quadrature with the mode, k_v (10^{-3}-10^{-7} Nm/rad) is a viscous torque coefficient that keeps the mode rotation linked to the natural plasma rotation Ω_*, V_{rs} is a geometrical coefficient, J (10^{-6} -10^{-8}kg m^2) is the mode moment of inertia. The large spreads in the parameters reflects the uncertainties in the physical mechanisms. The equations, linearized around the equilibrium $B_{eq0} \cong 0$, Ω_0, with $\Omega = \Omega_0 + \omega$, $\vartheta = \Omega_0 t + \varphi$, are:

$$d\omega/dt = -C_0/J\ \delta - k_v/J\ \omega \quad (\text{with } \delta = \varphi_e - \varphi) \qquad (5)$$
$$d\varphi/dt = \omega$$

The input φ_e is the external helical field phase and $C_0 = B_0 B_{e0} V_{rs}/\mu_0$ (0.1-10 Nm) is the peak external field torque.

C. *Measurements, Amplifiers, Coils and Vessel*

Because the pickup coils are located in the mid-plane they are largely insensitive to the coil flux ψ_{ev} in vacuum. Their integrated signal is proportional to $\psi_p + \psi_{pr}$ and so to $B - eB_e$. The feedthrough eB_e is a spurious pickup from the control field due to the fast plasma response. For a tenuous plasma $e=1$, but a precise estimate can be obtained only experimentally. The integrated signals from pickup coils, separated toroidally by 90 °, are proportional to :

$$\begin{vmatrix} B_{1m} \\ B_{2m} \end{vmatrix} = \begin{vmatrix} \cos\varphi & -\sin\varphi \\ \sin\varphi & \cos\varphi \end{vmatrix} \cdot \begin{vmatrix} B_{md} \\ B_{mq} \end{vmatrix} + \begin{vmatrix} B_{1n} \\ B_{2n} \end{vmatrix} \qquad (6)$$

$B_{md} = k_{rs}(B - eB_{ed})$, $B_{mq} = -k_{rs}\, eB_{eq}$.
k_{rs} is a geometrical factor due to the mode field decay $\sim r^{-3}$, and is a function of the position of the island r_s; B_n is the spurious pickup from other plasma fields.

The DFAS [2] in current control can be modelled, in first approximation, by a Laplace transfer function:

$$I_A = 500/(1+sT_A)\ R , \qquad T_A \cong 8\ \mu s. \qquad (7)$$

I_A is the output current and R is the input reference.

The coils produce an $m=2$, $n=1$ DC field in the order of $b_c \sim 0.1$ mT/kAturn (3 turns). The vessel screening reduces this field at high frequency by a factor 3.5 (~ 2 for bottom coils). The coils and vessel transfer function is:

$$B_e = 3\, b_c(1+s\,T_{v2})/(1+s\,T_{v1})\ I_A . \qquad (8)$$

$T_{v1} = 1.8$ms, $T_{v2} = 0.5$ms (top coils), 0.9ms (bottom coils). The fields produced by the coils and the vessel separated by 90° toroidally, B_{1e} and B_{2e}, generate field components in quadrature (q) and in phase (d) with the mode:

$$\begin{vmatrix} B_{ed} \\ B_{eq} \end{vmatrix} = \begin{vmatrix} \cos\varphi & \sin\varphi \\ -\sin\varphi & \cos\varphi \end{vmatrix} \cdot \begin{vmatrix} B_{1e} \\ B_{2e} \end{vmatrix} \qquad (9)$$

The complete DFSS model is shown in Fig. 3 where T_φ represents the sine and cosine transformation array between fixed co-ordinates (1,2) to co-ordinates rotating with the mode (d,q) at an angle φ from (1,2) .

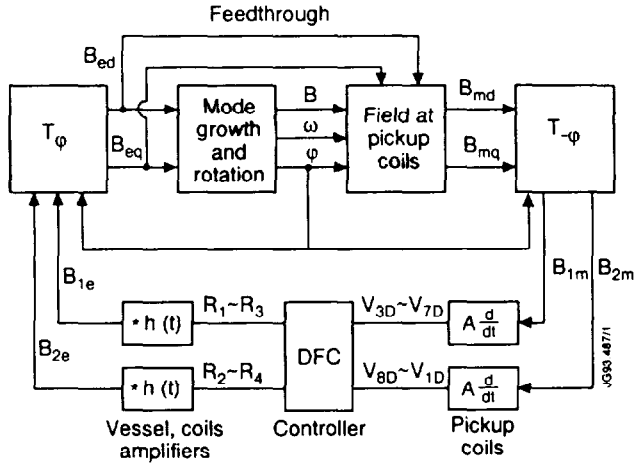

Fig. 3 Model of the Disruption Feedback Stabilisation System.

V. CONTROL REQUIREMENTS AND SYSTEM LIMITATIONS

A. *Mode Amplitude Control and Stability*

Considering a feedback field perturbation perfectly in phase opposition with the mode, with control law:

$$b_e = - k\, b \qquad (10)$$

and with (3), the closed loop time constant results:

$$T = 1/(k/T_* - \gamma). \qquad (11)$$

The closed loop system is stable when :

$$k > \gamma\, T_* = \Delta'_0\, r_s/4 \quad \text{(for tenuous plasma)} \qquad (12)$$

If the measurements are affected by the feedthrough e the control law becomes : $b_e = - k(b - e\, b_e)$.

An additional requirement for stability is then: $k\, e < 1$.

The feedthrough e, due to plasma response, limits the feedback gain k to 1 and the Δ'_0 that can stabilized to 4 m^{-1}. At least 90% feedthrough compensation ($e \sim 0.1$) is required to increase this theoretical stabilisation limit by a factor 10.

Other, less stringent limits, require the growth rate of the instability and the closed loop time constant to be slower then the system delays (10-20 μs).

B. *Phase Control and Stability*

The phase of the external feedback field must be kept in opposition to the mode field to obtain an efficient amplitude feedback with constant gain (k). The correct phase could be obtained (see Fig 3) if B_{1e} and B_{2e} were proportional respectively to B_{1m} and B_{2m}, but because the delays in the loop (vessel, amplifier, controller), the applied field is delayed with respect to the mode field. This delay will be compensated either by dynamic networks, compensating the system poles with zeros, or by rotating B_{1m} and B_{2m} in advance, multiplying them with a 2*2 rotational array $T_{\delta c}$.

If the mode rotation is dominated by viscosity ($k_v > C_0/\Omega_*$) the mode natural speed Ω_* is hardly changed by feedback. For low viscosity the equilibrium mode speed Ω_0 and the external field delay δ_0 can be calculated from the equations (Fig. 4) :

$$C_0 \sin \delta_0 = - k_v\, (\Omega_0 - \Omega_*) \qquad (13)$$

$$\delta_0 = \delta\, (\Omega_0) = \arg(K(i\Omega_0)). \qquad (14)$$

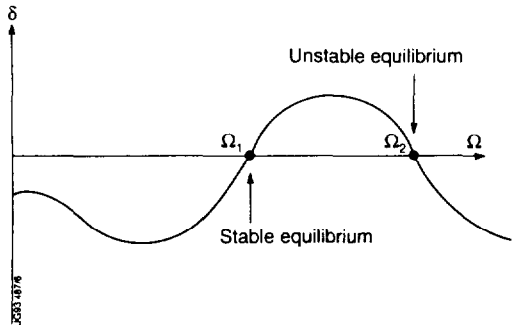

Fig. 4 Plot of control system delays $\delta = \arg(k(j\Omega)) - \arcsin(k_v(\Omega-\Omega_*)/C_0)$ in function of the mode speed Ω (for low viscosity k_v) giving one stable equilibrium speed Ω_1 and one unstable Ω_2.

Equation (14) represents the delay of the control system (composed of amplifier, vessel, controller and pickup coils and with Laplace transfer function K(s)) as a function of Ω.

Phase and speed stability conditions can be derived from (5) and the linearization of the argument of the transfer function $K(s = i\Omega)$ around the equilibrium speed Ω_0 :

$$h = \partial \arg(K(i\Omega)) / \partial\Omega |_{\Omega 0} , \quad (h \cong \text{-}2\text{-}20\mu s). \qquad (15)$$

If the control system (K(s)) delays are kept small up to the mode rotating frequency Ω_0 ($\delta < 5$-$10°$) and up to the closed loop system bandwidth (19), the whole control system can be linearized ($\delta = \delta_0 + \hat{\delta}$) and approximated by:

$$\hat{\delta} = h\, \omega \qquad (16)$$

Equation (16) is combined with (5) to obtain the closed loop system with time constant :

$$T_{cl} = J / (k_v + h\, C_0). \qquad (17)$$

Phase and angular speed stability require that:

$$h\, C_0 + k_v > 0. \qquad (18)$$

Either the high viscosity, k_v, keeps the plasma rotating at the natural speed, or $h > 0$ and the control system has phase anticipation increasing with frequency (Fig. 5). The second condition means intuitively that every time the mode is running faster than the equilibrium speed, the feedback opposition field must anticipate the mode, creating a braking torque that drives the speed back to the equilibrium point.

T_{cl} has been estimated ~ 1ms but, because of uncertainty in the parameters, phase compensation at high frequency will be performed with dynamic networks, extending the range of T_{cl} which can be sabilized to 10-20 μs.

For large phase delays of K(s) at angular frequency Ω_0 (30-50°) there is large coupling between amplitude and phase control and the stability analysis become complex.

C *Noise and Detectable signals*

The cost of high frequency power amplifiers has limited the available feedback field and the mode must be stabilised at a very small level before it locks or saturates. In extreme working conditions (minimum $r_s = 0.6$ a, maximum $\Delta'_0 = 10$ m^{-1}), fields at the wall of 1-10μT with pickup coil output signals of 0.3-1 mV must be detected. A very large input signal dynamic range (up to 10^5-10^6) needs to be maintained in order to cope with various plasma conditions. Hardware must minimise the transmission and electronic noise. However plasma noise (sawteeth, ELM`s,..) can saturate the system and must be filtered together with the amplifier chopper noise. The amplifiers will work in current control: in this way the pickup coil signals can be integrated, reducing the noise and aliasing in the digital controller.

VI. FEEDBACK CONTROLLER

The Disruption Feedback Controller (Fig. 5) is composed of an input conditioning stage, and a digital controller based on a cluster of four 40 MHz TMS320C40 Digital Signal Processors (DSP`s), capable of up to 40 MFLOPs each. A digital solution has been chosen to allow the flexibility to test different complex control algorithms, to adapt the control parameters to changing plasma conditions and to control and test the controller and its software modifications from the JET control room. Rogowsky coils are used to measure the four different coil

current derivatives, to estimate the external field and hence to obtain feedthrough compensation.

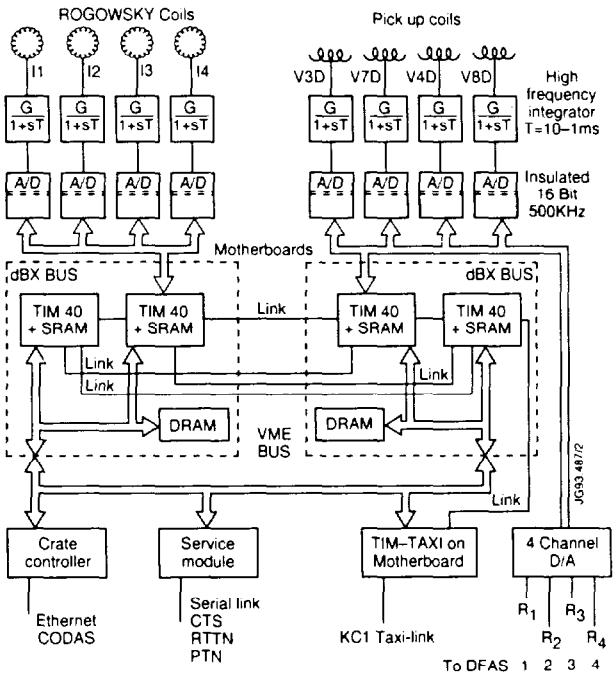

Fig. 5 Disruption Feedback Controller.

The input stage, amplifies and integrates the signals in the band of interest (0.1-10kHz) and acts as an anti-aliasing filter. It can also be shaped in frequency to give the required phase anticipation. The signals are acquired by eight ADC`s with 500kHz sampling rate, 16-bit resolution and a conversion and transmission delay of less than 3μs. Galvanic isolation of input signals is obtained digitally by a row of optoisolators after A/D conversion. The input stage is floating. Output references are sent to the amplifiers through a four channel, 12 bit DAC`s with a delay of less than 1μs. Two C40`s communicate with the ADC`s and the DAC`s through a 32bit, zero wait, C40 bus expansion. The C40 Communication links (16 Mbytes/s) are used to transfer data between processors. The total digital controller delay is expected to be less then 6 μs. A Taxi optic-link interface, mounted on a motherboard with an extra C40 processor, connects the digital controller with the JET magnetic diagnostic (KC1D) digital acquisition system. The main plasma parameters (current, toroidal field, position,..) are passed through this link every 2 ms to the digital controller to adapt control parameters in real time. The Digital Controller is interfaced to the JET computer system (CODAS) through the VME bus of the crate, a VME Crate Controller, and an Ethernet Link. This allows setting of parameters and monitoring from the JET control room. Triggering and timing are given to the controller by the JET Central Timing System, the Real Time Triggering Network and the Plasma Termination Network through a digital interface (Service Module).

VII. SOFTWARE

Two DSP`s are dedicated to the Fast Control algorithm and signal I/O. They have a program cycle time of 2-4μs. The other two DSP`s adapt the fast controller parameters at a slower time scale of ~100-400μs (Slow Control).

The Fast Control eliminates the n=0,2,.. plasma field by adding pickup coil signals from opposite octants. It rotates the pickup coil measurements to the Saddle coils co-ordinates and compensates for the pickup coils that are not located at the ideal distance of 90° toroidally. It compensates the feedthrough due to coils and plasma response by adding the Rogowsky signals properly weighted.

After obtaining a proper estimate of the mode field and position it compensates any residual phase delay in the system, and sets the correct loop gain. The proper current references are sent to the Amplifiers through DAC`s. All useful signals are stored in a round memory.

The Slow Control obtains data from the Fast Control and the TAXI link, estimates mode amplitude and mode speed and adapts the gain, phase and feedthrough compensation of the fast controller as a function of the plasma conditions. It also supervises the fast control, starting and stopping it, sensing timing events, or sensing control saturation conditions. It compensates for signal offset and DC fields and extends the system operation at low frequency. Slow signals are stored for monitoring and triggers for the fast round memory are generated.

CONCLUSIONS

The system analysis has shown some limits for the stabilisation of the m=2, n=1 tearing mode by magnetic feedback and has led to the design of the Disruption Feedback Controller described here. Particularly stringent limits have been found due to the feedthrough caused by the plasma response and the low signal to plasma noise ratio.

The experiments will verify if the scheme is a viable way to stabilise disruptions in tokamaks, and will contribute to the understanding of the physics of disruption precursors.

ACKNOWLEDGMENT

The authors would like to acknowledge very useful discussions with P. Noll, V. Marchese, E. Lazzaro and J.A.Wesson.

REFERENCES

[1] A. W. Morris et al.,"Feedback stabilisation of disruption precursors in a tokamak", Physical Review Letters, Vol. 64, No 11, 1990.

[2] M.A. Pick et al., " Full power operation at JET: consequences for in -vessel components ", Proc. 15th Symp. of Fus. Tech., Vol. 1, 1988, pp. 776-780.

[3] P. L. Mondino et al. , "The high power, wide bandwidth Disruption Feedback Amplifiers for JET ". Proc. 16th Symp. of Fus. Tech., Vol. II, 1990, pp.193-198.

[4] J. A. Wesson, Nuclear Fusion, Vol. 18, No. 87, 1978.

Power Optimisation in the RF Systems at JET and Future Devices

A G H Sibley, V Bhatnagar, G Bosia, M Bures, J A Dobbing, C Gormezano, J How, M Schmid, D Start, T Wade.

JET Joint Undertaking, Abingdon, Oxon, OX14 3EA.

POWER OPTIMISATION IN THE RF SYSTEMS AT JET AND FUTURE DEVICES

AGH Sibley, V Bhatnagar, G Bosia, M Bures, JA Dobbing,
C Gormezano, J How, M Schmid, D Start, T Wade
JET Joint Undertaking
Abingdon, Oxon., OX14 3EA

ABSTRACT

For the JET divertor phase starting in 1994, powerful Ion Cyclotron Resonant Heating (up to 24MW) and Lower Hybrid Current Drive (up to 10MW) systems will be available. To optimise their use in the large variety of plasma configurations which are planned at JET, it is essential that enhanced automatic control systems are installed to obtain the maximum power for both systems.

INTRODUCTION

The use of automatic control in both the ICRH and LHCD systems has been very successful in previous operating campaigns.

ICRH	• Automatic matching • Coupling using plasma position feedback (essential for RF only H-modes)
LHCD	• Launcher position control (flux saving with 7MA discharges)

For the 1994 campaign, automatic control will be expanded and applied to:

ICRH	*Power*
	Phase
	Frequency
	Tuning stubs
	Trombones (line stretchers)
	Conjugate Box
	Plasma position
	Demanded power feedback
	Real time total power
	Anode dissipation

LHCD	*Power*
	Phase
	Reflection coefficient control through:
	• Launcher position
	• Plasma position
	• Grill mouth density feedback
	Real time total power & profile control

(Items already under control are in Italics)

ICRH UPGRADE

For the Divertor phase, JET will have four 'A2' antenna arrays with a total generator power of 32MW [1].

With the installation of this new JET A2 antenna system, the control of power and phase of four conductors per array instead of two, required the design and construction of an upgraded control system.

The upgrade should solve several problems associated with:

- Accurate detection of arcs in the transmission line and antenna.
- Immunity from crosstalk due to multifrequency operation.
- Improved matching techniques for proposed Tritium pulses.
- Accurate power and phase control over the entire frequency range 23-57MHz (important for ITER).

The upgrade is based on experience gained with the original ICRH control and the JET LHCD system[2][3]. A block diagram is shown in Fig 1.

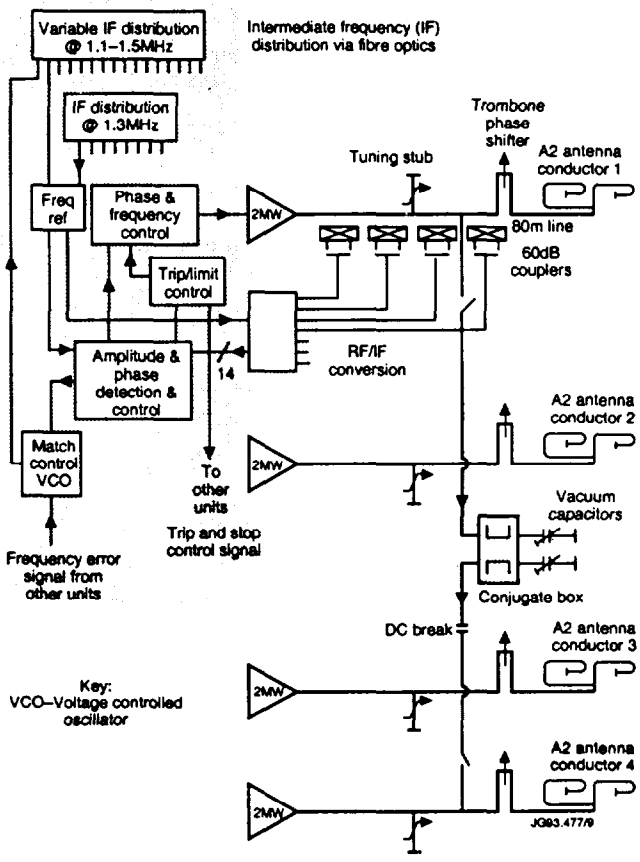

Figure 1. Block diagram of upgraded equipment

The major improvements are:

- Conversion of the coupler signals to a low intermediate frequency (IF) which ensures phase and amplitude stability. The handling and processing is also easier at a lower frequency.
- Filtering of the reflected power signals to reject RF Generators operating on adjacent frequencies thus enhancing arc protection.
- Integrated phase and frequency control ensuring a low phase noise source ideal for amplification up the 2MW level.
- Low frequency, 1.3MHz, phase reference distribution over fibre optics avoiding interference.
- Automatic testing of the reflected power trip (VSWR) at the beginning of every Tokamak pulse. Possible failures of the arc detection circuit are avoided.

A. Frequency & Phase Control

Frequency and phase control is achieved by placing the 2MW amplifier chain inside a Phase Locked Loop (PLL).

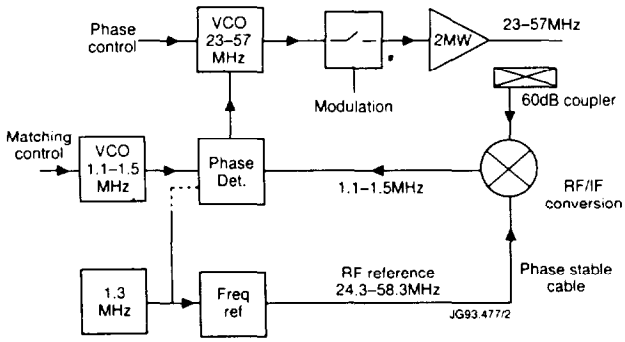

Figure 2. Frequency Translation Loop

The benefits are:

- Accurate control of the phase, either amplifier output or antenna current
- Stable low frequency oscillator (1.1-1.5MHz) controls output frequency
- Phase control over a full ±180° with detection to ±360°
- Integrated control loop simplifies electronics

B. Amplitude Detection

Due to deficiencies in the original amplitude detectors a new type based on a coherent detection principle has been developed.

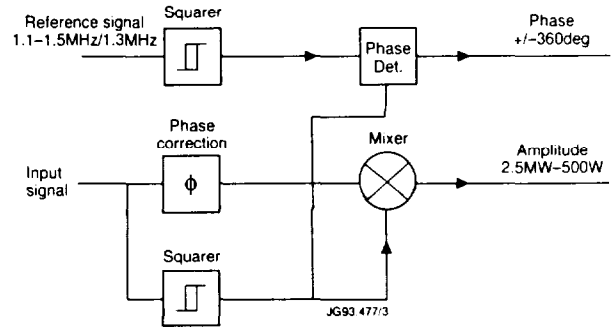

Figure 3. Coherent detector

Specification:

- Dynamic range of greater than 30dB
- Accuracy of 0.1dB over the frequency range 1.1-1.5MHz, phase independent
- Image rejection by careful choice of Intermediate Frequency (IF)
- Post detector filtering to reject unwanted signals and prevent interference with control loops

Tight bandwidth filtering of the reflected power signals is achieved by conversion to a fixed intermediate frequency of 455kHz and use of a narrow bandpass filter.

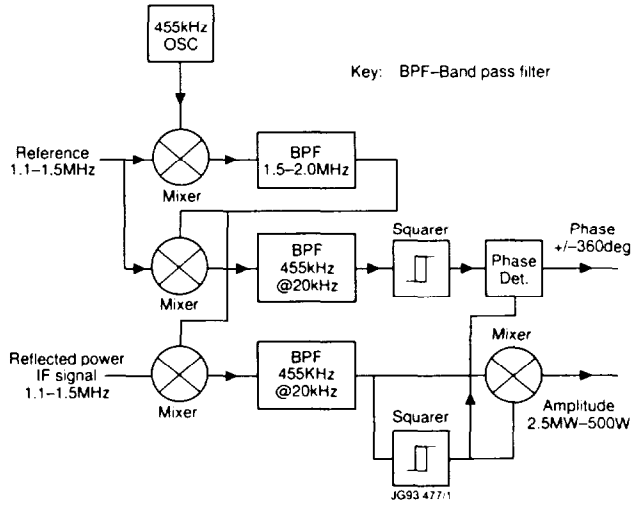

Figure 4. Reflected Power Processing

The filter bandwidth of ±20kHz is a compromise between a 50μs rise time for VSWR protection and rejection of adjacent unwanted signals.

Phase information is preserved as the reference signal follows an identical signal path before phase detection.

C. Amplitude Control

The amplitude control system has been enhanced as now four amplifier are required to be synchronously controlled. Trip and power protection control signals are now shared between four amplifiers.

Control of the antenna current, required for phased conductor experiments, is achieved by:

- Antenna current amplitude derived from maximum voltage on resonant transmission line
- Antenna current phase derived by simple algorithm from current phase at transmission line antinode
- Antenna current ratios can be altered to maximise array total power

The conjugate box equalises the generator powers by providing a return path for the antenna circulating power [4].

D. Automatic Matching Control

The automatic matching is based on the existing successful system implemented at JET but converted to the new IF system. Frequency and stub error signals are derived from RF Directional Couplers either side of the tuning stub[5]. With the mechanical tuning stub limiting the speed, fast automatic matching is enhanced by:

- Allowing the amplifier amplitude to vary by up to 15%
- Altering the output phase by up to ±15°

Arbitrary phased conductor operation is enhanced by the installation of new wide range phase shifters (trombones). This covers the electrical length variation of 1.5m in 10s, eighteen times faster than the originals.

E. Control System Simulation

The complete ICRH control system has been modelled by using the commercial SIMULINK simulation package on a 486 66MHz Personal Computer. It allows the control system to be represented in diagram form using standard function blocks.

The transmission line and antenna are represented as a set of 24 simultaneous equations with complex coefficients. The equations are solved by matrix inversion at each time step to give control system inputs.

The control system model computes controlled variables, frequency, tetrode output voltage & phase, stub length. The new variables form inputs to the transmission line model to be solved at next time step.

A typical simulation shows operation at 48MHz without the conjugate box and equal conductor currents phased at 90°. Note that one of the forward powers required is greater than 2MW, the maximum output power of the tetrode because no tube limitation has been applied.

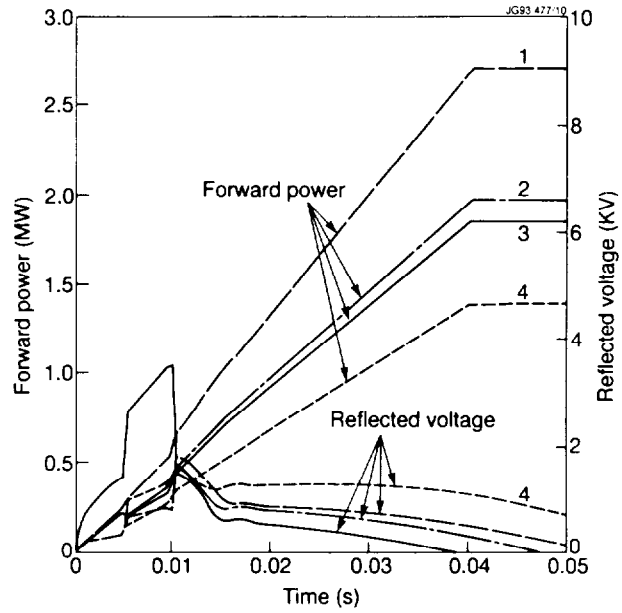

Figure 5. Typical Simulation

LHCD UPGRADE

In the 1991/1992 campaign, the launcher position was controlled in a feedback loop with a global reflection coefficient as the controlled parameter see Figure 6.

For the 1994 operational period, new feedback scenarios for the control of the launcher reflection coefficient are planned.

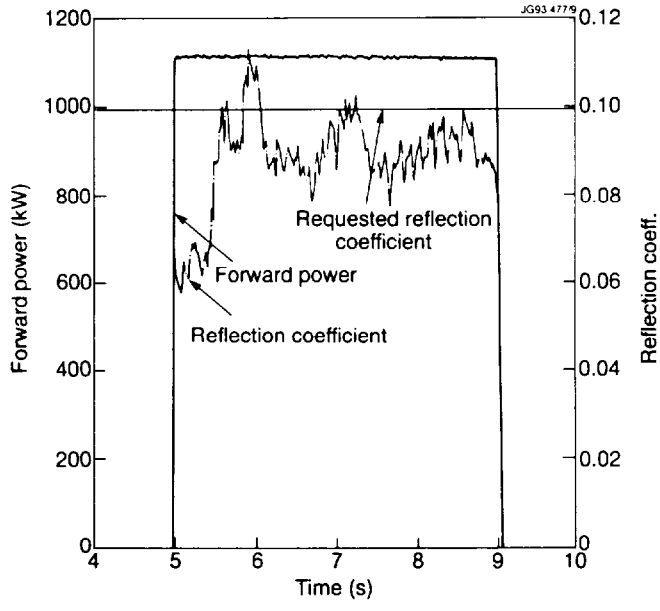

Figure 6. Feedback control on Reflection Coefficient

The plasma position control system is being enhanced to provide an integrated feedback system with the LHCD launcher. The plasma position will changed to keep the LHCD global reflection coefficient constant. If a limit is reached, a movement request will be made to the launcher position control system.

The launcher grill mouth density will be controlled via a dedicated Gas Introduction Module. This allows injection of gas near to the LHCD launcher during the plasma pulse to optimise coupling.

REAL TIME PLASMA CONTROL

Following the success of the real time plasma position control using the RF Coupling Resistance, a new control scenario is now planned for implementation on JET in 1994. Such a system is essential for the study of steady state Tokamak plasma scenarios.

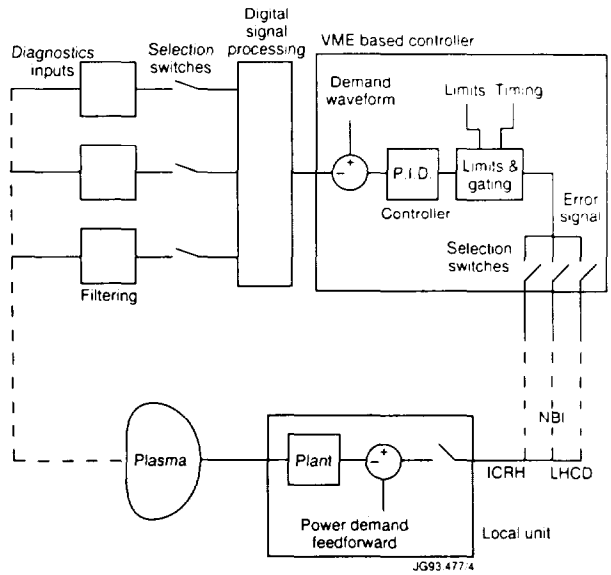

Figure 7. Real Time Plasma Control

By using real time outputs from key diagnostics, it will be possible to control any one of the following parameters in the JET plasma:

- Plasma stored energy using Beam and/or ICRH power feedback (burn control for ITER)
- Neutron yield (burn control for ITER)
- Ion or electron temperature using Beam and/or ICRH power feedback
- Plasma density feedback using Beam power
- Current drive feedback using loop voltage to control Lower Hybrid parameters
- Current density profile using flux loops, poloidal field and fast electron Bremstrahlung measurements to control the launched LH spectrum
- Impurity level feedback

ICRH & LHCD REAL TIME CONTROL

For both the ICRH and LHCD systems, a dedicated local VME based controller handles the processing of the Real Time Power Control error signals.

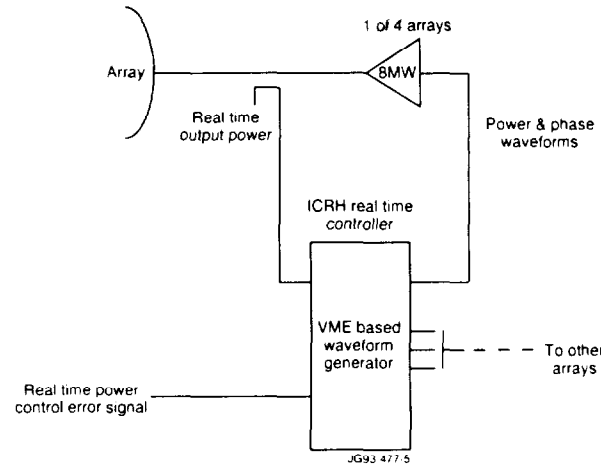

Figure 8. ICRH Controller

For the ICRH, it will provide all the power and phase waveforms for the RF Generators and via software will allow different control scenarios to be easily implemented. The local controller also processes the real time output power of each array and will adjust the demand to keep total output power constant in the case of a failure

For LHCD it allows real time amplitude and phase control of the LH waves' launched spectrum from the three independent antenna sections.

SUMMARY

The enhancements of the RF systems at JET should allow:

- Reliable high power operation
- Optimisation of the power handling in JET plasmas
- Preparation for operation with long, high power RF pulses in future devices (ITER)

REFERENCES

[1] A Kaye et al., Present and Future JET ICRH Antennae, Fusion Engineering and Design, in press.

[2] TJ Wade et al., Development if the JET ICRH Plant, Fusion Engineering and Design, in press.

[3] M Pain et al., 15MW Microwave Generator and Launcher of the LHCD Experiment on JET, 13 SOFE, Knoxville, October 1989.

[4] R Goulding et al., Design and Control of Phased ICRF Antenna Arrays, this conference.

[5] G Bosia et al., Automatic VSWR Control in JET ICRH Transmitters, proc 16th SOFT London, 1990, pp 1099-1103.

Construction and Testing of the JET Divertor Coils Inside the Vacuum Vessel

A Tesini, E Bertolini, N Dolgetta, J R Last, P Presle, G Sannazzaro, J Tait, G Dal Mut[1], C D'Urzo[1], A Laurenti[1], A Maragliano[1].

JET Joint Undertaking, Abingdon, Oxon, OX14 3EA.
[1] Ansaldo GIE, Genova, Italy.

Construction and Testing of the JET Divertor Coils Inside the Vacuum Vessel

A. Tesini, E. Bertolini, N. Dolgetta, J.R. Last, P. Presle, G. Sannazzaro, J. Tait, G. Dal Mut*, C.D'Urzo*, A. Laurenti*, A. Maragliano*, JET Joint Undertaking, Abingdon, Oxon, England, *Ansaldo GIE, Genova, Italy.

ABSTRACT

The JET Tokamak magnetic system has been enhanced by adding four resistive magnets inside the vacuum vessel to produce divertor plasmas. In factory the coil parts were manufactured and process techniques qualified. Assembly took place at JET, inside the vacuum vessel, including welding into Inconel casings and impregnation with epoxy resin.

INTRODUCTION

The construction of the JET divertor coils marked a significant step in magnet technology [1]. For the first time large coils were assembled, brazed and vacuum impregnated with epoxy resin not at the contractor's factory but inside a tokamak vacuum vessel, in a radiation and beryllium controlled environment. For 26 weeks the JET vacuum vessel was turned into an extension of the factory, with people working on two or four shifts (20-24hr days), six and also seven days/week. Assembly and resin impregnation of two coils at a time was done to optimise tools usage and save time [2].

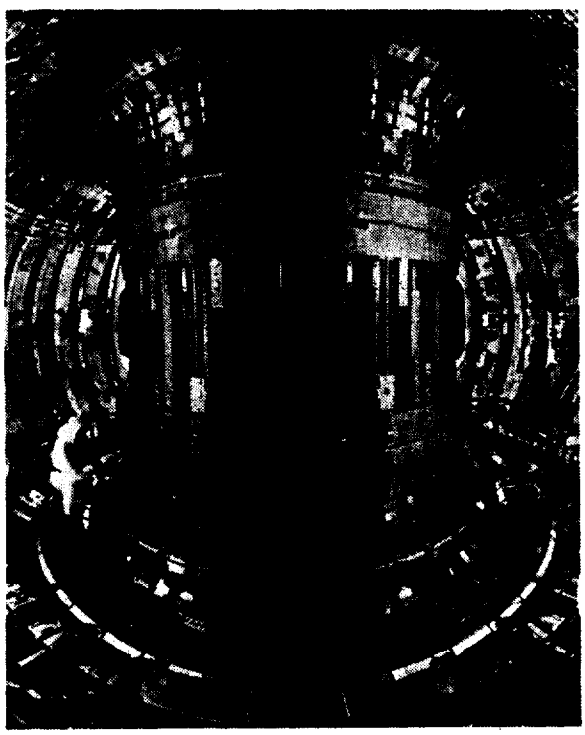

Fig. 1: Divertor Coils Installed in the Vacuum Vessel

DESIGN CONCEPT AND MANUFACTURING TECHNIQUE

The four JET divertor coils (D1, D2, D3, D4) were designed:

- to maximise the vessel volume available for plasma operations and
- to be assembled in situ, i.e. inside the vacuum vessel.

The concept of assembling pre-formed conductors was evaluated together with other more conventional manufacturing techniques like conductor tension winding and forming by rolling and found to offer the best assembly simplicity/assembly time ratio. Further, this solution allowed the use of light tools and modular jigs (i.e. the assembly tables) an important factor when working in a confined space. Each assembly sequence was carefully studied and planned with a CAD system.

Due to topological constraints the coils were built in the following sequence [3]:

1. Build of the 1.2mm thick Inconel casings by entering quarter sections into the vessel and welding in 360° jigs to form complete rings. During coil build the complete lids were stored near the vessel ceiling and the lower halves under a purpose built load bearing floor.
2. Insertion of assembly tables and build of coils D1-D4 and then D2-D3 (conductor bars introduced through a ~ $0.4m^2$ vessel port and placed onto the table, brazed, tested and insulated, to produce complete turns which are then compressed to give the correct coil cross-section). As the assembly table was common to coil D2-D3, coil D2 had to be built starting from the outer turns inwards.
3. Lifting of coils off the assembly tables, removal of tables from vessel and brazing of electrical terminals, welding of cooling pipes; application of ground insulation to terminals.
4. Lowering of coils on supports for ground insulation application.
5. Insertion of coils into the Inconel casings, shimming and welding of the lids.
6. Lowering of the coils in the impregnation position and in the post impregnation final position.

COIL PARTS AND TOOLS MANUFACTURE

17 tons of phosphorous deoxidised copper (59 × 30.5mm cross section bars with a 17mm diameter centred hole for the Freon coolant and several plates for machined parts) were procured in early 1991 and formed at the contractor's factory. All 220 pieces (~ 50% are standard curved conductors and ~ 50% are specially shaped pieces for vertical and radial transitions and for the hydraulic and electrical terminations) were formed using a combination of standard and newly designed tools. Some of these special tools, like the assembly tables, were used both at the factory for pre-assembly checks and trials and at JET for assembly inside the vessel. Other tools designed and built for work at JET were: a) brazing jigs, for conductor joining and alignment, brazing and stretching, b) lifting equipment, necessary for the completion of the coil electrical and hydraulic terminations, for the insertion into cases and for the final positioning at the bottom of the vacuum vessel. All coil parts and tools were ready for the start of the assembly work at JET scheduled for November 9th, 1992, 25 months after the contract was placed.

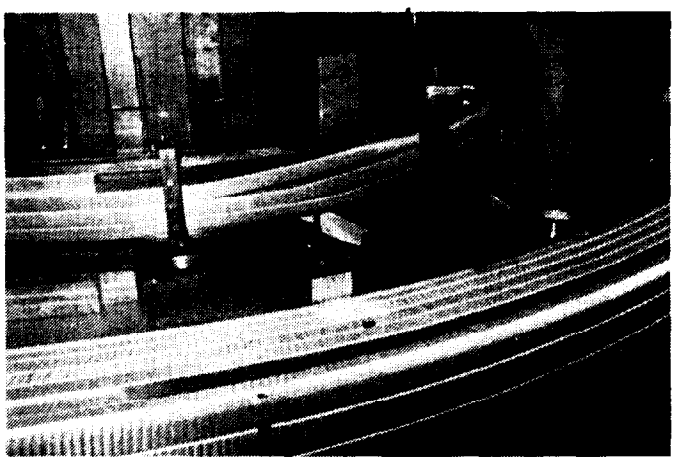

Fig. 2: Coils D1-D4 Prior to the Ground Insulation Application

ASSEMBLY

A. Vacuum Vessel Preparation

Before assembly of the coils the vessel was stripped down of all components (tiles, RF antennae, limiters, etc.) and cleaned to reduce the beryllium surface and airborne contamination, to allow personnel to work with reduced or no respiratory protection equipment. Sixteen aluminium beams made to follow the curved contour of the vessel ceiling for maximum headroom were installed and proof loaded. These provided several combinations of lifting points for the handling of the individual conductors using ropes and pulleys and for lifting of the coils, including their final positioning using three synchronised motorised lifting beams. Three lifting beams were used simultaneously to lift each coil at six positions. As the beam/pulleys/rope system is free to pivot around a horizontal centre line this was equivalent to a "three point lifting system".

B. Tools

Build of the modular assembly tables was simple and good precision was achieved by precisely machined side faces of the modules. Wedges, bolts and locating pins were used to obtain: a) the correct table diameter and planarity, b) to allow the table to collapse when extracting the complete coil, thus minimising upset of the coil geometry and ensuring that the final ground insulation is applied to a correctly shaped coil and to reduce the loading on the lifting equipment After use the assembly table top section was removed from the vessel and the support legs kept to support the coil during ground insulation application. The jigs used for brazing the conductors (two for work on two coils in parallel) were extremely compact due to the small space available between conductors. While this made their handling easy, the necessary joint alignment precision (0.2 mm joint gap) was not always easily achieved. This resulted in a lengthy conductor positioning operation and extra checking of the joint gap before reaching a satisfactory joint matching. The tool used for stretching the joint after brazing (to work harden the copper annealed during brazing) performed satisfactorily. The brazing and stretching tools were hydraulic powered using demineralised water to comply with the vessel clean condition requirements.

C. Brazing

The brazing process was controlled by two parameters: joint temperature, (~650°C) using a thermocouple in proximity to the joint, and time (joint pressure: 6-8MPa). The heating was kept short to minimise the extent of the copper annealed zone. A 50kW power supply situated outside the vessel fed two water cooled induction coils through two 15m long cables providing automatically controlled power for the brazing. A local control panel (in vessel) was used by the brazer to start and stop the brazing process. The saddle shape of the induction coil for copper joints brazing was optimised by adding steel laminations to obtain uniform heating of the copper cross section. The joint surface preparation and positioning prior to brazing was critical. Thorough cleaning and silvering of the copper joint (in vessel) and ultrasonic cleaning of the brazing material (Silphos, a copper/phosphorous/silver alloy) was done immediately before brazing to reduce the possibility of surface oxidation. Braze failures during coils D1-D4 assembly prompted a check of the brazing jigs. It was found that too large lateral forces produced incorrect bar alignment and uneven joint pressure. A complete strip down and recalibration was performed after completion of coils D1 and D4, followed by several test brazes to verify the correct performance of the jig and mechanical tests to assess the quality of the brazed joints.

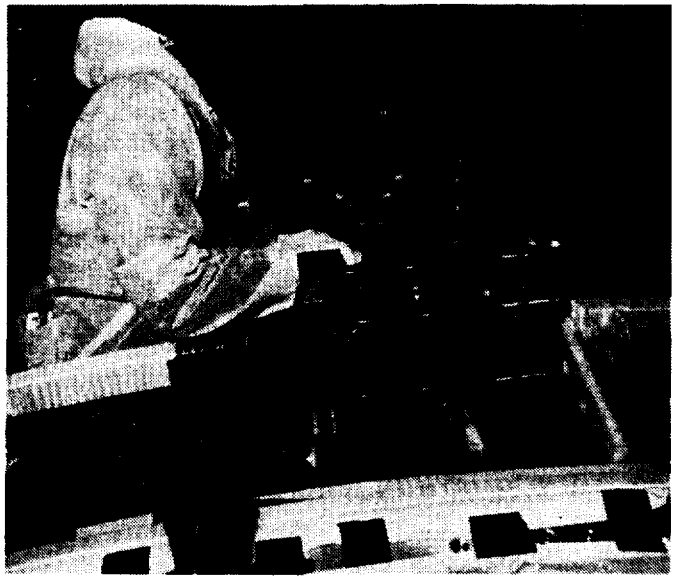

Fig. 3: Setting up the Brazing Jig and the Induction Brazing Coil

The rate of braze success improved from ~ 79% (coils D1-D4) to ~ 94% (coils D2-D3) (see also Table 1). Occasionally the induction coil power modulation failed to work correctly, notably when the feedback control thermocouple was not exactly positioned or securely touching the copper close to the braze line. In this case the brazing process was effectively controlled by eye from the time the Silphos alloy started flowing along the joint line. Every time a joint failed to pass the stringent x-ray test limits it was cut using a special cutting tool. Although the cut was originally done through the Silphos, better results were obtained by cutting a ~ 60mm section. The azimuthal position of the downstream joints on coils D1-D4 was not critical. The overall coil length was maintained by adding extra pieces of copper. On coils D2-D3 a ~ 200mm piece was cut and replaced (or in one occasion, the whole bar replaced). Here the joints position was fixed by the fixed location of the radial joggles. Vertical brazing of the electrical feedthroughs was straightforward, using a special support for the brazing jig and to guarantee good alignment of the conductors.

TABLE 1 BRAZED JOINTS BALANCE AT THE END OF THE JET DIVERTOR COILS BUILD.

Coil	Joints Nominal No.	Total Brazes	Passed	Failed and Re-brazed	% Failure
D1	42	57	46	11	19
D2	44	47	44	3	6
D3	48	51	48	3	6
D4	75	103	80	23	22

D. *Testing of the Brazed Joints*

After stretching and visual inspection, each brazed joint was x-rayed. A 300kV tube mounted on a special fixture was used to take two 0 deg and two 8 deg shots per joint. This allowed defect identification in the full section and in the reduced section of the conductor. Interpretation of the defect was not always easy. In a few doubtful situations the joint was cut and re-brazed. The maximum acceptable defect size was: 5 mm^2, i.e. 1.7% of the combined area side by side of the cooling channel hole and 40mm^2, i.e. 3.3% of the combined area top and bottom of the hole. A summary of the brazed joint success rate is given in Table 1. After x-ray each joint was pressure (2 bar) and leak tested (10^{-5} mbar.l/s).

E. *Coil Electrical Insulation and Insertion into the Casings*

All conductors were pre-insulated but the interturn electrical insulation needed to be completed locally after each brazed joint passed the x-ray, pressure and leak test. Glass reinforced epoxy shims were used during assembly to fill up the gaps between joggles and between coil and casing before the final weld of the casing lids (to minimise the number of epoxy resin rich areas). The coil ground insulation application was straightforward and done quickly by using three teams of two workers. The correct coil cross section was maintained, as during the brazing phase, by using clamps fitted at regular intervals, thus keeping the turns tight together. However, when these clamps were removed prior to the coil insertion into the case, some unsupported turns on coils D1-D4 dropped slightly. It was still possible to insert the coils in the casings and the problem was overcome by tighter winding for coils D2-D3. In some places the ground insulation thickness was reduced to clear the coil/casing gap still maintaining a good electrical insulation safety margin. During the last stages of the ground insulation application the following items were fitted: a) copper plates on top and bottom face of coil to spread part of the heat coming from the vacuum vessel at 350°C over the actively cooled conductors, b) de-gassing pipes to help removing gas evolved when radiolysis of the

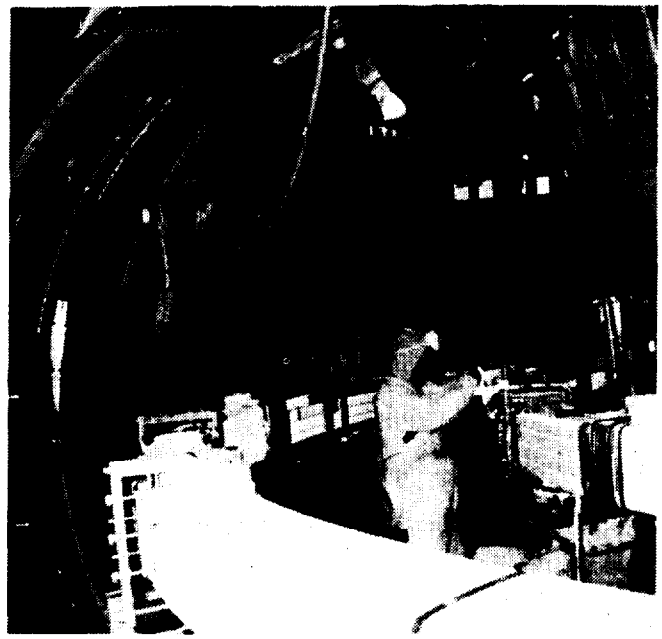

Fig. 4: Ground Insulation Being Applied To Coils D1-D4

resin occurs under fast neutron and gamma flux (as shown by resin irradiation tests performed at the JRC-Petten high flux reactor [4]). Further gas removal is obtained by pumping the coil/casing interspace (which should appear due to the application of release agent to prevent casing sticking to the epoxy resin) via a pumping box fitted outside the vessel, at the bottom of the casing tail.

The low lifting speed of the lifting equipment (0.1mm/min) and the possibility of separate rope tensioning minimised coil swinging during lifting and ensured uniform loading at the lifting points. The coils were inserted into their casings by lifting the casing around the coil while this was resting on eight, 200mm long, 22mm diameter rods inserted through holes in the casing bottom. A total Inconel length of ~140m for the four casings was tack welded in stages and then continuously welded to close the four coil casing lids. The casings were finally vacuum leak tested ready for the resin impregnation.

Fig. 5: Coil D4 Insertion Into Casing

TABLE 2: COIL/CASING BUILD DETAILS

Coil No	Average Diameter (mm)	Mass (Tons)	Inner/Outer Diameter Coil./Casing Av. Gap (mm)	Coil/casing Vertical Av. Gap (mm)
D1	4197	3.5	6.4/0	3.1
D2	5004	3.8	7.7/1.4	4
D3	5694	4.3	3.9/4.7	3.5
D4	6793	7.1	1.5/0	2.5

F. Vacuum Impregnation with Epoxy Resin

The resin system used for the JET divertor coil contains the base epoxy with hardener and plasticizer. No accelerator was used to allow a very slow impregnation of the tight glass/kapton insulation without risk of premature setting. The resin impregnation equipment, situated outside the vessel, consisted of resin mixer, ~ 200m of 12.5mm diameter copper pipes, vacuum pumping system, temperature and vacuum gauges. The resin inlet ports were equally spaced at the bottom of each casing, with the electrical feedthrough fed separately via a resin tank welded to the casing tail. Special clamps limited the casing deformation in areas where the dimensional interface with other divertor components was critical. Thermal insulation was applied around the coils during the impregnation and the curing cycle to reduce the thermal losses and minimise the electric heating power requirements. The coil tails, the resin inlet/outlet flanges and the boxes at the bottom of the tails were also heated by external heating tapes. To avoid resin spillages inside the vacuum vessel the resin in the pipes was fully cured using additional electric heating elements before pipework disassembly.

Special sliding supports were fitted to allow coil thermal expansion during the heating cycle. The heating necessary for the coils drying/impregnation/curing was provided by a 2000A, 30V DC power supply feeding the coil conductors (using the vessel as an oven was originally regarded too complex). Before impregnation the coils were heated to 90°C under vacuum to dry the electrical insulation and flushed with CO_2.

The impregnation was done by gravity under vacuum using the casings as a mould. The process was complete when the resin overflowed through copper pipes connected to ports at the top of the case into an expansion tank located outside the vessel. When this was half full, the vacuum was broken and re-made several times to push-pull the resin inside the coil and improve the coil resin filling with 300 mbar max overpressure (instead of 4-6 bar normally used in factory).

After the curing process, i.e. after removing the resin pipes, it was discovered that in some areas between coil and casing the resin had not fully cured, (low value of the glass transition temperature was measured on some resin samples). Although the interturn insulation had fully cured (as the resistance temperature measurements showed) it was decided to complete the outer resin layer curing before the coils went into operation. The corrective action was taken as soon as the tight JET shutdown programme allowed. An extensive testing campaign was carried out to evaluate the best recuring cycle and the effects of reheating on partially cured resin. This included consultation with the resin manufacturer, the assessment of the degree of polymerisation of part cured resin before and after different heating cycles and the manufacture of

TABLE 3: CHARACTERISTICS OF THE IMPREGNATION PROCESS

Vacuum level	1-10mbar
Temperature rate of rise	5°C/hr
Resin impregnation time	12hr
Resin gelification	100°C for 10hr
Resin curing	135°C for 24hr

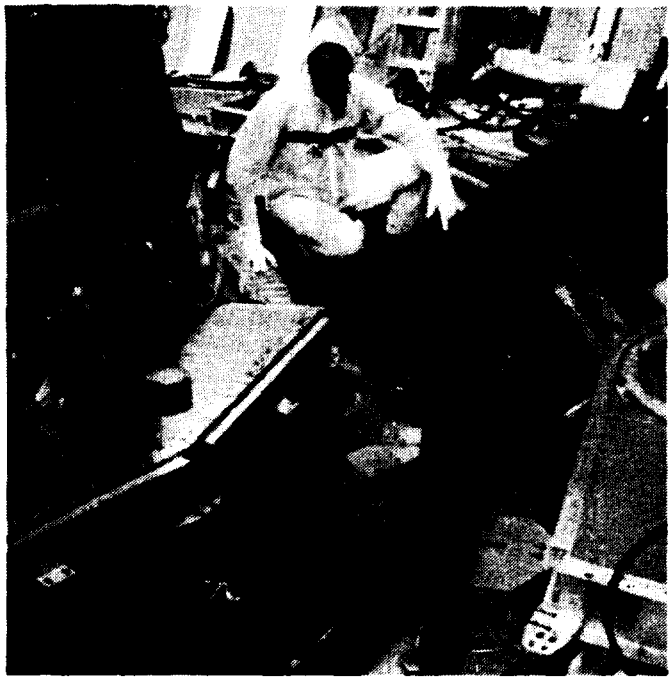

Fig. 6 Resin Pipework Installation on Coils D2-D3

two simplified models which repeated the curing conditions previously found at JET. These models subsequently underwent an "optimum" recuring cycle. It was concluded that: a) complete resin polymerisation could be achieved provided that a suitable recuring cycle is followed, b) the mechanical shear strength characteristics of the insulation system are not impaired if part cured resin is subjected to a correct recuring cycle. Four months after completion of the last two coils the recuring operations was successfully performed. This time the vacuum vessel was set up to act as an oven in air, using the vessel baking plant as the prime source of heating together with the ohmic heating of the four coils.

TABLE 4: CHARACTERISTICS OF THE RE-CURING

Temperature rate of rise	3°C/hr up to 90°C
	2°C/hr up to 130°C
Temperature of the copper	130°C for 50hr
	142C for 50hr
Maximum Temperature of the vessel	155°C
Maximum Temperature of the air in vessel	140°C
Temperature decay rate.	5°C/hr

G. Electrical Tests

Tests were performed to confirm that the coils' electrical insulation was sound. The test values were lower than those normally used in factory (as the divertor coils were complete and finally installed), but higher than those which would be normally found in fault condition during operation. The tests were: a) on the complete coil but before ground insulation application (DC resistance measurement, ampere turn measurement to confirm correct number of turns, resistance/inductance vs frequency measurements @ 20Hz - 50kHz), b) on the complete coil, inserted into the case, after the final weld of the casing lids (high voltage test by capacitance discharge, monitoring the voltage and current waveform, at reduced value before resin impregnation and at 6kV-interturn and 8kV-ground after resin curing, c) inductance and resistance measurement vs a wide range of frequencies to provide a data base for future reference and monitoring of any developing faults. The test results were compared with a model which includes the case and the vacuum vessel to establish the sensitivity limits of interturn fault detection.

CONCLUSIONS

Completion of the JET divertor coils in confined conditions and on schedule demonstrates that fusion magnets can be built away from the factory.

Non-conventional coil manufacturing techniques and novel working conditions were experienced. We hope that this pioneering work will be valuable to future large fusion machines if magnets are to be built on site.

ACKNOWLEDGEMENTS

The dedicated work of many colleagues of JET and Ansaldo contributed significantly to the successful completion of the JET divertor coil. The co-operation of JET First Wall Division members and of the GEC site contractor is also gratefully acknowledged.

REFERENCES

[1] J.R. Last et al., "The JET Divertor Magnetic Configuration and Coil Design", Proceedings of the 16th Symposium of Fusion Technology, London, UK, 3-7th September 1990, vol. 2, pp. 1614-1618.

[2] E. Bertolini et al., "The JET Divertor Coils", IEEE Transactions on Magnetics, January 1992, vol. 28, number 1 [Proceedings of the 12th Conference on Magnet Technology, Leningrad, USSR, 24-28th June 1991, pp. 275-278].

[3] E. Bertolini et al., "The JET Divertor Coils - Manufacture and Assembly", Proceeding of the 17th Symposium on Fusion Technology, Rome, Italy, 14-18th September 1992, vol. 1 pp. 783-787.

[4] R. Metz, G. Sordon, G.P. Tartaglia "EPIRO-TP272 Irradiation Report", JRC-Petten, Netherlands, September 1993.